Electrochemical/Electrospray-Mass Spectrometric Studies of the Oxidation of Iodide and Cyanide at Gold and Platinum Electrodes as well as Gas Phase Multiply-Charged Fullerene C_{60} Anions.

Except where reference is made to the work of others, the work described in this dissertation is my own or was done in collaboration with my advisory committee. This dissertation does not include proprietary or classified information.

Tan Guo

Certificate of Approval:

William E. Hill Professor Department of Chemistry	Andreas Illies, Chair Professor Department of Chemistry
Vince Cammarata Associate Professor Department of Chemistry	Rik Blumenthal Associate Professor Department of Chemistry

Stephen L. McFarland
Acting Dean
Graduate School

Electrochemical/Electrospray-Mass Spectrometric Studies of the Oxidation of Iodide and Cyanide at Gold and Platinum Electrodes as well as Gas Phase Multiply-Charged Fullerene C_{60} Anions.

Tan Guo

A Dissertation

Submitted to

the Graduate Faculty of

Auburn University

in Partial Fulfillment of the

Requirements for the

Degree of

Doctor of Philosophy

Auburn, Alabama
August 15, 2005

Vita

Tan Guo, son of Yuan, Suxia and Guo, Shenghui, was born on March 1, 1973, in Xian, China P. R.. He graduated from Daqing High School in 1991, and then he entered Harbin Institute of Technology in September 1991, and graduated with a Bachelor of Engineer degree in chemistry in July 1995. After a two-year's industry employment working as an assistant engineer in Daqing Institute of Research and Design, he entered Changchun Institute of Applied Chemistry, Chinese Academy of Sciences, and graduated with a Master Degree of Science in Physical Chemistry in July 2000. He entered Graduate School, Auburn University, in August 2000. He married Xia Wang, daughter of Liu, Xuxiu and Wang, Fagui, on December 16, 2001.

Dissertation Abstract

Electrochemical/Electrospray-Mass Spectrometric Studies of the Oxidation of Iodide and Cyanide at Gold and Platinum Electrodes as well as Gas Phase Multiply-Charged Fullerene C_{60} Anions.

Tan Guo

Doctor of Philosophy, August 15, 2005
(M.S., Changchun Institute of Applied Chemistry, Chinese Academy of Sciences 2000)
(B.E., Harbin Institute of Technology, 1991)

136 Typed Pages

Directed by Dr. Andreas Illies

In this dissertation, we introduce a new spherical thin-layer flow cell to interface electrochemistry with electrospray mass spectrometry. The successful applications of the electrochemistry with electrospray mass spectrometry are reported.

A spherical thin-layer flow electrochemical cell, which is characterized by easy access to the working electrode for cleaning and a high conversion efficiency, is developed. The cell has a relatively small dead volume from $5 - 10\,\mu$L. Calculated Reynolds (Re) numbers predict that the flow pattern around the working electrode is laminar. Both static cyclic voltammograms and hydrodynamic voltammograms at different scan rates indicate that the cell design meets the requirements of a thin layer flow cell. The multi-step oxidation of iodide and the oxidation of cyanide as well as the stepwise reduction of C_{60} were studied.

It was found that $B(C_6H_5)_4^-$ is a suitable internal standard for negative-ion studies in acetonitrile. The multi-step oxidation results of iodide demonstrate that the apparatus is capable of these very challenging electrochemistry/electrospray mass spectrometry experiments. With iodide at a platinum electrode, we observe well-behaved oxidation to tri-iodide (I_3^-). Experiments on iodide at gold electrodes are more complex, showing AuI_2^- as well as I_3^-. The AuI_2^- mass spectrometric ion intensity varies in a complex way throughout the applied electrochemical voltage range studied; we propose that this variation involves the adsorption of I^- on the gold electrode surface.

With cyanide at a platinum electrode, we observe $C_5N_5^-$, which is due to the oxidation of cyanide to cyanogen followed by the stepwise condensation of cyanogen with cyanide. At the gold working electrode, the surface oxidation of the gold to gold cyanide complex is observed. This is due to the high stability constant of the gold cyanide complex in acetonitrile.

Gas phase observation of C_{60}^-, C_{60}^{3-} and C_{60}^{4-} anions generated at platinum electrodes and detected by electrochemical/electrospray mass spectrometry is reported. The anions are electrochemically generated from solutions of C_{60} dissolved in mixtures of toluene and acetonitrile. The gas phase observation of C_{60}^{3-} and C_{60}^{4-}, despite the fact that they have negative electron affinities, is a result of a repulsive Coulombic barrier to electron loss. These studies, which demonstrate the gas phase stability of C_{60}^{3-} and C_{60}^{4-}, illustrate the promise of electrochemical/electrospray mass spectrometry for the studies of metastable anions.

Acknowledgments

The author would like to thank Dr.Illies and Dr. Cammarata for their help as well as the committee members for their time and suggestion.

The author would also like to express his deepest appreciation to his wife and his parents for their support and encouragement during the course of this dissertation.

Style manual or journal used Journal of the American Chemical Society (together with the style known as "auphd"). Bibliograpy follows van Leunen's *A Handbook for Scholars*.

Computer software used The document preparation package TEXLatex (specifically LATEX) together with the departmental style-file `auphd.sty`. Matlab 6.5, Adobe Acrobat 6.0, Microsoft Excel 2000, GSview 6.0, MassLynx DataBridge, Origin 7.0.

Table of Contents

List of Figures

List of Tables

Chapter 1

Introduction and Literature Review

1.1 Introduction

The online combination of electrochemistry and mass spectrometry (EC/MS) can be traced back as far as the 1970s. [1] A literature search reveals that research applications of EC/MS have increased greatly in recent years, although this area has never been a primary technique for either electrochemistry or mass spectrometry.

Electrospray mass spectrometry, a soft ionization method, [2] can be used to transfer ionic species that are present in the solution phase into the gas phase without significant fragmentation. This makes it possible to probe short-lived intermediates and products derived during electrochemical reactions in solution and analyze them as a function of the working electrode potential. Experiments can be carried out at close to real time by using this technique. [1, 3, 4] An electrochemical flow cell with high electrochemical conversion efficiency is an important part of the electrochemistry/electrospray mass spectrometry (EC/ES-MS) experimental apparatus. However, it has also been recognized that electrospray ionization sources act as controlled-current electrolysis cells. [5] When an electrochemical cell is coupled with an electrospray source, two problems commonly arise, namely electrochemical cell potential interference due to the high voltage at the electrospray tip and severe electrospray signal attenuation by the supporting electrolytes. [6] The objective of the present study is to develop a new electrochemical flow cell and to apply the EC/ES-MS method to several scientifically significant problems. These are briefly described below and are presented in more detail in later chapters of this dissertation.

Iodide and Cyanide at Platinum and Gold Electrodes

Early investigations of the electrochemical oxidation of the iodide-iodine system in different solvents at a platinum electrode mainly focused on the adsorption behavior of the ions and the kinetics and mechanisms of the reactions. [7–13] The adsorption behavior of iodide ions on a smooth electrode in aqueous solution was investigated by Pirtskhalava. [10] Good agreement between the experimental and theoretical polariographic characteristics of the iodide-iodine system in acetonitrile was reported by Piccaradi, [11] and the electrochemical properties of iodide in different organic solvents with a wide range of dielectric constants was reported by Iwamoto. [9] The kinetics and mechanism of electrochemical oxidation of the iodide-iodine system were investigated using a rotating platinum disk electrode by Giordano in two solvents, acetonitrile and dimethylsulphoxide (DMSO). [14] The results showed that two polarographic waves were present in the system, and the difference between the half-wave potentials of the two waves was related to the stability constant of tri-iodide ion species in the solvents.

A number of studies have discussed the electrochemistry of gold(I) and its halide complexes in both aqueous and non-aqueous solutions. [15–22] The structures of gold iodide complexes, such as AuI_2^-, AuI_4^-, were investigated by Kissner, [23] and Bard reported scanning tunneling microscopy images of iodide adsorbed on Au(111) surfaces from aqueous solutions. [18] The catalytic activity of halide ions towards the electrochemical oxidation of gold electrodes in acetonitrile has also been reported. [24] Gerischer examined the influence of water on the formation of an oxide layer on gold in acetonitrile and found that the water was a reactant both in the formation of an oxidation layer and reduction of the layer. [22]

The chemistry of gold cyanide complexes has been well studied. Early results show that a monolayer of cyanide on the gold electrode plays a role in the gold dissolution in the cyanide solution. [24–26] The formation of gold cyanide complexes is primarily the result of the high stability constant.

Cyanide oxidation has attracted considerable attention because it is a general waste treatment process to clear the contaminants in the industrial waste-water. The oxidation of cyanide gives cyanogen, which is a reactive which can participate in many reactions. [27] The mechanism of formation of $C_3N_3^-$ and $C_5N_5^-$ by reaction of cyanogen with cyanide, which depends on the mole ratios of cyanogen and cyanide, was proposed by Wiley. [28]

In this dissertation, we report our results on the electrochemistry of iodide as well as cyanide at gold and platinum electrodes using EC/ES-MS in Chapter 3.

Fullerene C_{60}.

The electron-accepting ability of C_{60} in solution has attracted much attention from chemists since it was first discovered in the 1980s. [29–34] Molecular orbital theory calculations reveal that C_{60} is a good electron acceptor and is capable of oxidation states up to negative six in solution. This is due to its triply degenerate and energetically low-lying lowest unoccupied molecular orbitals (LUMO). [35, 36] The reversible stepwise reduction of up to six electrons in C_{60} was first demonstrated by cyclic voltammetry following early molecular orbital calculations. [37] The field of gas phase chemistry involving fullerene ions and its derivatives has experienced tremendous growth during the last decade. Studies of C_{60} have provided very promising opportunities to explore exciting new areas of science. Positively multi-charged gas phase fullerene ions with charge states ranging from 4+ to 1+ have been reported. [38–40] However, observations of multiply-charged fullerene anions in the gas

phase are fairly rare. So far, only singly and doubly charged gas phase fullerene anions have been reported. [41]

In the research presented in Chapter 4 of this dissertation, multiply-charged C_{60}^{n-} (with n up to 4) anions were studied using the EC/ES-MS. We observed C_{60}^{-}, C_{60}^{3-}, C_{60}^{4-}, but the di-anion, C_{60}^{2-}, was not observed. Possible reasons for this are discussed.

1.2 Literature Review

1.2.1 Electrochemistry/Mass Spectrometry

Electrochemistry deals with the chemical action of electricity and the production of electricity by chemical reactions. [42] This field encompasses a great variety of phenomena. Electrochemical reactions are different from homogeneous chemical reactions in that the amount of products formed at the working electrode is usually comparatively small. Many electrochemical techniques, such as linear scan voltammetry, polarography, the pulse voltammetry method, and the controlled-current methods, have been devised in order to obtain thermodynamic data about electrochemical reactions, to generate products or unstable short-lived intermediates such as radicals, and to detect trace amounts of metal ions and other organic or inorganic species. [42, 43] Though electrochemistry is well established as a field, the immediate detection of electrochemical reaction products shortly after their formation on a working electrode has been a difficult task.

Mass Spectrometry (MS) is an analytical tool that is primarily concerned with the separation of molecular or atomic species according to their mass to charge ratio. [44] Because mass spectrometry is capable of providing comprehensive information on molecular masses of unknown species and short-lived intermediates directly, as well as providing clues on molecular structures, the online combination of electrochemistry and mass spectrometry holds the great promise to be a powerful new approach. The main goal is to detect electrochemical reaction products, by-products, or unstable intermediates shortly after their formation on a working electrode. The initial combination of electrochemistry and mass spectrometry can be traced back as early as the 1970s. [1]

Bruckenstein and Gadde first used an online combination of electrochemistry with mass spectrometry in order to study gaseous products of fuel cells. [1] In their work, gaseous electrochemical products were collected in a vacuum system, and then the products were analyzed by electron impact ionization. Later, Heitbaum and Wolter used a porous Teflon membrane covered by a 100 μm layer of an electrocatalyst that functioned as a working electrode as well as the interface to the mass spectrometer. [3, 45] To allow direct real time detection of volatile electrochemical reaction products or intermediates, Heitbaum and Wolter significantly improved the vacuum system by including two pumping stages. Due to the improved vacuum design, this type of electrochemical and mass spectrometric interface was capable of measuring rates of product formation. It was sensitive enough to detect desorption products corresponding to a single monolayer of adsorbed species at porous electrodes. To distinguish this technique from other methods, this method was called "Differential Electrochemical Mass Spectrometry" (DEMS).

DEMS is thus similar to membrane introduction mass spectrometry, which has been widely used to detect trace amounts of non-polar molecules in water. [46] In general, a thin, non-polar silicon or Teflon membrane is used to achieve the separation of reactants from water. The non-polar membrane has the advantage of preventing the diffusion of water into the mass spectrometer.

DEMS is ideally suitable to both the real time detection of electrochemical reaction products and the study of the adsorbates on single crystal electrodes. [47] With this method, analytes present in quantities of less than 1 nL can be easily detected. [48] When coupled with electron impact ionization mass spectrometry, DEMS can be used for quantitative measurements of electrochemical reaction rates and the electrode surface coverage. The drawback of DEMS is that only volatile products can

be detected. Later, a technique incorporating rotating disc electrodes (RDE) coupled with mass spectrometry was developed, this method allowed the study of fast electrochemical reactions. [49] Using this rotating inlet system, the transfer efficiency can be determined under controlled diffusion conditions. However, due to the difficulties in interfacing the liquid environment of electrochemistry with the gas-phase environment of mass spectrometry, the combination of these two techniques has been limited to studies of the volatile species, and has thus received little attention from chemists working either in electrochemistry or mass spectrometry.

Over the past decade, several new ionization methods, including thermospray (TS) [50–56] and electrospray (ES), [57–60] have been developed. This has made interfacing the liquid environment of electrochemistry with the gas phase in the mass spectrometer much more practicable. Hambitzer and Heitbaum [51, 52] were the first to study nonvolatile species in solution using electrochemistry coupled with thermospray ionization in the 1980s. Brajter-Toth [56] and Yost [54, 55] then expanded this technique by combining it with high performance liquid chromatography (HPLC), demonstrating a powerful new analytical method in the study of biological redox reactions.

Other approaches have been taken by other groups. For example, Bartmess and Phillips combined electrochemistry with fast atom bombardment ionization (FAB). [61] In their work, the neutral analyte species were ionized by electrochemical redox reactions on the FAB tip before sputtering the samples with a Xe atom beam. Other techniques, such as coupling electrochemistry with mass spectrometry (particle beam interface and atmospheric pressure chemical ionization (APCI)), along with variable ionization-interfaces have also been attempted. [62]

The online combination of electrochemistry with electrospray mass spectrometry (EC/ES-MS) became more common in the 1990's. [63, 64] This interface enables the detection of nonvolatile solutes. It has been proven that EC/ES-MS is a powerful technique for the direct on-line investigation of electrochemical reactions, it holds promise for studies of the mechanisms of electrochemical reactions. As revealed by a literature search, the number of reports of the online combination of electrochemistry with electrospray mass spectrometry is increasing. It is the EC/ES-MS technique that was used for the research for this dissertation. To trace the history of EC/ES-MS, it is necessary to first look at the history of electrospray and mass spectrometry.

1.2.2 Electrospray and Mass Spectrometry

The idea of using electrospray ionization as a source for generating gas-phase ions followed by mass spectrometry was first proposed by Dole in 1968. [65] In this pioneering study, electrospray ionization was used to detect polymeric species, such as polystyrenes. However, the observed gas phase ions were not themselves ionized in the solution, and this made the results suspect. Pole extended this work by proposing an electrospray ionization mechanism, the charge residue model, and this model has become important in developing new applications of electrospray. [65]

Finally, in 1984, Yamashita and Fenn [57] introduced electrospray mass spectrometry. At approximately the same time, Aleksandrov and coworkers [66] reported their independent development of electrospray mass spectrometry. Since then, the development of electrospray mass spectrometry has revolutionized the application of mass spectrometry for biochemical and pharmaceutical fields due to the fact that many biochemical systems involve ions in solution.

Electrospray ionization is unique among the mass spectrometric methods in terms of both the principles on which it is based and the instrument required to perform the experiments. It is an ionization (desolvation) technique by which ions present in solution can be transferred into the gas phase, after which the gas phase ions can be detected by mass spectrometry. Electrospray ionization results in very little fragmentation and is one of the softest ionization methods available in mass spectrometry.

The overall process involved in the production of gas phase ions by electrospray includes three major steps: [2] the production of charged droplets at the electrospray needle tip; the shrinkage of relatively large charged droplets by solvent evaporation and droplet fission; and the transfer of ions from the solution phase into the gas phase. The latter is an extremely endothermic and endoergic process. Of the three steps, only the first two are well understood.

Electrospray charged droplets are produced by pneumatic nebulization, which is shown in Figure 1.1. Usually, a metal needle with a small inner diameter (ID) (typically 0.1 mm ID and 0.2 mm OD) serves as the electrospray tip. A counter electrode is located 1 - 3 cm from the needle and a high voltage of $\pm 2.0 - 5.0$ kV is applied to the metal needle, forming a high electric field in the air at the tip of needle, $\vec{E}c = 10^6$ V/m. The sign of the potential depends on whether positive or negative ions are to be detected. When an analyte is forced through the needle, the electric field is sufficiently high to penetrate the solution, forming a double layer on the surface of the Taylor cone. This disperses the emerging solution into a very fine spray of charged droplets. These charged droplets have the same polarity as that applied to the electrospray tip. The second stage involves solvent evaporation, during which the droplets shrink and the surface charge increases. Eventually, at the Ray-

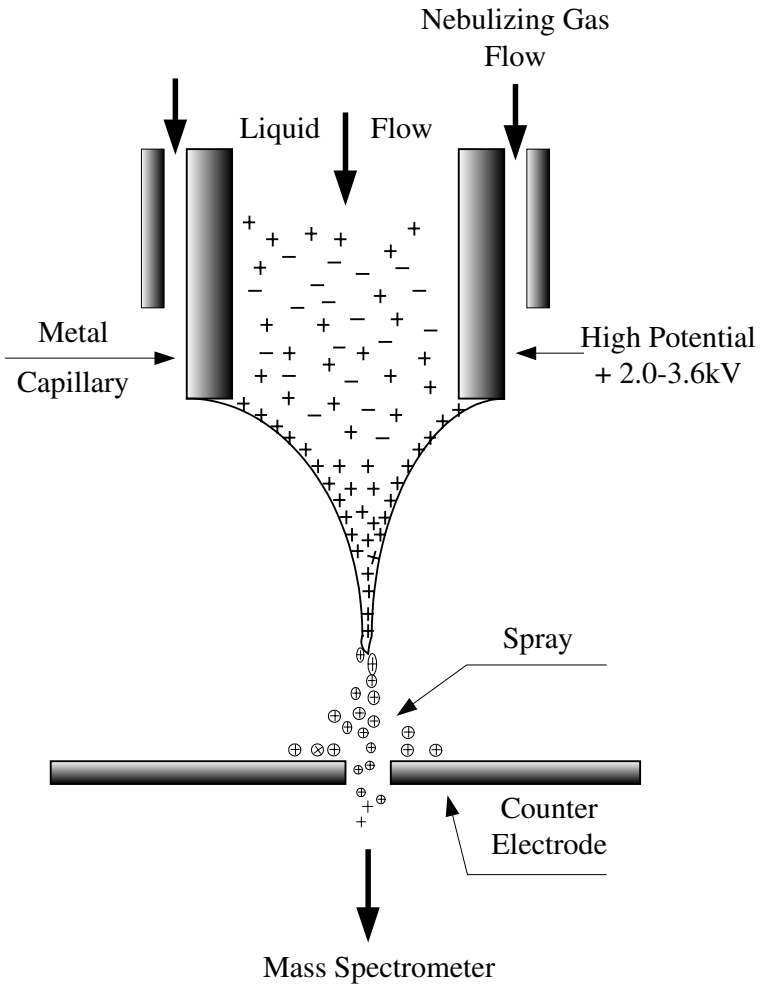

Figure 1.1: Schematic of the Electrospray Process Producing Positive Ions.The Polarity of the Applied Potential Determines the Polarity of the Ions Produced. [2]

leigh limit, equation 1.1 [67] describes how the coulombic repulsion overcomes the droplet's surface tension [68] and the droplet explodes.

$$q_{Ry} = \pi(64\gamma\varepsilon_0 R^3)^{\frac{1}{2}} \tag{1.1}$$

where γ is the surface tension; q_{Ry} is the surface charge of the droplet; R is the radius of droplet and ϵ_0 is the permittivity of vacuum.

The coulombic explosion forms a series of smaller, lower charged droplets. These are the precursors of all the gas phase ions. The first stages of the electrospray ionization process are relatively well understood. The later stages of the mechanism, however, become increasing complex and are not well understood. It is these later stages that ultimately gives rise to the gas phase ions.

Two mechanisms have been proposed to explain the final stage of the evaporation of droplets remaining near the Rayleigh limit. [67] The first is the charged residue model proposed by Dole, et al. in 1968, [65] shown in Figure 1.2. In this model, the formation of gas phase ions depends on the development of extremely small droplets, which contain only one naked analyte ion. The ions in solution are never emitted from the charged droplet's surface at any point during the whole process. Repeated solvent evaporation followed by coulombic explosions ultimately produces droplets, which contain only naked analyte ions. The formation of multiply charged ions is dependent on the neutral analyte's available surface sites and on the correct conditions being present.

A detailed consideration of, and support for, this mechanism was presented by the Röllgen [69, 70] and Kebarle groups. [2] They reported the observation of $M(MX)_n^+$

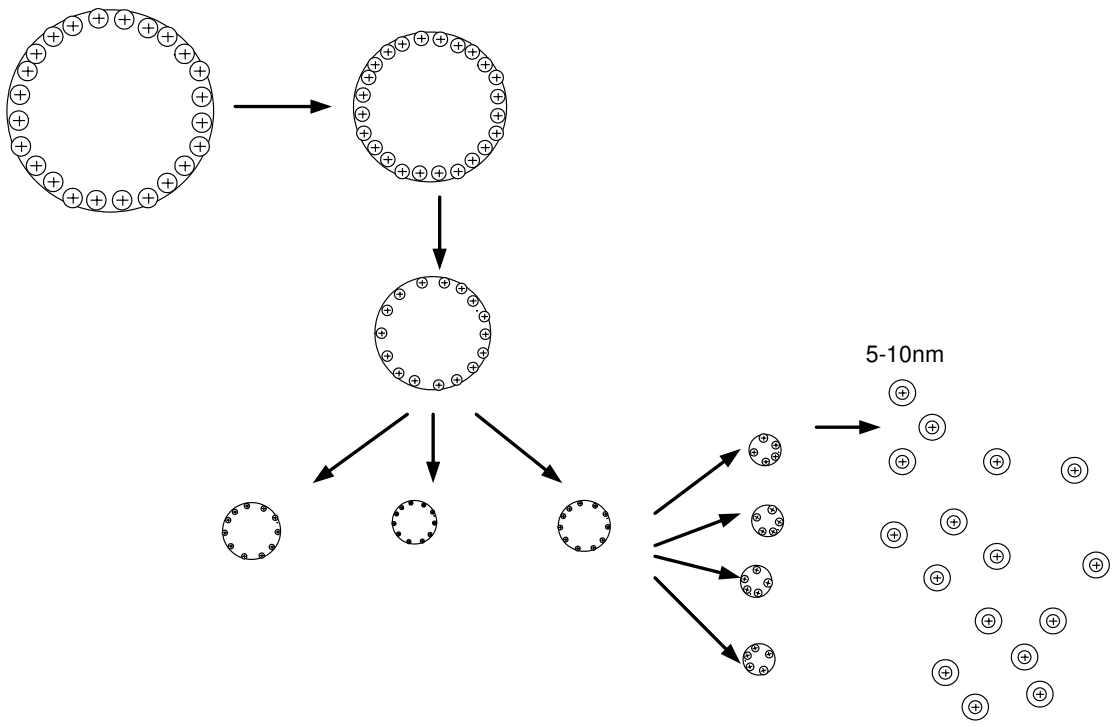

Figure 1.2: Dole, et al. Charge Residue Model. [65]

and $(MX)_nX^-$ clusters from solutions containing (NaCl, KCl, NaBr and CsCl), where the highest intensity was at n=1. These results agreed with the prediction of the charged residue model.

The second possible mechanism is the ion evaporation model, shown in Figure 1.3, proposed by Iribarne and Thomson. [59, 60] In principle, it is similar to the charge residue model at the very beginning. The formation of the charged-droplets follows the same sequence of evaporation and explosions when Rayleigh instabilities occur. However, unlike the charge residue model, Iribarne and Thomson's model argues that prior to a charged droplet reaching the ultimate stage contemplated by Dole, the electric field on the droplet surface becomes strong enough to overcome solvation, and solute ions from the droplet surface are emitted into the ambient gas. For charged droplet sizes ≤ 10 nm, the direct emission of ions from the solution thus becomes possible. The emission process is certainly dominant over the coulombic fission. Iribane and Thomson also derived equation 1.2 based on transition state theory, which can be used to predict the rate of ion evaporation from the charged small droplets.

$$k_I = \frac{K_B T}{h} e^{-\Delta G^{\ddagger}/K_B T} \tag{1.2}$$

where K_B is Boltzmann's constant, h is Planck's constant, and $\Delta G^{\ddagger}$ is the Gibbs free energy of activation.

Experimental evidence supporting the ion evaporation model was presented by Loscertales and Fernandez de la Mora, [71] who studied the electrospray mechanism by producing a monodisperse cloud of charged droplets. The mechanism was verified by measuring the charge, q, and diameter, r, of the residual particles remaining after

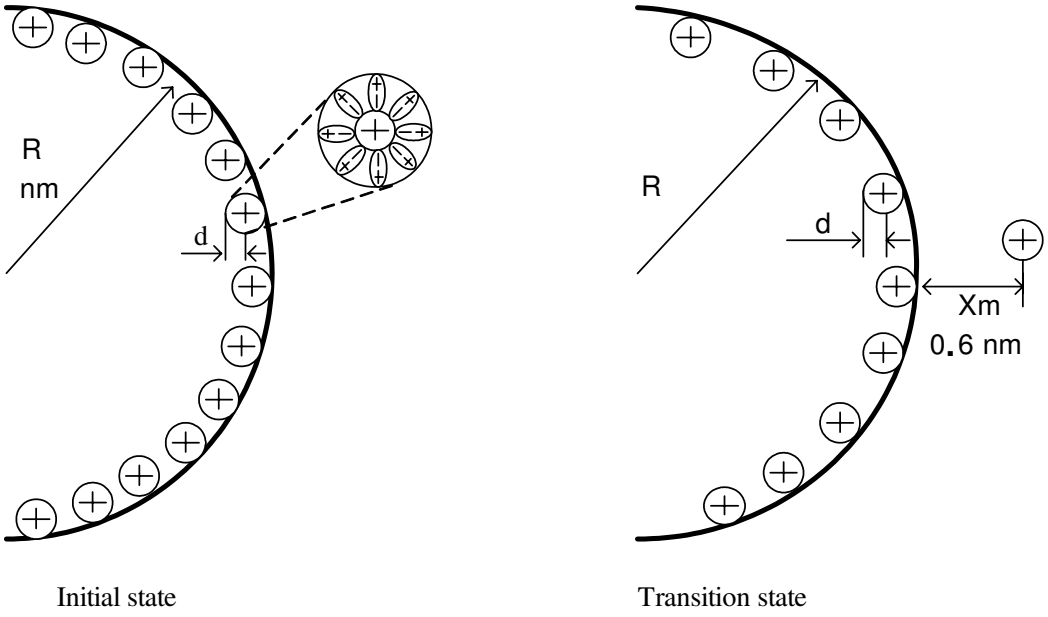

Figure 1.3: Ion Evaporation Transition State and Initial State Models. [59]

complete evaporation of the electrospray solvent. The experimental results showed that the electric field E on the surface of the droplet is independent of r when the droplets contain small monovalent dissolved ions. A consequence of this is that on a clean surface, the rate of ion ejection from a charged droplet is simply related to the rate of solvent evaporation. The measured ionization rates were well represented by the results from the ion evaporation model.

It possible that the ion formation during the electrospray process involves contributions from both solvent evaporation and ion ejection, and that the dominating process depends on the chemical and physical characteristics of the solvent.

1.2.3 Electrochemistry/Mass Spectrometry Flow Cells

Several research groups have reported successful applications of EC/ES-MS. [4, 72–78] This combination has proven to be very effective for investigating electrochemical processes. [55, 63, 79–84] The overriding strength of the method is that it promises the full characterization of the details of electrochemical reactions. In a recent paper, Permentier and Bruins reported the study of electrochemical oxidation and the cleavage of small proteins, insulin and α-lactalbumin, by EC/ES-MS. This method is also feasible for use in analyzing molecules such as tyrosine and tryptophan. These results indicated the possibility of developing a new technique with which to study enzymatic and protein digestion. [85]

A difficulty in implementing EC/ES-MS is that the electrochemical cell is operated relative to ground potential, while the electrospray tip operates at a high potential (usually $\pm 2.5 - 3.6$ kV), and current leakage may occur between the two. In addition, for experiments conducted in organic solvents, tetraalkylammonium salts,

often used as supporting electrolytes, can severely attenuate ES-MS signals; [6] hence it is often necessary to use low concentrations of supporting electrolytes.

The central part of the EC/ES-MS setup is the electrochemical cell and the analyte flow in the cell. In contrast to homogeneous chemical reactions, the amount of product generated on the working electrode surface is relatively small in an electrochemical reaction. In order to generate sufficient products at working electrodes to be detected by mass spectrometry, a flow cell must have a high electrochemical conversion efficiency, well-defined hydrodynamics, and allow easy access to the working electrode. The cell design should also take into account the optimal positions of the reference electrode, counter electrode and working electrode.

A wide range of electrochemical cell designs have been developed for electrochemistry/mass spectrometry, these are discussed below.

Flow Cells for Electrochemical/Electron Impact Mass Spectrometry

A typical electrochemical cell used in the DEMS setup is shown in Figure 1.4. [1, 45] In this method, electron impact ionization mass spectrometry is used, hence the DEMS cell is particularly suitable for studying electrochemical reactions that generate gaseous or volatile species such as CO, CO_2 and H_2. A critical part of the cell is the Teflon membrane used to separate the solution from the vacuum chamber. The membrane, typically 75 nm thick, has a nominal pore width of 20 nm and a porosity of 50%. The Teflon membrane is mechanically supported by a glass or steel frit. An electrocatalyst layer, generally platinum, is deposited onto the Teflon membrane, producing a catalyst layer with a typical thickness of $50 - 80$ nm. The hydrophobicity of the Teflon membrane stops the diffusion of aqueous solvents though the membrane, whereas dissolved volatile products and gaseous species can penetrate the pores and be detected by electron impact mass spectrometry. The critical pore

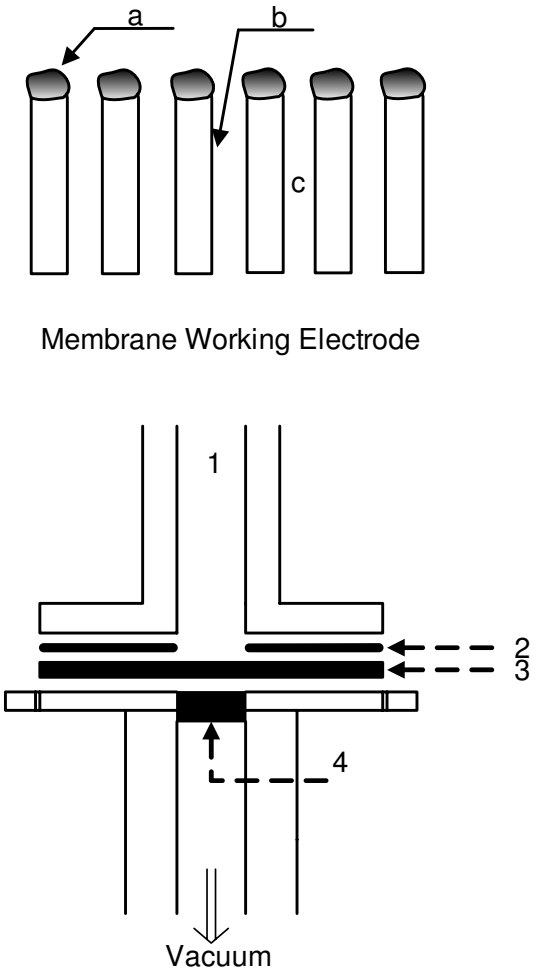

Figure 1.4: Schematic Diagram of the DEMS Cell. [45]
Top: Membrane working electrode. a, Electrocatalyst; b, Teflon-membrane and c, Pore size $\approx 0.02\ \mu m$.
Bottom: EC/MS interface. 1, Glass Body; 2, Teflon-spacer; 3, Working Electrode and 4, Steel frit.

size depends on the surface tension of the liquid and contact angle of the solution with the Teflon membrane. [1, 45] The size of the pores, calculated for water, is less than 0.8 μm. A cell with this type of working electrode has a very small dead volume. The response time of this cell for a electrochemical reaction is about 0.8 s. [48] Since the ion intensity determined by electron impact mass spectrometry is directly proportional to the incoming flow of the gas ($J_i = K^0 J_I$), rates of product formation can be measured by recording the ion current.

Tegtmeyer [49] developed a rotating porous electrode to be used as the inlet system coupled with mass spectrometry. For an approximately 100 nm thin sputtered platinum pore electrode, the transfer efficiency is greater than 0.9, this efficiency can be obtained even at high rotating speeds. [49] The diffusion layer from the macroscopic surface of the electrode to the Teflon membrane is comparable to the diffusion layer in the bulk electrolyte.

Flow Cells for Thermospray and Electrospray Mass Spectrometry

Because thermospray and electrospray interfaces can transfer the analyte into the gas phase and ionize nonvolatile species without significant fragmentation, many types of electrochemical flow cells have been coupled with thermospray or electrospray mass spectrometry. [4, 72–78] Of the many geometries possible, three are most commonly used: thin-layer, wall-jet, and tubular cells. The most widely used of these are the flow cells based on the thin-layer and wall-jet configurations, shown in Figure 1.5. [42] Here the flow channel is formed by applying pressure to a thin Teflon gasket, which results in a very small dead volume ($\sim$ 1 μL). The working electrode is embedded in a block in the cell. A high electrochemical conversion efficiency results from the thin layer of sample solution flowing parallel to the planar working electrode surface.

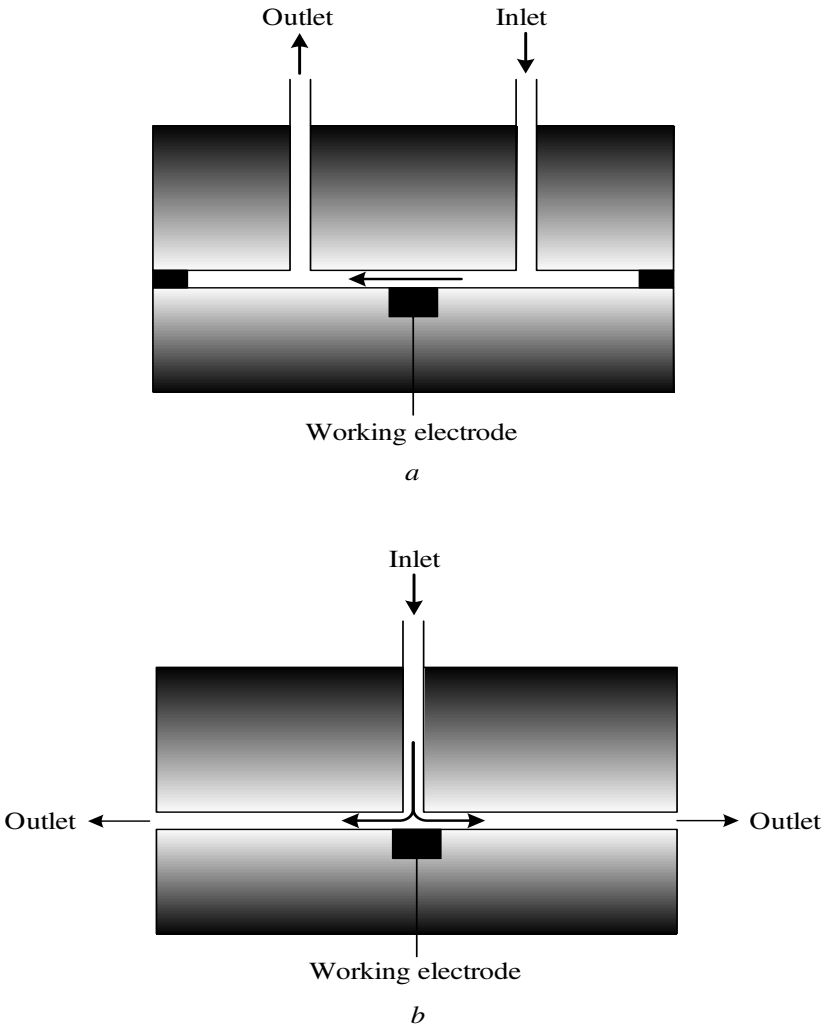

Figure 1.5: Thin-layer (a) and Wall-Jet (b) Flow cells

The design of many electrochemical flow cells available commercially are based on the thin-layer flow electrode. In order to achieve high conversion efficiency and high electrolyte flow rates, most thin-layer flow cell designs have sacrificed the separation of the counter and working electrodes. A simple two-electrode electrochemical flow cell was used both by the Bond and Van-Berkel groups. [76, 86] These EC/ES-MS setups used two metal capillaries. The connection between the electrospray mass spectrometer and the pump was made through these two metal capillaries, which also served as the working and counter electrodes.

A three-electrode flow cell without separation of working and counter electrodes was developed by Anne Brajter-Toth's group. [79,80] A porous flow-through electrode was used as the working electrode. The electrochemical process occurring on the working electrode was characterized as a complex electrochemical reaction. The cell design sacrifices the separation of counter, working, and quasi reference electrodes in order to achieve a high cell conversion efficiency and high electrolyte flow rates. A three-electrode flow cell with a 12 cm^2 reticulated vitreous carbon graphite-working electrode has also been introduced. [54, 55, 63]. The advantage of this cell design is the ease of access to the working electrode. However, the design of the thin-layer flow cell has a high ohmic loss, which results in the observation of no limiting current for ferrocyanide reduction over the whole potential range measured.

To decrease the response time of this EC/ES-MS system, Cole and coworkers placed an electrochemical cell at the very end of the tip of the electrospray nozzle. [87, 88] In this configuration, the auxiliary electrode of the electrochemical cell functions also as the electrospray tip. However, this type of setup requires the potentiostat itself to be connected to the electrodes, therefore making it subject to the high potential at the electrospray tip, $\pm 2.0 - 4.5$ kV. A similar design was adopted in ref [54],

where a stainless steel electrospray needle functioned as both the working electrode of the three electrode cell and the electrospray tip. The potential is controlled by a battery instead of a potentiostat due to the high potential at the electrospray tip.

A three-electrode thin layer flow cell without separation of working and counter electrode compartments has also been used by van Berkel and co-workers for EC/ES-MS. [4,74,76,84,90,91] This thin layer flow electrolyte was typically about 16 μm thick. [4, 84, 90, 91] Due to the small dead volume of the cell, this design was characterized by over 50% conversion efficiencies for flow rates below 50 μL/min. [4] The response time of this EC/ES-MS system was on the order of 1 s. However, a high ohmic drop in the thin layer cell caused a considerable deviation in the voltammetric response from reported data and the cyclic voltammetry measured in a conventional electrochemical cell.

Hambitzer et al. first introduced electrochemical thin layer flow cells with separation of the working and auxiliary electrode compartments using a thermospray technique as the interface to combine the electrochemistry and mass spectrometry (TSIMS). [51, 92] The separation of the individual compartments was achieved by using glass frits. This flow cell design had a smooth, metal working electrode with a relatively large surface area of about 1.5 cm^2, and flow rates through the cell were on the order of 1 mL/min. This cell design has another advantage, as it can simultaneously record voltammograms and the potential dependent abundance of products and reactants of the electrochemical reaction.

In a recent paper, Modestov and Ovadia Lev introduced a new, radial, miniature, three-electrode flow cell. [93] The cell is characterized by low resistive losses and high conversion efficiency. The three-electrode compartments were separated to prevent the counter electrode reaction by-products from entering the product stream reaching

the mass spectrometer. The authors developed a mathematical model describing and theoretically predicting the convection diffusion in the radial cell over a wide range of parameters. The performance of the cell was demonstrated by studies of dimethylaminomethyl ferrocene (DMAMF) oxidation. The mathematical model was validated using the simple single electron charge transfer reaction of DMAMF.

In chapter 2, we introduce a new spherical thin layer flow cell to interface electrochemistry with mass spectrometry.

1.2.4 Oxidation of Iodide and Cyanide at Platinum and Gold Electrodes

The oxidation behavior of iodide on platinum and gold working electrodes in non-aqueous solutions, covering a wide range of dielectric constants, has been extensively studied since the 1970s. [7–12] The kinetics and mechanisms of iodide $\rightarrow$ tri $-$ iodide in acetonitrile were studied using a rotating disk electrode from $0 - 30\,^{\circ}\mathrm{C}$. The anodic and cathodic processes showed two well-defined waves, which were related to the oxidation of iodide and tri-iodide. The limiting currents increased linearly with the square root of the rotation speed of the platinum rotating electrode at a constant solution composition. The results also showed the kinetics of the electrode reactions involving iodine-iodide couples and iodide adsorption on platinum electrodes in both dimethylsulfoxide (DMSO) and acetonitrile solutions. The formation of an adsorbed iodide film on the platinum electrode was confirmed by a Tafel plot (4RT/F). The diffusion coefficients (D_i) of iodide and tri-iodide in acetonitrile and DMSO at $20\,^{\circ}\mathrm{C}$ were determined to be 1.68×10^{-5} cm^2/s and 1.55×10^{-5} cm^2/s. [7] The rate determining step was found to be the electron transfer reaction on the platinum rotating disk electrode by evaluating the kinetic parameters of the diffusion coefficients.

The early cyclic voltammetric studies of acetonitrile solutions containing iodine and iodide and tri-iodide on platinum electrodes showed four waves, two for the anodic reactions and the other two for the cathodic reactions. [13] For solutions containing an excess of iodide, two anodic waves and only one cathodic wave were observed. The two anodic waves were related to the oxidation of iodide and tri-iodide, while the cathodic wave was due to the reduction of tri-iodide.

Formation of a iodide adsorption layer on the platinum electrode surface occurs when the iodide concentration exceeds $\sim$ 5 mM. [9] The kinetics and mechanism of formation, growth and dissolution of the iodide film were studied under both fixed potential and open circuit conditions. [9] The oxidation behavior of an iodide film on the platinum electrode was studied by a rotating ring disk electrode. [9] A hydrodynamic modulation was used to study the oxidation behaviors under potentiostatic steady state conditions at a constant rotation speed. The experimental results showed that the disk current was controlled by the mass transport coupled with the equilibrium of the iodide-iodine couple. The thickness of the adsorbed iodide film depended on the flux of iodide at the film-solution interface. A consideration of the diffusion coefficient of iodide indicated that the iodide transport through the film followed the Grotthuss chain transfer mechanism. Further calculations indicated that the iodide film relaxation processes were slower than the relaxation of the diffusion layer.

A number of studies have discussed the detailed mechanisms of the initial stages of the electro-oxidation of gold. [16–20, 23] The absorption of anions, such as halides or oxyanions ClO_4^-, are known to play a major role in the initial stages of oxidation of gold.

Oxidation of gold can be catalyzed by halides in acetonitrile. [23] The reaction can be inhibited by traces of water. Experimental results have shown that the gold

electrode surface may be covered by a mono-ionic halide layer in the presence of even a small amount of halide. The catalytic effect of halide in acetonitrile increases in the order of coordinating ligands ($Cl^- < Br^- \ll I^-$). A positive potential at the gold electrode can promote a strong halide adsorption. [19, 20, 23]

It is well known [27] that cyanide can be oxidized by numerous chemical reactions. Previous results show that the electrochemical oxidation of cyanide in aqueous solution gives cyanogens. [94] Tri-cyanide is the most easily made pseudo-halogens. A pseudo-halogen is similar to the halogens in their physical and chemical properties. [95] A well-known reaction of cyanogens is the nucleophilic addition. [27] The possible mechanism of stepwise formation of $C_3N_3^-$, $C_5N_5^-$ and $C_7N_7^-$ was proposed. [28]. Although $C_3N_3^-$ was proposed as a pseudo-halogen ion, the structure of $C_3N_3^-$ can not be treated as the linear structure as of the tri-halogen ions. [96] This is because a linear $C_3N_3^-$ results in a very unstable structure which requires the centrally located nitrogen atom to have a positive charge. The studies of the formation of $C_5N_5^-$ and $C_7N_7^-$ in the non-aqueous solution suggested that the addition processes involved a two stepwise cyanogens condensation with cyanide. [28]

In Chapter 3, we will study the oxidation behavior of iodide and tri-iodide as well as cyanide at platinum and gold working electrodes using the EC/ES-MS method.

1.2.5 Fullerene C_{60}

It was first discovered that vaporization of graphite by laser irradiation produced stable C_{60} and C_{70} clusters in 1985. [97] These clusters, known as fullerenes, have attracted significant attention from scientists in chemistry, physics and material sciences. This widespread interest in fullerenes is due, in part, to their chemical

properties. [98,99] One of the most characteristic chemical properties of C_{60} is its unusual ability to accommodate negative charges. The structure of C_{60} is described as a truncated icosahedron composed of 32 faces, of which 12 are pentagonal and 20 are hexagonal. [35] The closed-shell configuration consists of 60 π-electrons in 30 bonding molecular orbitals. Early theoretical molecular orbital calculations predicted that C_{60} would have three low-lying degenerate unoccupied molecular orbitals (LUMO) at the T_1u level, 2 eV above the highest occupied molecular orbitals (HOMO) H_u. Figure 1.6 shows a potential energy diagram for the orbitals. This electron configuration makes C_{60} a good stepwise electron acceptor for up to six electrons. [36,100,101]

Electrochemical Generation of C_{60} Ions in the Solution Phase.

Shortly after the advent of the technique of producing gram quantities of pure buckminsterfullerene (C_{60}), attempts to confirm the theoretical predictions of C_{60} electron accepting ability were begun. [102–105] The methods commonly used for the generation and study of C_{60} multi-charged anions in solution phase include: cyclic voltammetry (CV), ultraviolet or visible light (UV) absorption, electron paramagnetic resonance (EPR) and nuclear magnetic resonance (NMR). A literature search reveals that the most significant discoveries about C_{60} multi-charged anions in solution phase have been the result of finding the right cyclic voltammetric conditions, including the cell temperature, the solvent, the working electrode material, the scan rate and the supporting electrolyte. [37]

However, between 1990 and 1991, CV experiments recorded only five reversible reduction peaks of C_{60}. This is because of the limitations of the solvent potential window. In 1992, three groups [104,106,107] reported the detection of the reversible

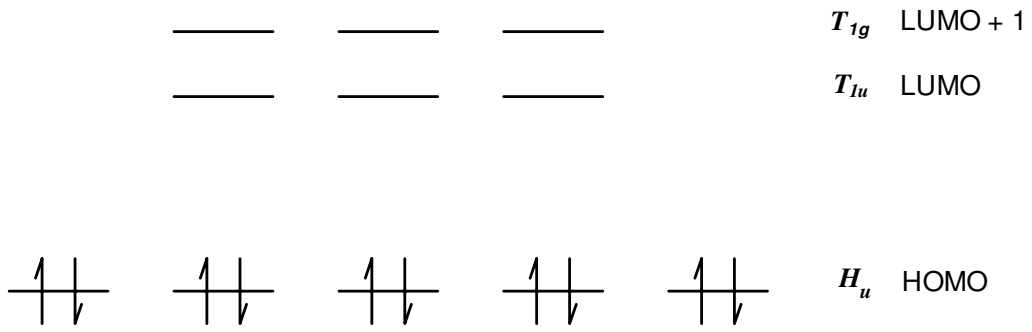

Figure 1.6: Three Low-Lying Degenerate Lowest Unoccupied Molecular Orbitals of C_{60}. [36]

stepwise addition of six electrons to C_{60} by cyclic voltammogram in solution phase. Qie's group recorded the six successive, reversible reduction peaks using CV and differential pulse voltammetry in a mixed-solvent system at -10 °C. The solvent system consisted of toluene and acetonitrile in a 5 to 1 volume ratio. The potential separation between two consecutive peaks was almost constant, at 450 ± 50 mV. This is consistent with the earlier theoretical predictions. [107]

Given the well-defined, distinct reduction potentials of fullerenes, it is natural that classical electrochemical methods, such as controlled potential bulk electrolysis and potential sweeps, are widely used to generate C_{60}^{n-} $(n = 1 - 6)$. [102]

C_{60}^{n-} $(n = 1 - 3)$ ions were electrochemically generated by square wave voltamogram, then EPR was used to study the anions. [108, 109] The results showed that a dynamic Jahn-Teller distortion is operative in all three anions.

Electrosynthesis and electrodoping of ${C_{60}}^{n-}$ $(n = 1 - 3)$ films were studied using an electrochemical quartz crystal microbalance in acetonitrile solution. [110] The results indicated that C_{60} films could be electrodoped with Bu_4N^+ cations from solution upon electroreduction at appropriate potentials. [110]

Fullerides and fullerene cations have electronic absorptions throughout the visible and ultraviolet spectral regions. The C_{60}^{n-} $(n = 1 - 5)$ ions have distinctive near-infrared (NIR) spectra, as reported by Lawson, [111] Heath and coworkers, [112, 113] and Baumgarten and coworkers. [31]

In a recent paper, Bruno and coworkers reported the first electrochemical reversible generation of ${C_{60}}^{2+}$ and ${C_{60}}^{3+}$ ions in ultra-dry dichloromethane (DCM) solutions. [114] The experiments were carried out using supporting electrolytes containing low nucleophilic and high oxidation resistant counteranions, such as $[Bu_4N]AsF_6$. These were used because of their high electrochemical oxidation potential (as high

as 4.7 V vs SCE). [115–117] The CV curve they recorded showed two reversible one-electron oxidation peaks, at the $E_{1/2}$ = 1.27 and 1.71 V (*vs.* Fc^+/Fc), that were attributed to the oxidations of C_{60} to $C_{60}{}^+$ and $C_{60}{}^{2+}$, respectively.

Chemical Generation of Fullerides

Given the fact that nearly 450 mV separates the stepwise reductions of C_{60}, an alternative method for generating C_{60}^{n-} anions is to use chemical reducing agents that are specific for a desired reduction rate and state. In this manner, a careful stoichiometric control of strong reducing agents is usually required in order to produce soluble C_{60} anions or salts, because the solvents that dissolve C_{60} and its anions often do not dissolve the C_{60} salts. [118, 119]

Due to the powerful reducing abilities of alkali metals (Li, Na, K, Rb, Cs), they have been successfully used in organic solutions or liquid ammonia to chemically generate $C_{60}{}^{n-}$ (n up to 5) anions. [120, 121] However, this method requires an *in situ* monitoring of the reduction state to stop the reduction at the level of reaction desired. Successful generation of $C_{60}{}^{n-}$ (n up to 6) anions using this method is reported. [122, 123],

C_{60}^{n-} anions were produced by simply sonicating a C_{60} solution in the presence of an excess of lithium, sodium metal or potassium naphthalide. The -3 state of C_{60} was generated by a sonication of C_{60} tetramethylethylenediamine solution with an excess of potassium. [121–124] Alkali metals are active and difficult to handle, but reducing agents of complexants, such as crown ethers or cryptands, are relatively inert and easier to handle, so they provide an attractive alternative choice for reducing C_{60}. [125]

A complexed alkali metal is usually characterized by a low solubility in the solvents into which C_{60} anions dissolve, thus crystallization of the salt in the solution is easily accomplished, and further reductions can be halted by separating the products from the excess of alkali. Using this method, $Na(dibenzo-18-crown-6)^{+}$ salts of ${C_{60}}^{n-}$ for n (1, 2, and 3) were successfully isolated from THF solutions. [126–128] The highest charged fulleride anion so far isolated using this method is ${C_{60}}^{4-}$. The complexant 2.2.2-cryptand was used as the reducing agent. [129]

Generation of C_{60}^{n-} $(n = 1-6)$ using alkali metals is superior to using electrochemical methods for some purposes, because no supporting electrolytes are needed during the reduction. The drawback is that it is difficult to control the stoichiometry, and products must be quickly isolated from the excess of alkali metal in order to avoid over-reduction.

An ingenious way to control the stoichiometry and monitor the C_{60} reduction state is to use an electron carrier to control the electron transfer. [130] In this method, the desired level of C_{60} reduction can be determined by the added carrier molecules. By using cryptand as an electron carrier without sonication, ${C_{60}}^{n-}$ (n=4) anions have been successfully generated with an excess of alkali metal in THF. [123] Huang and coworkers reported the generation of ${C_{60}}^{n-}$ $(n = 1-3)$ salts using an electron carrier, 1-methylnaphthalene, as well as stoichiometric control of alkali metal. [123–125]

Other attempts to generate C_{60} [130] have made use of the coordination and organometallic compounds, such as Cr(TPP) (tetraphenylporphyrinato) and cobaltocene, as reducing agents. These compounds have precisely defined redox potentials, which makes them well-suited as reducing agents for the generation of fullerenes anions. [130–134] Schmelzeisn-Redeker et al. [70] reported generation of ${C_{60}}^{n-}$(n=1) salt by treatment of $[Cr(TPP)(THF)_2]$ with C_{60} in toluene/THF solvent mixture.

The redox potential can be shifted into the appropriate range by adding THF, and the Cr(III) can be stabilized via coordination.

Observation of C_{60} Ions in Gas phase

Gas Phase C_{60} Cations. Studies of gas phase fullerene C_{60} cations by using the mass spectrometry have been a major subject of research of C_{60} in the last decade. Ionization of gas phase neutral C_{60} has been accomplished by various methods such as electron impact, [39] collisions with fast atoms, [136, 137] neutral particles, [138] ions with high charge states as well as cluster ions, [139] photons with energies up to 340 eV, and surface collision [140]. It was found that C_{60} needs to capture at least 45 eV of energy in order to allow the ionization and subsequent dissociation of C_2 loss. [38]

Much of experimental work of the electron-fullerene interaction has been devoted to the study of the formation of singly and multi-charged C_{60} cations. Märk and coworkers [141] reported the first measurements of cross-section functions for the production of the various parent C_{60}^{z+} and the most abundant fragment ions C_{60} by single electron collision. The electron energies range from threshold to up to 1000 eV. A crossed-beam apparatus was used in order to achieve the accurate determination of partial ionization cross-sections. The results show both an unusually large parent ion cross section and irregularities in the production of multiply charged parent and fragment ions.

The electron-impact induced fragmentation of fullerene was also studied by Salzborn group. [39] The results show that two different processes dominate the cross section for the loss of C_2 fragment. At low electron energies, the electron-fullerene interaction leads to the direct excitation of the fullerene. When the electron energies are greater

than 100 eV, the dissociation of the fullerene is due to an unsuccessful ionization. It is the higher energy part of the cross section that shows a dependence on the charge state, q, of the precursor ion.

The dissociation of fullerene ions C_{60}^{z+} (z=1,2,3,4) upon the excitation undergoes a series of C_2 losses, equation (1.3), only even-numbered fragment of ions are observed.

$$C_{60}^{z+} \longrightarrow C_{60-2m}^{z+} + C_{2m} \tag{1.3}$$

There are three different cooling mechanisms proposed for the excited fullerene cations, i.e. radiative cooling, [142] the release of neutral or charged particles, [143, 144] and the evaporation of electrons. [145]

Gas Phase C_{60} Anions. Multiply charged fullerene anions (C_{60}) are very common in condensed phases, and their existence and stability have been proven, but their observation in the gas phase has been problematic. $C_{60}{}^{-}$ is readily detected in negative ion mass spectrometry, [31, 146–149] however, like other multiply-charged anions (MCAs), reports of observations of gas phase multiply charged fullerene anions are fairly rare.

Gas phase C_{60}^{2-} and C_{70}^{2-} [150, 151] have been observed by Fourier transform mass spectrometry. In this method, a probe with a fullerene film coated tip was placed in the source chamber of a Fourier transform/ion cyclotron resonance (ICR) mass spectrometer. A laser was used to desorb the C_{60} film. In order to distinguish the signal of the second harmonic of the monoanion C_{60}^{-} from the signal of the dianion C_{60}^{2-}, C_{60}^{-} was selectively ejected from the ion trap by single-frequency resonant irradiation at the ICR orbital frequency of C_{60}^{-}. [150] At a backgroud pressure of 10^{-5} Pa, the

lifetime of C_{60}^{2-} is about 10^{-2} second. The observed abundance ratios of M^{2-}/M^{-} are between 0.02-0.20. [150]

An attempt was also made to generate gas phase C_{60}^{2-} by attaching two successive electrons to the fullerene neutral in the gas phase. [150] In this method, C_{60} was thermally desorbed to interact as a vapor with a low-energy electron beam. [150] Only C_{60}^{-} was obtained, so attachment of a second electron to C_{60}^{2-} was unsuccessful in this method. Thus, this proves that the laser desorption technique ejects C_{60}^{-} and C_{60}^{2-} directly from the metal surface. [150] Dianionic adducts of C_{60} with $F_{47,48}$ [152] and $(CN)_{2,4,6}$ [41] attached are also observed.

A literature search reveals that the observation of gas phase C_{60}^{n-} ($n > 2$) to date has not yet been reported. A consideration of the electron affinities (EAs) of C_{60} provides a simple rationale for this fact. [153] The EA of C_{60} is 2.65 eV, [154] whereas the pseudo-potential calculations indicate the second EA of C_{60}^{-} is in the range of 0.1-0.4 eV. [150] The fact that ${C_{60}}^{2-}$ is only observed under extremely energetic conditions, while dianions of higher fullerenes are much more common in negative ion spectrometry, has been attributed to the more positive EAs for the larger molecules and the ability of the larger fullerenes to mitigate coulombic repulsion. [155, 156]

In Chapter 4, C_{60} reduction is studied by using the EC/ES-MS technique. Gas phase observation of C_{60}^{-}, C_{60}^{3-} and C_{60}^{4-} anions generated at platinum electrodes and detected by electrochemistry/electrospray mass spectrometry is reported.

Chapter 2

Cell Design for Electrochemistry Electrospray Mass Spectrometry

Abstract

In this chapter, we introduce a new spherical thin layer flow cell with a relatively small volume, experimental conditions suitable for electrochemistry electrospray mass spectrometry using the cell are also described. The flow pattern through the cell is estimated by calculating the Reynolds (Re) number. The cell is characterized by easy access to the working electrode for cleaning and a high electrochemical conversion efficiency. The performance of the spherical thin-layer flow cell is demonstrated in this chapter by off-line electrochemistry.

2.1 Introduction

One of the major advantages of the combination of electrochemistry electrospray mass spectrometry (EC/ES-MS) is to simultaneously record the voltammetric and mass spectrometric responses, thus mechanisms of electrochemical reactions can be probed by this method. In order to successfully achieve this goal, a good design for an electrochemical flow cell is necessary.

Various home-built and commercial flow cells, which are based on thin-layer flow electrodes, have been coupled with electrospray mass spectrometry to study different types of electrochemical reactions under a variety of conditions. [4, 74, 75, 77, 79, 80, 85, 91] A challenge of designing a flow cell is to provide easy access to the working electrode for cleaning, thus meeting the requirements for different electrochemical reactions. At the same time the cell should have a small dead volume and a predictable

electron conversion efficiency. A good flow cell design also should fulfill the transition from a qualitative description of the composition of cell effluent to quantitative analysis.

No matter what the purpose of the cell, when designing a new flow cell, some criteria should be considered for optimizing the cell design: the design and construction of a electrochemical flow cell should meet the basic requirements of the desired level of precision required for the electrochemical measurements, optimum electrode geometry, the chemical reactivity of the system, the working temperature of the system and the scale of the system. The cell material also should be resistant to chemical attack of the solution loaded in the cell and it should be reasonable easy to change solutions and to clean the cell between the measurements.

When a thin-layer flow cell is coupled with electrospray mass spectrometry, the following additional criteria should be considered in order to meet the special challenges posed by EC/ES-MS studies.

1. The degree of conversion of the analyte in the cell should be easily estimated or calculated.

2. The cell should be connected to the electrospray source by a "bridging" line which enables fast substance transfer and protection of the electrochemical equipment from current leaks from the electrospray needle.

3. The reference and counter electrodes should be separated from the working electrode to prevent the mixing of products of the reactions in the two compartments.

4. Since electrospray ionization sources have been recognized as controlled-current electrolytic cells, [72, 75, 157–160] operation of the electrostatic sprayer necessitates passage of currents in the test liquid. The interference of these currents on the liquid sample composition needs to be minimized relative to effect of electrochemical flow cell.

2.2 A New Electrochemical Flow Cell, Construction and Operation Details

Part of the work presented in this dissertation was to develop a new low-cost electrochemical flow cell with a predictable conversion efficiency. In order to make the new flow cell configuration meet the special challenges posed by EC/ES-MS studies, our first concern was to build an easy access working electrode for cleaning which could meet the requirements for the various electrochemical reactions to be studied. This goal was achieved by using high purity gold or platinum balls as the working electrode.

The working electrodes were made from gold (99.9999%) or platinum (99.9999%) wires (1 mm OD). The gold or platinum working electrodes themselves were fabricated by melting a $\sim$ 2 mm diameter ball in a reducing H_2/O_2 flame at one end of the wire. Then the gold or platinum ball was annealed in the H_2/O_2 reducing flame for 30 mins prior to use. A freshly annealed electrode was always used for all off-line and on-line electrochemical experiments. The annealed electrodes have polycrystalline surfaces with surface areas between 0.124 and 0.264 cm^2. The surface areas were measured by the reduction of $K_3[Fe(CN)_6]$ in aqueous solution. Teflon heat shrink tube was used to seal the reminder of the gold/platinum wire, allowing only the ball-shaped electrode to be exposed to the solution.

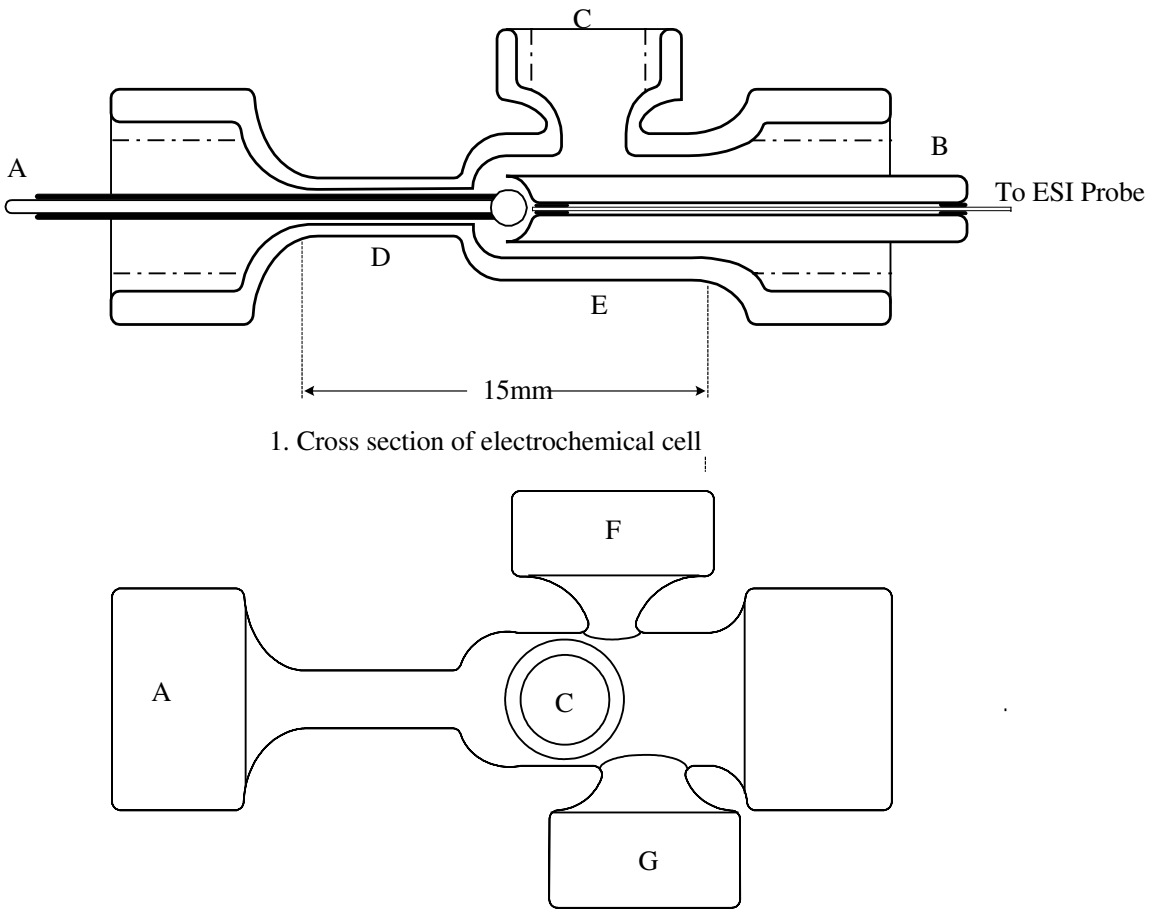

Figure 2.1: Schematic of the Electrochemical Flow Cell

The design of the electrochemical cell is shown in Figure 2.1. A schematic diagram of the electrochemical working electrode and ion collection region are shown in the top of Figure 2.1. The flow cell body is made from a Pyrex glass tube with two coaxial cylindrical chambers, D and E. Chamber D (ID 2.5 mm) is for the working electrode inlet, and E with a larger ID (4 mm) is for a cup-shaped glass tube outlet. The working electrode is placed at one end and the cupped collection assembly leading to the mass spectrometer at the other end. The collection assembly is composed of a fused silica capillary and a convex thick-walled Pyrex capillary tube. A and B show the placement of the working electrode, the cupped collection assembly and the flow around the working electrode into the capillary.

A 800-900 mm long untreated silica capillary (ID 0.1 mm, Supelco) was used to connect the electrochemical flow cell and electrospray probe. The assembly, B in Figure 2.1, is composed of a fused silica capillary, which is glued into a convex thick-walled Pyrex capillary tube using 24-hour-cure Torr Seal (Varian). This epoxy prevented leaks and solvent attack against the glue. The advantage of using a 800 - 900 mm long untreated silica capillary (ID 0.1 mm) as a duct line connecting the electrochemical flow cell and the electrospray probe is that the silica capillary electrically isolates the electrochemical cell from the electrospray tip potential, this results in a reduction of current leaks from the electrospray needle.

A Swagelok fitting and Teflon tube (ID 0.25 mm) was used to connect the silica capillary to a homemade electrospray probe. The design of homemade probe is based on the Micromass factory-built electrospray probe. All other connections were made either by O-rings or Supelco septa (Diameter 11 mm).

Two types of home-made reference electrodes were used, aqueous (Ag/AgCl) and nonaqueous (Ag/Ag^{+}). The choice depended on the experimental conditions and the

requirements for the desired level of precision of the electrochemical measurements. The reference electrode was placed over the working electrode upstream of the working electrode (Figure 2.1, part C). To separate the reference electrode from the working electrode, the reference electrode was connected to the working electrode chamber using a double salt bridge with a fine Vycor glass frit. The entire electrochemical cell was maintained at room temperature.

A Cole Palmer Series 74900 syringe pump with a flow rate of 1.0 mL/hr was used to provide the constant mobile phase and produce the spray. The syringe pump was connected to the cell by a Teflon tube (0.25 mm ID) with a Swagelok fitting.

The cell volume is determined by the cup-shape collector (Figure 2.1 part B). A well made "cup" has a volume of 5 - 10 μL. The gold or platinum ball, serving as a working electrode, was placed into the center of the "cup" without touching the inner wall of the "cup". The "cup" functions as the collector, which collects the products generated at the surface of the working electrode. The flowing solution between the spherical working electrode surface and the inner wall of the "cup" serves as a spherical flow thin-layer, and the products formed on the electrode surface are guided into the 800 mm untreated silica capillary to the electrospray probe. In this configuration, the cell dead volume of the spherical flow cell can be limited to a relatively small volume, thus meeting the requirements posed by the EC/ES-MS experiments.

A piece of platinum mesh, used as counter electrode, was connected directly to the working electrode compartment. This configuration maintains a small cell volume and at same time provides reasonably easy assembly of the electrochemical cell. In order to isolate possible counter electrode reactions from the flow stream into the electrospray source, the counter electrode was placed outside the cup-shaped

collector and upstream from the working electrode. A drawback of this configuration, however, is that an uneven current distribution could develop.

The electrochemical cell body was always cleaned using a solution mixtures of sulfuric acid (98%) and H_2O_2 (30%) (piranha solution) [161] and dried in a vacuum oven at 80 °C for at least 72 hours prior to use. The working electrodes were cleaned by rinsing sequentially with distilled water, hydrofluoric acid 49%, piranha solution, [161] distilled water, HPLC grade methanol and fresh acetonitrile. The electrodes were then stored in acetonitrile in a glove bag under an argon atmosphere. The assembly of the electrochemical cell was carried out in a glove bag under argon and all solutions were degassed for at least 15 minutes with dry Grade 5.0 Ar gas before use.

2.3 Flow Pattern

Since the way solutions pass over a working electrode can greatly affect the electrochemical processes happening on the electrode surface, [162] it is important for us to understand the solution flow pattern around the spherical working electrode. To study the flow around a spherical working electrode, a Reynolds (Re) number, [163] equation(2-1),was used to estimate the various fluid properties at different velocities. The Re is defined as:

$$R_e = \frac{\rho\, v\, d}{\mu} \tag{2.1}$$

The specific values for our cell using acetonitrile are: ρ is the density of acetonitrile at 20 °C, 0.776×10^3 kg/m^3; v is the mean velocity of acetonitrile, 1.26×10^{-5} m/s - 3.44×10^{-2} m/s; d is the diameter of working electrode, 2.0×10^{-3} m and μ is the viscosity of acetonitrile, 3.5×10^{-4} kg $\cdot$ m^{-1} $\cdot$ s^{-1}

Fast flow rates can substantially decrease the residence times of the analyte in the electrospray, and reduce unwanted electrochemical reactions at the electrospray needle. [5] Fast flow rates, however, can also cause an increase in the charged droplet sizes in the electrospray, therefore affecting the transfer of solvated ions from the liquid phase to the gas phase. To maintain a high conversion efficiency, the source temperature must be adjusted to match the operating flow rate. In this dissertation, various flow rates, ranging from 1 - 5 mL/hr, were used to meet the requirements of the various electrochemical reactions studied.

For mathematical simplicity, the electrolyte flow in the cell is assumed to be a fluid passing a sphere. [163] The electrolyte has the slowest flow rate when it is flowing through the upstream part of the spherical electrode. As the velocity of electrolyte is increased, the cross section area is decreased when solution passes the spherical thin-layer channel. The velocity reaches a maximum of 3.44×10^{-2} m/s at the entrance of the silica capillary where the smallest cross section area, (7.85×10^{-4} mm^2), is encountered.

Based upon above analysis, the calculated Re number is less than 1, we, thus, assume fully developed laminar flow [163] when the electrolyte is flowing through the spherical thin-layer channel as shown in the top part of Figure 2.2.

If a fluid with a sufficient high flow rate passing through the cell, the Re number is high (> 10), and then a weak turbulence could develop in the downstream part of the working electrode, [163] shown in bottom of Figure 2.2. In this case, products formed on the working electrode surface could react further on the electrode surface due to the turbulence. Nevertheless, a laminar flow is developed at a flow rate of 1 mL/hr, which is the most often used flow rate in this dissertation.

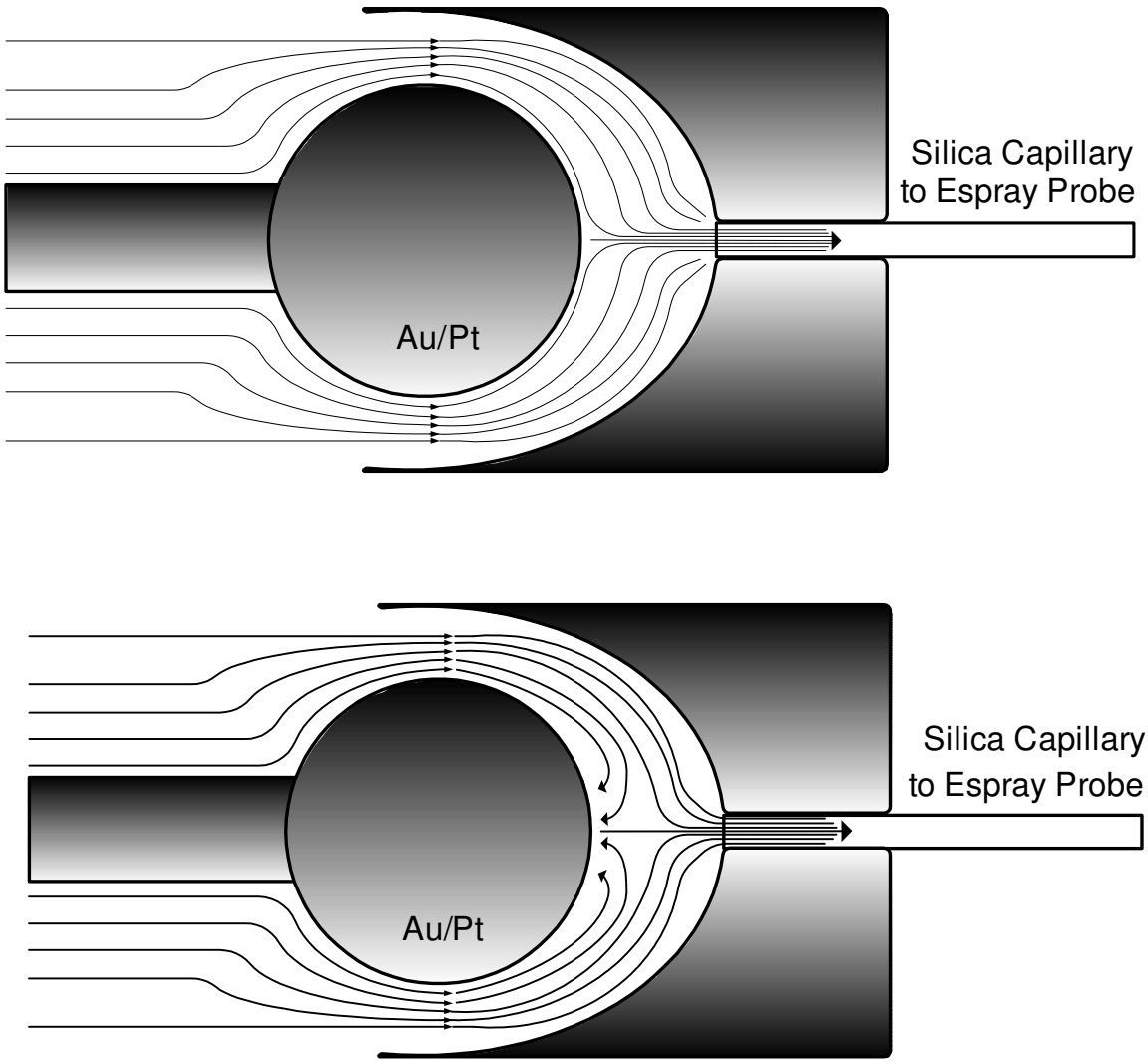

Figure 2.2: Flow Pattern Around the Working Electrode

2.4 EC/ES-MS Experimental Conditions

Solvents Used. In classical electrochemical measurements, the choice of solvent is determined by the electrochemical system to be studied. Non-aqueous solvents usually offer a wider usable potential range. These solvents include the aprotic solvents, such as: dimethylformamide, dimethyl sulfoxide, dichlorobenzene, trichloromethane, propylene carbonate and acetonitrile. [43] These solvents have the tendency of simplifying the electrochemical reactions and they have the ability to stabilize radicals or other intermediates produced during electron transfer process. [43] When choosing a suitable solvent, some important criteria, such as the voltage limits, dielectric constant, dipole moment, protic character, and solubility of reactants and product must be considered.

The most important of these properties are the voltage limits and dielectric constant of the solvent. The voltage limits define the accessible potential range available for the electrochemical oxidation or reduction process. A large dielectric constant, in general, promotes the dissociation of ionic solutes, thus decreasing the cell resistance. Since electrolytic conductivity is always necessary, a dielectric constant value larger than 10 is usually necessary to avoid experimental difficulties. [43] A low cell resistance minimizes the iR drop resulting in a better electrode potential measurements.

EC/ES-MS, however, imposes more restrictions on the solvents than conventional electrochemical experiments. Of most concern is how the solvent used in the electrochemical system affects the electrospray process, such as the formation of charged-droplets and the transfer of solvated ions into gas phase. Surface tension is also an important factor because it determines the charged droplet sizes that remain near the Rayleigh instability range, equation (1-1).

Experimental results show that the electrospray current is a function of the conductivity σ of the solution, equation (2-2). [6]

$$I = H\sigma^n \tag{2.2}$$

where: $n = 0.2 - 0.4$, σ is the conductivity of solution and H is a constant.
The dielectric constant is not directly related to the ion transfer process from the solution phase to the gas phase, but it can affect the conductivity of the solution which is related to the formation of charged-droplets. Other physical properties of the solvents, such as the boiling point, are not directly related to the transfer of ions from the charged-droplets to the gas phase, but a solution with high boiling point could affect the sizes of charged-droplets at the operating source temperature.

In this dissertation, the most often used solvents are acetonitrile and acetonitrile/toluene mixtures. Acetonitrile is a relatively inert solvent, and is resistant to both oxidation and reduction. It, also, is an excellent solvent for many compounds. Its dielectric constant of 37 allows good conductivity, minimizing the iR drop in the electrochemical cells. [43] Standard procedures are available to easily dry and purify acetonitrile and dissolved oxygen can easily be removed by simply bubbling a dry clean inert gas, such as Ar, N_2, through the solvent. [164]

Supporting Electrolytes. Since most organic solvents used for studying electrochemical reactions are nonconductors, it is necessary to add inert soluble supporting electrolytes to the solutions. A concentration of 0.1 M is often used. [43] There are several ways in which the supporting electrolyte affects the solvent medium. The primary function is to regulate the cell resistance and mass transport by electrical migration. It also may determine the structure of the double layer, and be involved in

the formation of ion-pairs with the electroactive species. The supporting electrolyte may also limit the potential window due to its redox properties. The most often used supporting electrolytes in aprotic solvents are the tetraalkylammonium salts such as, $[Et_4N]ClO_4$, $[Et_4N]BF_4$, $[Et_4N]ClO_4$, $[n-Bu_4N]BF_4$. [42, 43, 165, 166]

A high concentration of supporting electrolyte must, however, be avoided when studying an electrochemical reaction using the EC/ES-MS technique. The tetraalkylammonium salts are soluble in many aprotic solvents, and are resistant to oxidation and reduction, but these ions usually have high surface activities compared with the analytes. Hence, they tend to form clusters in gas phase during the electrospray process. Formation of clusters suppresses and changes mass spectrometric signals. In addition, a solution with a high concentration of supporting electrolyte can act as a conductor between the electrochemical cell and the high potential electrospray needle. This causes potential voltage floating of the electrochemical cell as well as significant current leakage from the electrospray needle. Another reason for avoiding a high concentration of supporting electrolyte in EC/ES-MS is because a high concentration of supporting electrolyte can significantly suppress mass spectrometric signals of the analytes. [6]

2.5 Off-line Electrochemical Characterization of the Cell

The performance of the spherical thin-layer flow cell was characterized by off-line static and hydrodynamic cyclic voltammograms of the rapid one electron reversible reaction, $[Fe(CN)_6]^{3-/4-}$, using solvents and electrolytes applicable to EC/ES-MS.

Solvents and Chemicals. Electrochemical grade potassium hexacyanoferrate ($K_3[Fe(CN)_6], 99\%$) was purchased from Fluka (St. Louis, MO), and potassium chloride (KCl) was obtained from Aldrich Chem. Co. All chemicals were used as received.

Aqueous solutions of 1 mM $K_3[Fe(CN)_6]$ were prepared in 0.1 M KCl. Deionized water with a measured resistance of 18.6 MΩ was used to make all the aqueous solutions.

Electrochemical Methods. A Model BAS Epslion-EC potentiostat with data system version 1.31.65NT and firmware version 1.30a (Bioanalytical Systems Inc.) were used for off-line EC/ES-MS experiments. A platinum-mesh electrode was used as the counter electrode. A Ag/AgCl reference electrode was connected to the cell through a double salt bridge. All potentials are quoted versus aqueous Ag/AgCl and all the measurements were done twice. Origin version 7.0 (Microcal Software, Inc.) was used to plot the Nernstian curves and linear-fits.

Measurements of the Gold Electrode Surface Areas. In order to be qualitative about the electrochemical measurements, it is important to know the working electrode surface areas. The gold working electrode surface areas were measured by using an electrochemical method, linear sweep voltammetry. [42] A fast one electron reversible redox reaction, was used to produce cathodic and anodic peaks, equation (2.3), [167].

$$[Fe(CN)_6]^{3-} + e^- \rightleftharpoons [Fe(CN)_6]^{4-} \tag{2.3}$$

Figure 2.3 shows a typical cyclic voltammogram of 1 mM $[Fe(CN)_6]^{3-}$ at a gold electrode in a 0.1 M KCl aqueous solution. The separation of anodic and cathodic peaks is 65 mV (theoretical value is 59 mV). [42] The two peaks are symmetrical in terms of their heights and shapes. It is evident that the redox reaction is a one-

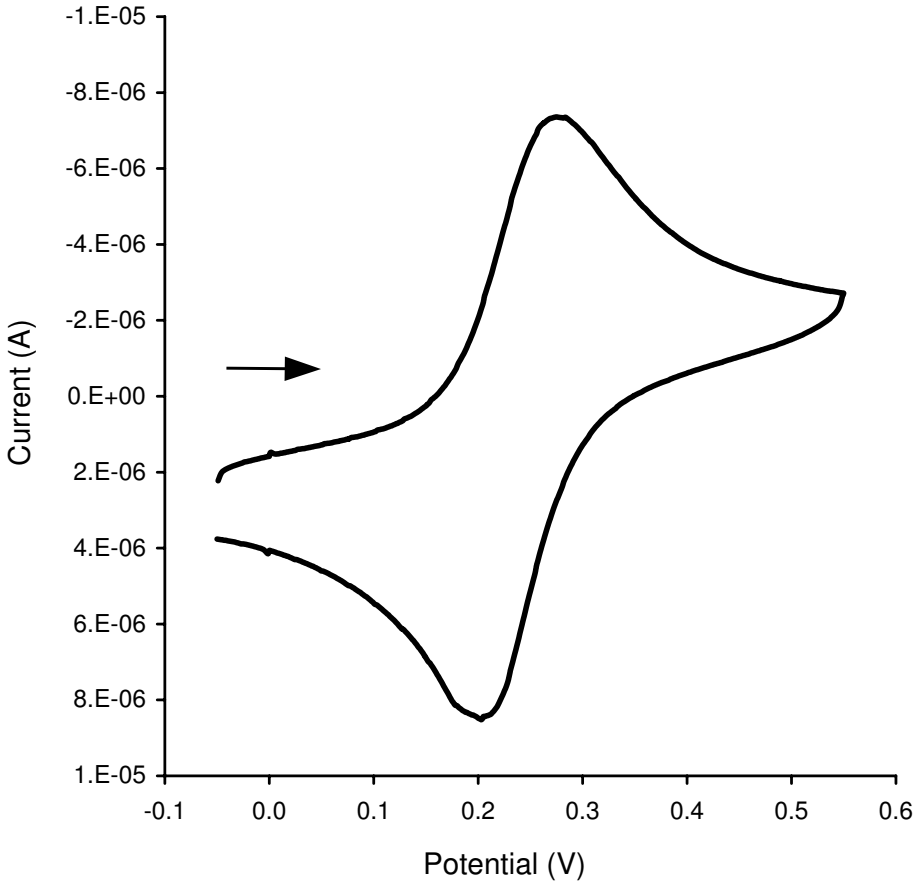

Figure 2.3: CyclicVoltammogram of $[Fe(CN)_6]^{3-}$ in H_2O at the Pt Electrode, V *vs.* Ag/AgCl

electron reversible reaction under these experimental conditions. Therefore, the cathodic or anodic peak height, i_p, is linearly related to the square root of the scan rates at the $[Fe(CN)_6]^{3-}$ concentrations, equation (2.4). [167]

$$i_p = (2.69 \times 10^5) n^{\frac{3}{2}} A D_0^{\frac{1}{2}} {C_0}^* \nu^{\frac{1}{2}} \tag{2.4}$$

In this equation, A is area in cm^2, D_0 is diffusion coefficient in $cm^2 \cdot s^{-1}$, C_0 is concentration in $mol \cdot cm^{-3}$, and ν is scan rate in $V \cdot s^{-1}$, n is the number of electrons. The diffusion coefficient (D_0) is taken as $7.63 \times 10^{-6}\, cm^2/s$. [168]

With this equation, the working electrode surface area can be derived by plotting the i_p vs. $\nu^{1/2}$ as shown in Figure 2.4. The slope of the linear i_p *vs.* $\nu^{1/2}$ dependence in Figure 2.4 yields the working electrode surface area. In our experiments, the calculated working electrode surface areas range from 0.124 to 0.264 cm^2.

Results and Discussion. Static cyclic voltammograms of 1 mM $[Fe(CN)_6]^{3-/4-}$ at voltammetric scan rates of 1-4 mV/s are shown in Figure 2.5. Peak-shaped voltammograms are observed at all scan rates. This indicates that rate of electron transfer exceeds the rate of mass transfer on the working electrode surface under these experimental conditions, which is not expected at the slow scan rate of 1 mV/s. The potential differences of the two peaks, however, are much greater than 59 mV, and increase as a function of the scan rate, these result from the high cell resistance.

The well-defined anodic and cathodic peaks are observed even at a scan rate of 1 mV/s. This may be caused by the small distance between the spherical working electrode and the "cup" wall. Given a scan time on the order a hundred seconds, one can estimate that the thickness of the diffusion layer is about several hundred

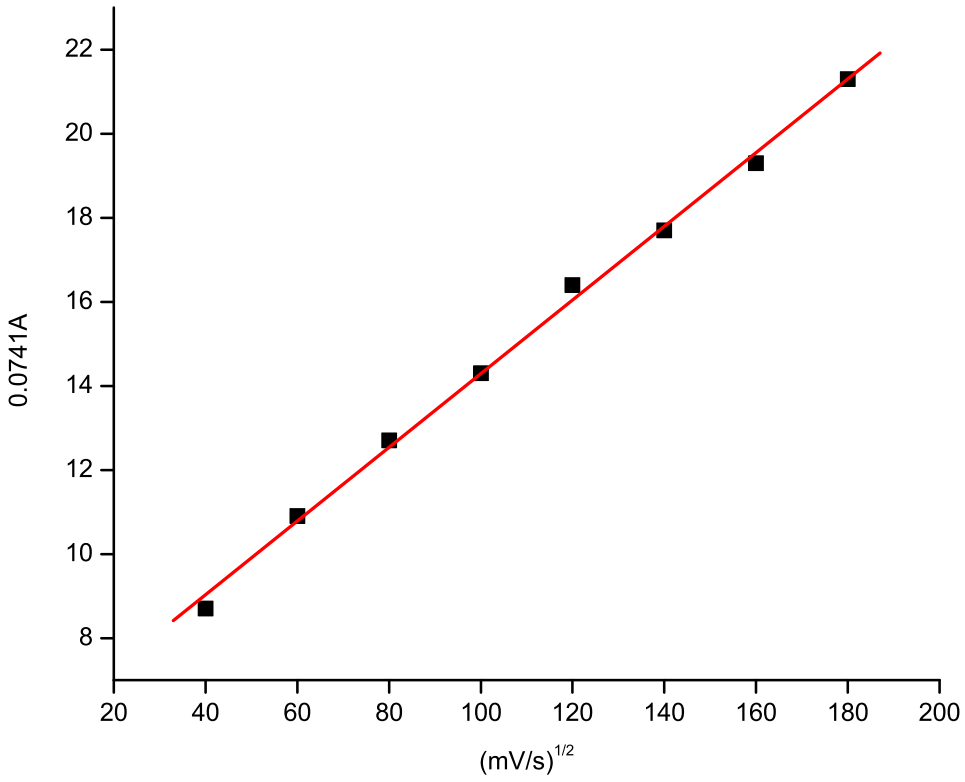

Figure 2.4: Peak Current (i_p) *vs.* Square Root of Scan Rates ($\nu^{\frac{1}{2}}$)

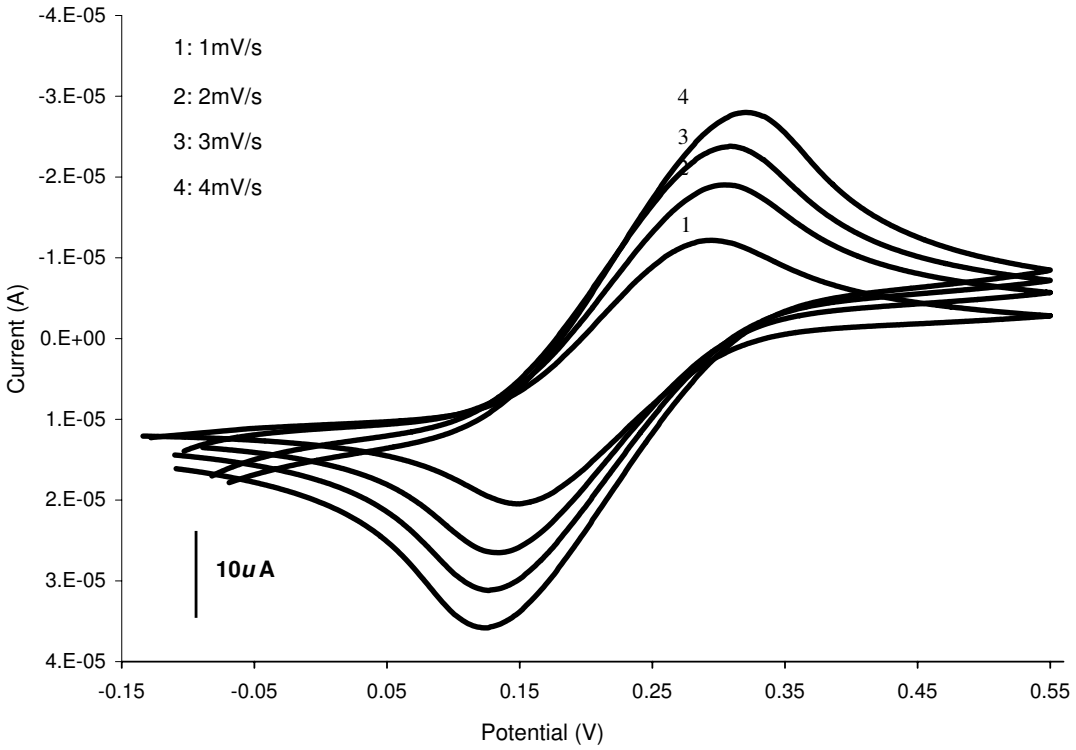

Figure 2.5: Static Cyclic Voltammograms of $[Fe(CN)_6]^{3-}$ at Various Scan Rates, V *vs.* Ag/AgCl

μm, [169] which could be greater than the size of spherical channel between the electrode and the cell wall.

Figure 2.6 shows hydrodynamic cyclic voltammograms of 1 mM $[Fe(CN)_6]^{3-/4-}$ at a flow rate of 1 mL/hr. The scan rates range from 1 mV/s to 6 mV/s with a step increase of 1 mV/s. When the flow rate is greater than 2 mL/s, the rate of electron transfer rate is greater than the mass transfer rate, and thus, peak-shaped hydrodynamic cyclic voltammograms are observed. At low scan rates, 1 mV/s and 2 mV/s, constant limiting currents were observed at high over-potentials. This indicates that the electron transfer rate is controlled by the mass transport of analyte in the cell.

In order to be more quantitative about the shapes and sizes of the hydrodynamic cyclic voltammograms obtained at scan rates of 1 mV/s and 2 mV/s, a logarithmic analysis of the current i relative to the potential (E) is carried out for laminar flow developed at a flow rate of 1 mL/hr. The redox reaction of $[Fe(CN)_6]^{3-/4-}$ is a rapid one electron reversible reaction. This electron transfer process has a typical Nernstian response. [170] With only $[Fe(CN)_6]^{3-}$ initially present at the millimolar level in solution, an equation in terms of electrode potential is written as follow: [170]

$$E = E_{1/2} + \frac{RT}{nF} \log \frac{i_L - i}{i} \tag{2.5}$$

Where i_L is the limiting current and F is the Faraday constant 96485.3 C/mol.

When a system conforms to equation (2-5), a plot of E *vs.* $\log[(i_L - i)/i]$ will give a straight line with a slope of $59.1/n$ mV (here $n = 1$) or $2.3RT/(nF)$. In our experiments, the measured limiting currents at scan rates of 1 mV/s and 2 mV/s are, respectively, 3.5846×10^{-5} A and 3.7482×10^{-5} A,

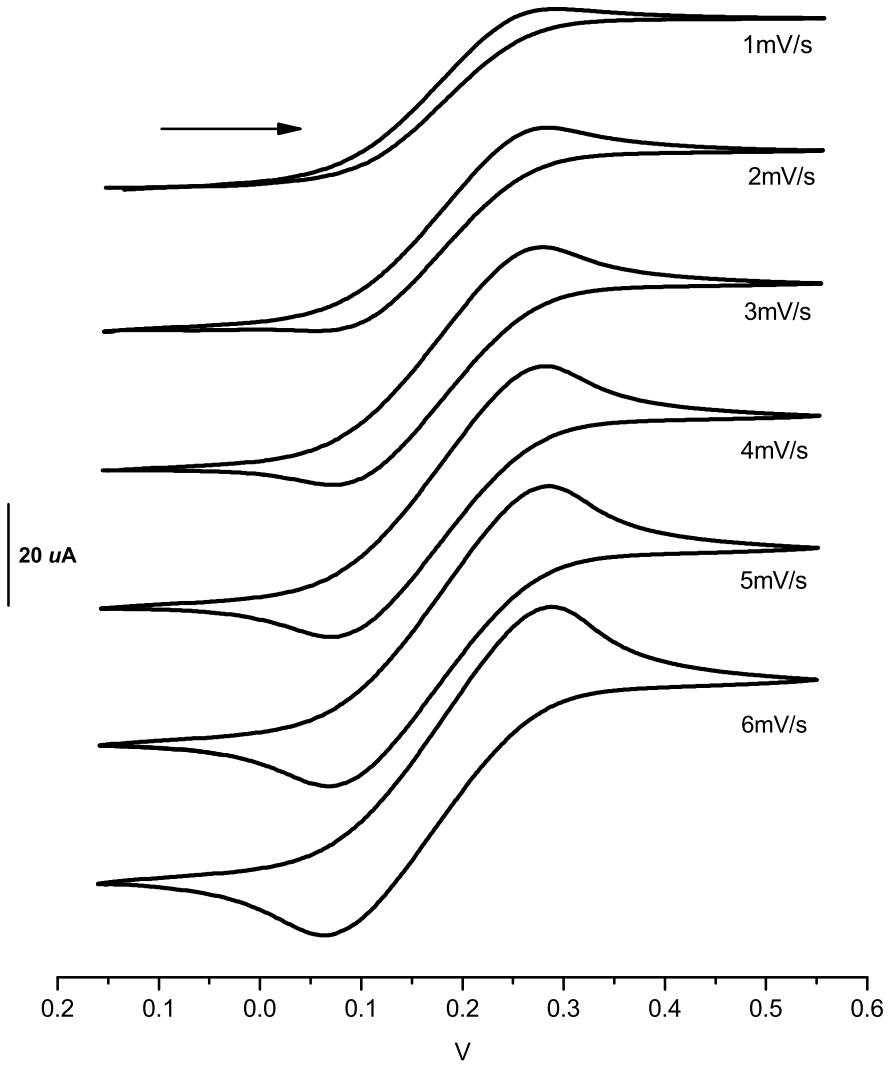

Figure 2.6: Hydrodynamic Cyclic Voltammograms of $[Fe(CN)_6]^{3-}$ at Various Scan Rates, V *vs.* Ag/AgCl

Logarithmic plots of E *vs.* $\log\left[(i_L - i)/i\right]$ in the low over potential range are shown in Figure 2.7. The data corresponds to a scan rate of 1 mV/s. Linear fits of the curve give slopes ranging from 63.31 mV to 68.8 mV (theoretical 59.1 mV) This indicates that Nernstian behavior of $[Fe(CN)_6]^{3-/4-}$ occurs at the working electrodes at low-over potentials.

The cell conversion efficiency is defined as the ratio of the number of moles of analyte reacted on the working electrode over the number of moles of analyte flowing through the cell per unit time. It is very important factor to determine the quality of the design of a flow cell.

The amount of analyte, $[Fe(CN)_6]^{3-}$, pumping through the flow cell at the flow rate of 1.0 mL/hr, which is the flow rate that is mostly used in this dissertation, is 2.778×10^{-10} mol/s. At the steady state region, the constant limiting current is 35.85 μA and 37.48 μA at the flow rates of 1 mV/s and 2 mV/s, respectively. The amount of electron transferred at the working electrode per unit time is calculated as 3.716×10^{-10} mol/s. The calculated results show that number of moles electrons transferred per unit time is slightly greater than the number of moles of analytes flowing through the cell per unit time. This indicates that the flow cell has high electrochemical conversion efficiency as well as that some analyte could diffuse to the back of the ball-shaped working electrode, shown in Figure 2.2, and thus participate the electrochemical reactions.

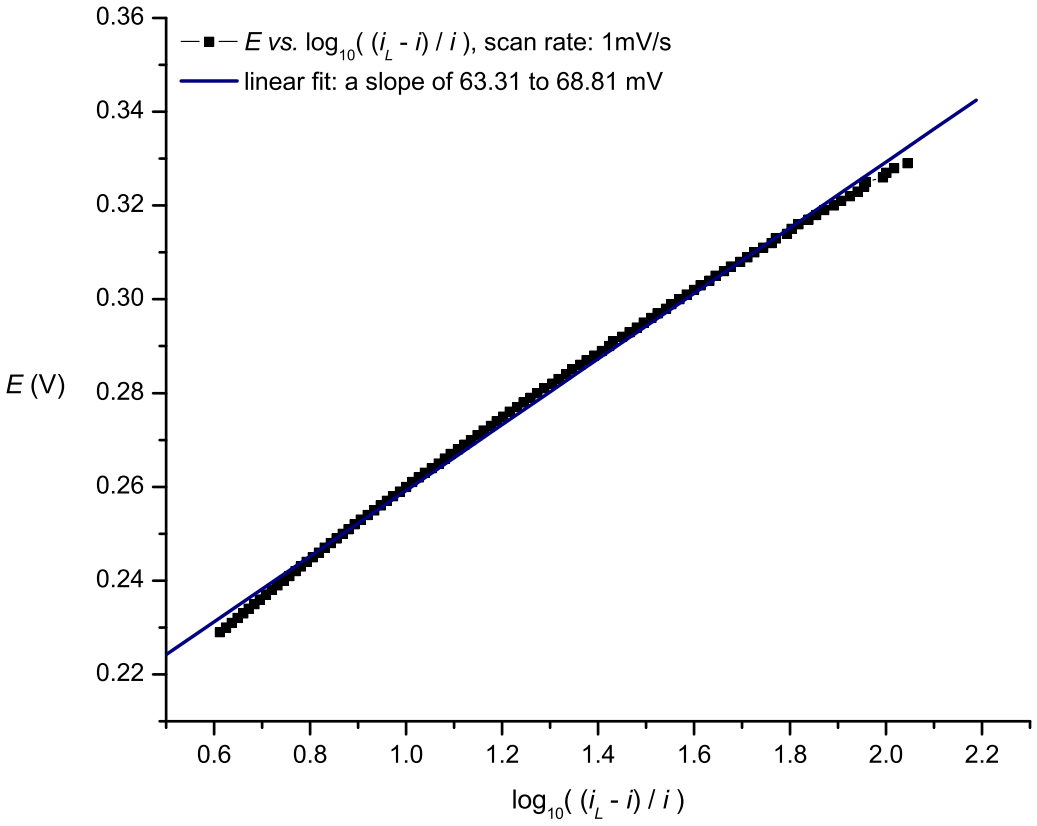

Figure 2.7: Nernstian Plot for the Scan Rate of 1 mV/s

2.6 Conclusions

A spherical thin-layer flow electrochemical cell, characterized by easy access for replacing the working electrode and a high conversion efficiency, was developed. The cell has a relatively small cell volume, 5 - 10 μL. Calculated Re numbers predict that the flow pattern around the working electrode is Laminar flow. Both the static cyclic voltammograms and hydrodynamic voltammograms at different flow rates indicate that the cell design meets the requirements of a thin layer flow cell.

The drawbacks and the advantages of the cell design are summarized as follow:
Drawbacks:

- The cell design sacrifices the separation of counter and working electrode in order to achieve a small dead volume.
- The cell design consists of too many hand-made components, which makes difficult to assembly.
- The counter electrode was placed the upstream of the working electrode, which may cause an uneven cell current density distribution.

Advantages:

- The cell design has easy access for cleaning the working electrode.
- The cell has a high conversion efficiency.
- A well-made "cup" volume is about 5 - 10 μL and functions as a collector.
- At low flow rates, between 1 - 5 mL/hr the fluid around the working electrode has well-developed Laminar flow.

- Counter electrode reactions are separated from the working electrode reactions by placing the counter electrode upstream of the working electrode.

The cell just described was used in the experiments to be described in Chapter 3 and 4. A 800 mm silica capillary was used in the on-line EC/ES-MS experiments to connect the electrochemical cell to the electrospray probe. This silica tube isolates the high potential at the tip preventing current leakage from the electrospray needle.

Chapter 3

I^- and CN^- at Gold and Platinum Electrodes

Abstract

We report results on the electrochemistry of I^- and CN^- at gold and platinum electrodes using an electrochemical flow cell described in Chapter 2 coupled to an electrospray mass spectrometer. We demonstrate that our apparatus is capable of these very challenging electrochemical/electrospray experiments and that $B(C_6H_5)_4^-$ is a suitable internal standard for negative-ion studies in acetonitrile. With I^- at a platinum electrode, we observe well-behaved oxidation to I_3^-. Experiments on I^- at gold electrodes are more complex, showing AuI_2^- as well as I_3^-. The AuI_2^- mass spectrometric ion intensity varies in a complex way throughout the applied electrochemical voltage range studied; we propose that this variation involves the adsorption of I^- on the gold electrode surface. In experiments on CN^- at the gold electrode, we observe $Au(CN)_2^-$ at 0 V. This arises from the surface oxidation of the freshly annealed gold electrode. In the platinum electrode case, the oxidation of cyanide yields cyanogen. Addition of one mole of CN^- to two moles of C_2N_2 gives the $C_5N_5^-$.

3.1 Introduction

We chose to study the iodide system because it undergoes a well-understood multi-step oxidation, and the iodide absorption onto electrode surfaces is well understood. [7, 8] Studies of the electrochemical oxidation of iodide to iodine in different solvents at platinum electrodes have focused on the kinetics and mechanisms of the reactions and the adsorption of ions on the electrode surfaces. [7–13, 15] Agreement

between experimental and theoretical polarographic characteristics of the oxidation of iodide in acetonitrile was reported by Guidelli and Piccaradi, [12] while the electrochemical properties of iodide in different organic solvents [10] with a wide range of dielectric constants were reported by Iwamoto. A two-step oxidation of iodide to iodine was proposed. The kinetics and mechanism of the electrochemical oxidation of iodide to iodine have also been investigated in acetonitrile and dimethylsulfoxide with a rotating platinum-disk electrode by Arvia. [7,8] The results showed two polarographic waves, and the difference between the half-wave potentials of the two waves was related to the stability constant of tri-iodide in the solvent. The adsorption of iodide on a smooth electrode in aqueous solutions has been investigated by Bagotskv, *et al.* [11] It was found that the adsorption formed a stable adlayer that dramatically influenced the surface reactivity.

Numerous studies have focused on the electrochemistry of gold and its halide complexes in both aqueous and non-aqueous solutions. [16–22] Metallic gold can be dissolved as gold complexes in acetonitrile with strongly coordinating ligands by both chemical or electrochemical oxidation. [23] The stepwise stability constants for AuI and AuI_2^- complexes in acetonitrile, determined by Fenske, are given below. [24] These stability constants indicate that AuI and AuI_2^- are stable in acetonitrile.

$$K_1 = \frac{\mathrm{AuI}}{[\mathrm{Au^+}][\mathrm{I^-}]} \qquad \log \mathrm{K_1} = 17.1 \tag{3.1}$$

$$K_2 = \frac{[\mathrm{AuI_2^-}]}{[\mathrm{AuI}][\mathrm{I^-}]} \qquad \log \mathrm{K_2} = 6.7 \tag{3.2}$$

In acetonitrile, halide ions have been found to be adsorbed on smooth gold surfaces, [11, 15] especially when a positive potential is applied to the gold. The halide

adlayer plays an important role in subsequent electrochemical reactions. It has been reported that halide adsorption on the gold electrodes shifts the oxidation potential for the oxidation of iodide to iodine to more negative values. [24] Scanning tunneling microscopy images of iodide adsorbed on gold(111) surfaces from aqueous solution have been reported by Bard. [18] The atomic images of the iodide adlayers provide direct evidence for the organization of the adlayer.

The chemistry of gold cyanide complexes has been known since the 17th century. The treatment of heterogeneous gold and electrolyte (cyanide, halide) interface as a model system for studying other interfacial processes has been a subject of many investigations.

Previous results, obtained using surface structure sensitive techniques, [25, 26], show that the process of gold dissolution first starts from the formation of monolayer of AuCN on the gold electrode in the presence of O_2.

The adsorption of CN^- ions on gold single crystals was monitored by visible-infrared difference frequency generation (DFG). [26] The results showed a significant effect of the surface orientation on the adsorption strength of cyanide. The interface between polycrystalline gold electrodes and the cyanide aqueous solution as a function of the potential and cyanide concentration was studied by polarization-modulated Fourier transform infrared reflection absorption spectroscopy (FT-IRRAS). [25]

In situ atomic scale scanning tunneling microscopy (STM) images of gold(111) films undergoing dissolution in aqueous cyanide solutions have been reported. [183] The STM images provided direct evidence that the complete disruption of gold(111) surface took place in less than 1 min at high concentrations of cyanide ($> 10^{-4}$ M) in the presence of oxygen.

Electrochemical oxidation of cyanide at platinum electrodes has been studied by various electrochemical methods in aqueous solution. [172] The results suggest that the cyanide oxidation is a non-reversible one-electron transfer process that is characterized by diffusion control at the platinum electrode. The oxidation product is cyanogen.

Cyanogen is an active species and can be involved in many reactions in both aqueous and non-aqueous solutions. The reaction of cyanogen with cyanide is one of the least studied areas of cyanogen chemistry. [27] A reversible reaction between cyanogen and cyanide yields $C_3N_3^-$, but, to date, there is no direct evidence to prove the exitance of this species in both aqueous and non-aqueous solutions. The proposed reactive anion $C_3N_3^-$ is an important intermediate in the process of formation of many cyano-carbons. The structure of $C_3N_3^-$ was studied by using the MNDO molecular orbital method, [96] the result shows that C_{2v} is the most stable structure. Addition of two cyanogens to cyanide ion yields $C_5N_5^-$ in a step-wise mechanism. [28]

In this chapter, we present our results of electrochemical studies of iodide and cyanide oxidations at gold and platinum electrodes using the EC/ES-MS method.

3.2 Experimental Section

Experimental Chemicals and Solutions. Potassium iodide (KI, 99.0+%), sodium tetraphenylborate ($Na[B(C_6H_5)_4] \geq 99.5\%$), potassium cyanide (KCN, 99%), potassium chloride (KCl, 99.8%), and acetonitrile (CH_3CN, HPLC grade) were obtained from Fisher. Tetrabutylammonium cyanide ($[Bu_4N]CN > 95\%$) was from Aldrich. All salts were used as received.

A 0.1 mM $K_3[Fe(CN)_6]$ in 0.1 M KCl aqueous solution was used to measure the areas of the working electrodes with $K_3[Fe(CN)_6]$ and KCl acting respectively

as probe molecules and supporting electrolyte. [43] Acetonitrile was dried over CaH_2 under N_2 gas for at least 4 hours prior to use. [164] The solutions were thoroughly degassed with high-purity dried argon (Grade 5.0) for at least 10 min before starting each experiment. $[Bu_4N]CN$ was dried at least 48 hours under vacuum at 30 °C before use.

Instrumentation and Electrodes. A VG-Trios-2000 quadrupole mass spectrometer with VG electrospray source was used in these experiments. Here we report results on anions; the mass spectra were acquired in negative-ion mode, and 50 scans at a scan rate of 1 scan/s. The ES tip voltage was $\sim$ 2.89 kV, the source temperature was 60 °C, and the cone voltage was 20 V. Since the residence time of solutions in the sampling area of the electrochemical cell is 18 - 30 seconds, the time delay between two consecutive potentials was 60 seconds.

A Bioanalytical System Inc. CV-27 potentiostat was used to apply potentials to the homemade three-electrode electrochemical cell, Figure 2.1, and to record the cell current. The potential ranged from 0.0 to 1.9 V with potential steps of 0.1 V. A Bioanalytical System Inc. Epsilon-EC potentiostat was used to obtain conventional cyclic voltammograms for comparison purposes. Matlab version 6.5 was used to process all mass spectral data and plot the 3-D figures. Origin version 7.0 and Microsoft Excel 2000 was used to plot other figures.

Working Electrodes and the Electrochemical Setup. A schematic diagram of the electrochemical working electrode and ion collection region is shown in Figure 2.1. The platinum-mesh was used as the counter electrode. A Ag/AgCl reference electrode was connected to the cell through a double salt bridge. All potentials are quoted versus aqueous Ag/AgCl. The connections to the cell were made through Viton O-rings or through Supelco Thermogreen LB-2 septa. A Cole Palmer Series

7490 syringe pump with a flow rate of 1.0 mL/hr was used to provide the constant mobile phase and produce the spray.

It was found that current leakage could be avoided by using an 800 - 850 mm long (ID 0.1 mm) untreated silica capillary connecting the electrochemical cell with the electrospray probe tip. The entire electrochemical cell was maintained at room temperature.

The organic stream in the cell and the duct line connecting to the ESI source fulfills several functions: it minimizes the liquid conductivity in the transfer line from the flow cell to the ESI probe due to its small cross section area (0.785 mm^2) and relatively long distance. Therefore it disconnects the high voltage of the ESI needle and the working electrode. An organic solute and low concentration of electrolytes also quenched chemical reactions between the oxidation products and the reactants, thus reducing compositional changes in the duct line.

The working electrodes were made from gold (99.9999%) or platinum (99.9999%) wires (OD 1 mm). Before use, the electrodes were cleaned by rinsing sequentially with distilled water, hydrofluoric acid 49%, piranha solution, [161] distilled water, HPLC grade methanol and fresh acetonitrile. The electrodes were then stored in acetonitrile in a glove bag under an argon atmosphere. The assembly of the electrochemical cell was carried out in a glove bag under Ar.

All the electrochemical measurements were done twice.

3.3 Results and Discussion

Internal Standard. High conductivity of the electrolytic solution is usually preferred in conventional electrochemical measurements to decrease the potential drop

between the working and reference electrodes. However in the EC/ES-MS experiments, the conductivity of the electrolyte solution is kept low for two reasons.
A low solution conductivity minimizes interfering currents due to the high potentials at the electrospray tip. Low electrolyte concentrations also avoid attenuation of the electrospray signals. [6] An organic solute and low concentration of supporting electrolyte also discourages the possible chemical reactions between the products with the supporting electrolyte, thus reducing compositional changes in the silica capillary.

As stated before, the reason we choose the iodide system is that it undergoes a well-understood multi-step oxidation, and iodide absorption onto the electrode surfaces. The formation of solvated K^+ and I^- ions is readily achieved in acetonitrile because of its high dielectric constant (36). Therefore, the iR drop can be minimized without using a high concentration of supporting electrolytes under the experimental conditions. The internal standard $NaB(C_6H_5)_4$, acting also as a supporting electrolyte, in the acetonitrile solution was used at low concentrations ($10^{-4} - 10^{-5}$ M). Different concentrations of $NaB(C_6H_5)_4$ were evaluated and a concentration of 0.02 mM appeared optimum.

Figure 3.1 shows a three-dimensional plot of the absolute ion intensity versus mass to charge ratio and applied electrochemical potential for 0.02 mM $NaB(C_6H_5)_4$ in acetonitrile using a platinum electrode. Data were collected in 0.1 V increments from 0.0 to +1.9 V. These data clearly show the intensity of the tetraphenylborate anion, $B(C_6H_5)_4^-$, does not change with applied potential. A similar result (not shown) was found for $B(C_6H_5)_4^-$ at gold electrodes. These results demonstrate that $B(C_6H_5)_4^-$ is a suitable internal standard for experiments at both platinum and gold electrodes; hence all mass spectra were normalized to the $B(C_6H_5)_4^-$ intensity at m/z 319. Sodium tetraphenylborate also has the advantages of good solubility and good

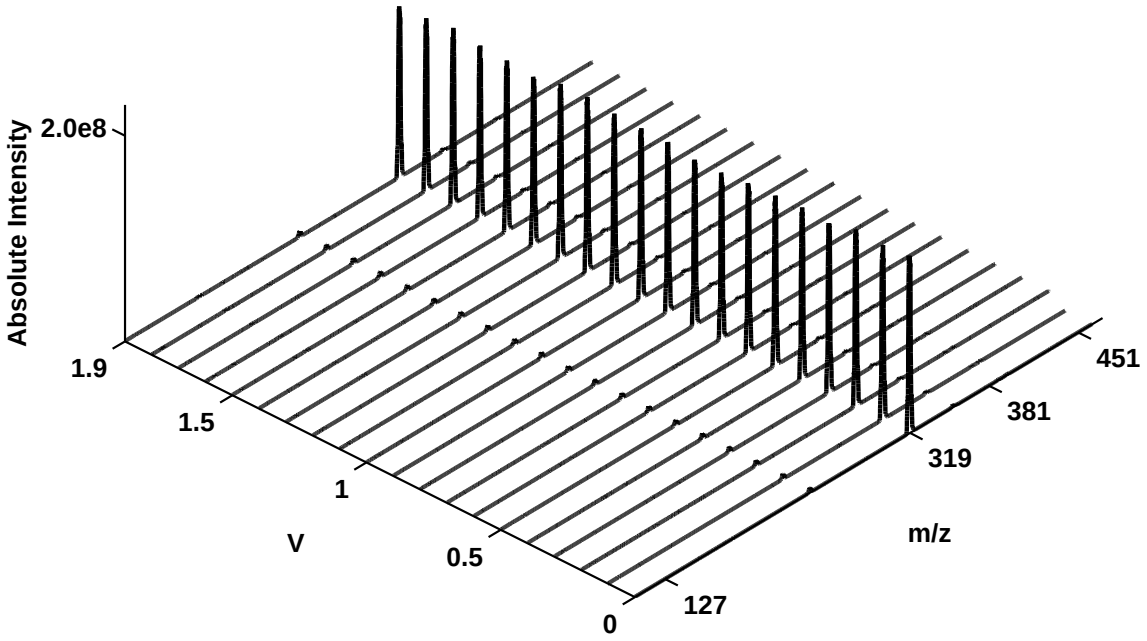

Figure 3.1: Three Dimensional Plot of EC/ES-MS Mass Spectra $B(C_6H_5)_4^-$ as a Function of Applied Electrochemical Cell Potential

voltage limits in acetonitrile, and the peak at m/z 319 lies in a convenient mass range. The other advantage of using $NaB(C_6H_5)_4$ as an internal standard is the ions did not appear to suppress the electrospray signal when present in micromolar quantities in the electrospray solution. [6, 88]

3.3.1 Iodide at Platinum and Gold Electrodes

Platinum Working Electrodes. The cyclic voltammogram of a 0.5 mM KI and 0.02 mM $NaB(C_6H_5)_4$ solution in acetonitrile at scan rate 10 mV/s is shown in Figure 3.2. Two anodic peaks and one cathodic peak are recorded in Figure 3.2. The first and second anodic peaks correspond, respectively, to the oxidation of I^- and I_3^-, consistent with the literature. [7] The reactions are illustrated by following equations:

$$2I^- \rightleftharpoons I_2 + 2e^- \qquad \text{Wave I} \tag{3.3}$$

$$I_2 + I^- \rightleftharpoons I_3^- \tag{3.4}$$

$$2I_3^- \rightleftharpoons 3I_2 + 2e^- \qquad \text{Wave II} \tag{3.5}$$

$$I_3^- + 2e^- \rightleftharpoons 3I^- \tag{3.6}$$

Only one cathodic peak corresponding to the reduction of I_3^- (reaction 3.6) is observed, since in acetonitrile the equilibrium constant for reaction (3.4) is $\sim 4 \times 10^6$ at 20 °C. [7] Thus, most I_2 is rapidly removed by reaction (3.4) and it is not available for re-oxidation in the reverse of reaction (3.3) or (3.5). This result can be contrasted with aqueous results where the equilibrium constant is smaller (K = 768) and one anodic peak and two cathodic peaks are observed. [7]

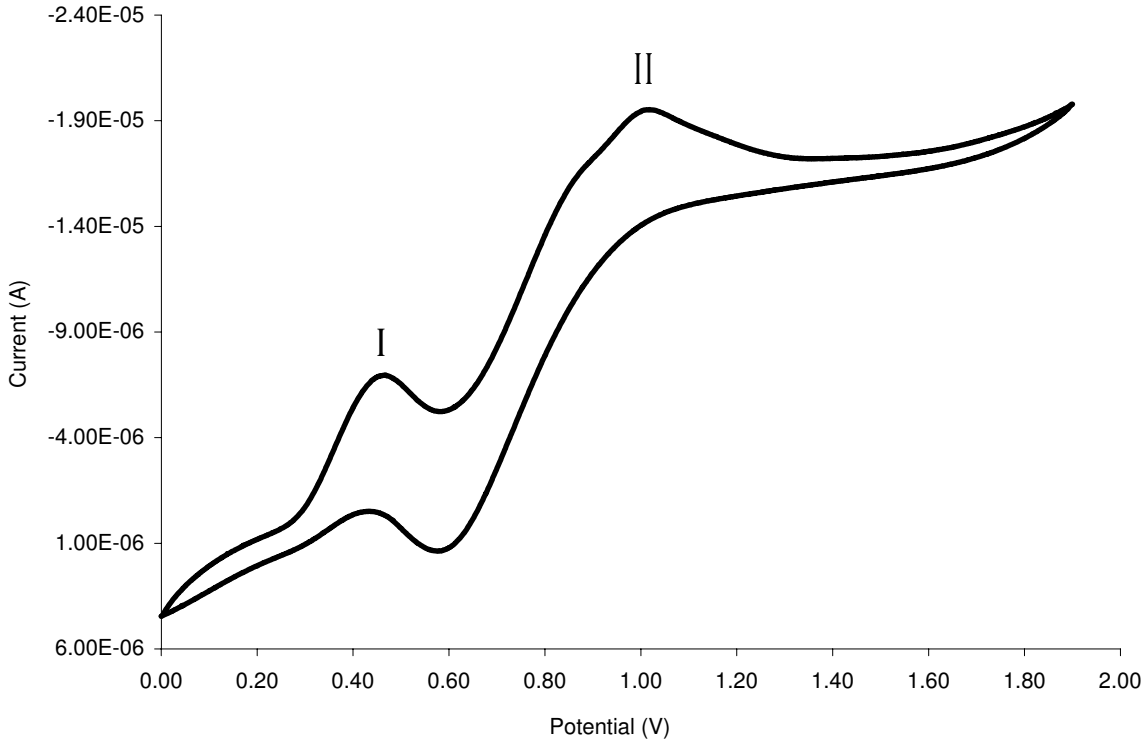

Figure 3.2: Cyclic Voltammetry of I^- at the Platinum Electrode, Scan Rate: 10 mV/s, V *vs.* Ag/AgCl

Figure 3.3 shows the hydrodynamic cyclic voltammogram of a 0.5 mM KI and 0.02 mM $NaB(C_6H_5)_4$ solution in acetonitrile. The scan rate is 1 mV/s, and the flow rate is 1 mL/hr. In contrast to the static cyclic voltammetry (Figure 3.2) where two anodic peaks, assigned to oxidation of I^- and I_3^- respectively, are observed, the hydrodynamic cyclic voltammetry (Figure 3.3) has only one clear anodic peak which can be assigned to the oxidation of I^-. No clear peak is observed for the oxidation of I_3^- in Figure 3.3. When the potential is scanned in the positive direction, the anodic current increases with increasing potentials, Figure 3.3. This is because the flow solution in the cell can bring the analyte, I^-, to the working electrode surface and remove the product, I_3^-. A steady state current is observed at potentials greater than 1.6 V. This indicates that convection dominates at high potentials range (1.6 - 1.9 V), rather than an electron transfer or a diffusion.

Figure 3.4 shows the results of a normalized EC/ES-MS experiment of the oxidation of KI in acetonitrile at a platinum electrode at potentials from 0.0 V to +1.9 V in 0.1 V increments. The peak at *m/z* 381 corresponds to I_3^- and first appears at $\sim +0.3$ V; it increases slowly until $\sim +1.6$ V, beyond which it increases more rapidly and then plateau. This is in agreement with the pattern recorded by hydrodynamic cyclic voltammetry, Figure 3.3, showing a plateau when the potential is greater than 1.6 V. The peak at *m/z* 319 ($B(C_6H_5)_4^-$) appear relatively constant throughout the voltage range. The small peak at *m/z* 293 is due to KI_2^-, which is believed to be the cluster of $[(KI) \cdot I]^-$. This peak, originating from I^-, is also relatively constant over the entire voltage range. These results clearly demonstrate the formation of I_3^- resulting from the oxidation of I^-.

The data from Figure 3.4 are also shown in Figure 3.5 where the absolute intensity of the ($B(C_6H_5)_4^-$), I^- and I_3^- are plotted versus the applied electrochemical potential.

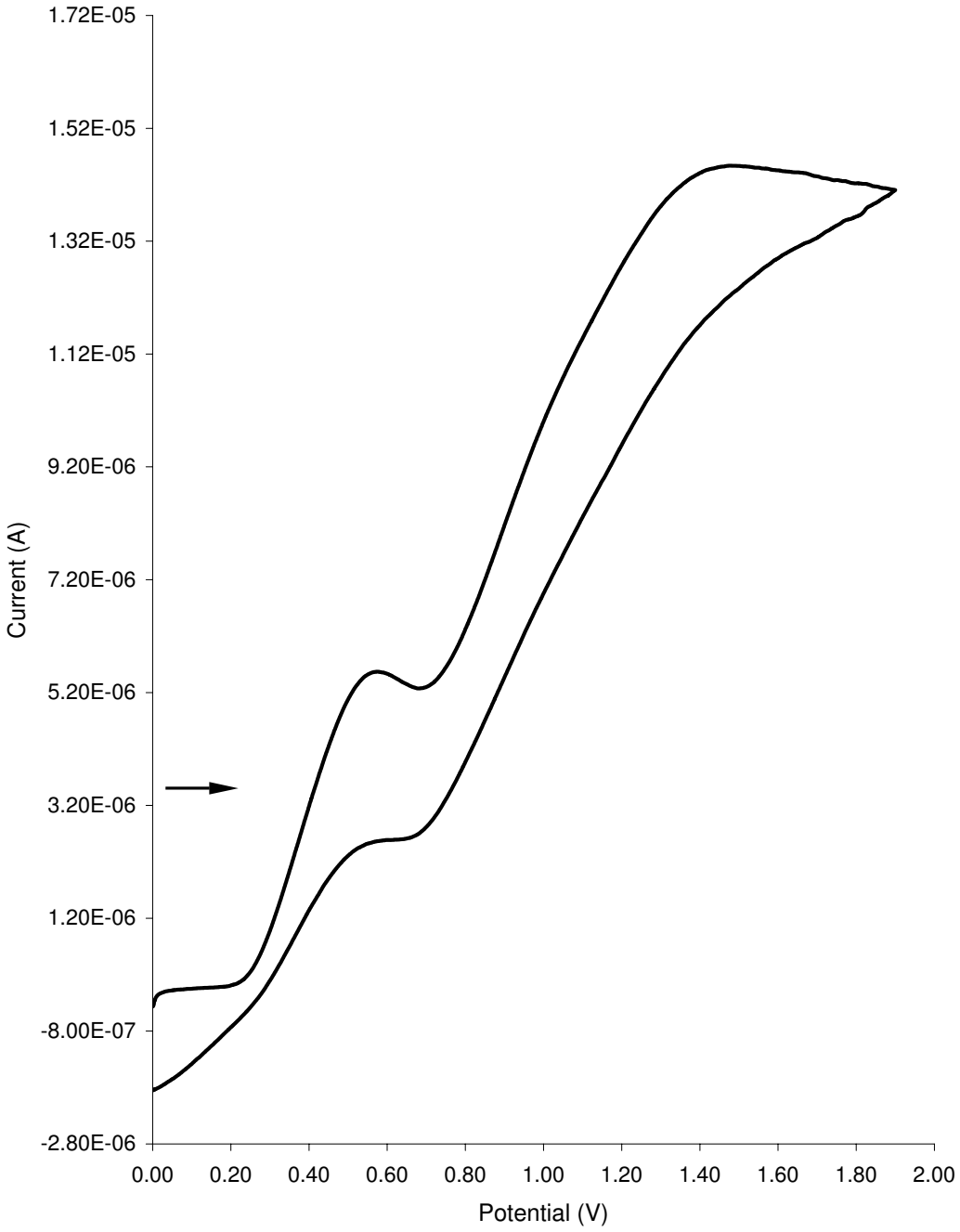

Figure 3.3: Hydrodynamic Cyclic Voltammetry of I^- at the Platinum Electrode, Flow Rate: 1 mL/hr, Scan Rate: 1 mV/s, V *vs.* Ag/AgCl

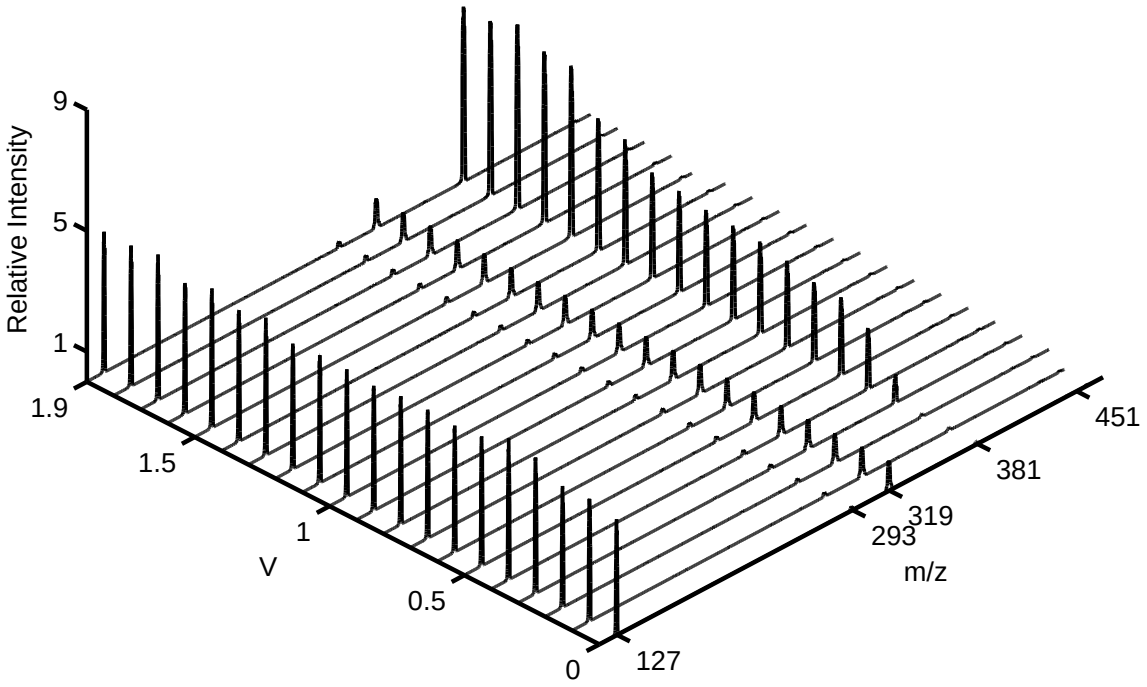

Figure 3.4: Three Dimensional Plot of EC/ES-MS Mass Spectra I^- at the Platinum Electrode as a Function of Applied Electrochemical Cell Potential

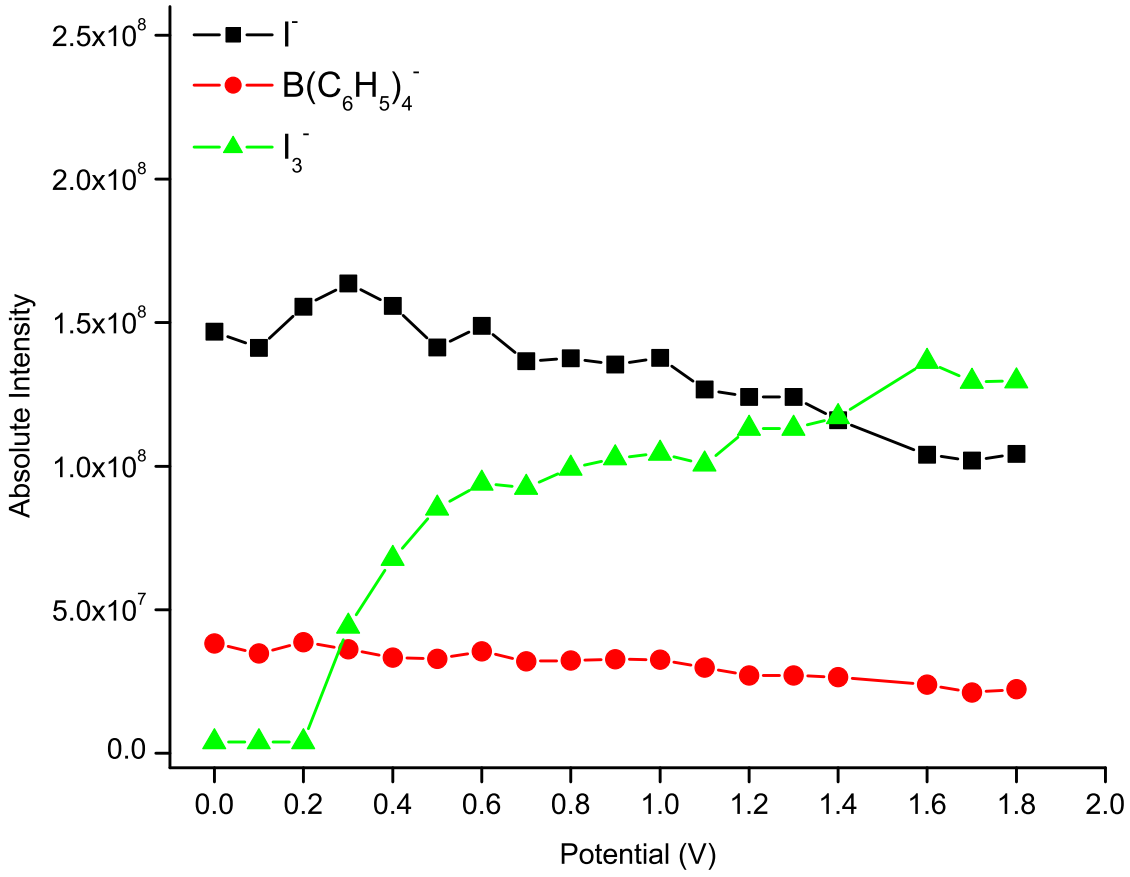

Figure 3.5: Absolute Ion Intensity *vs.* Potential, I^- at the Platinum Electrode

This figure shows an important trend; the absolute intensities of ($B(C_6H_5)_4^-$) and I^- decrease as the potential is increased and I_3^- is formed. The decreasing intensity of the I^- could be interpreted as a decrease resulting from the conversion to I_3^-.

However, such an explanation would not account for the steady decrease in the $B(C_6H_5)_4^-$ intensity which is constant in the control experiment. A more plausible interpretation is that there is an increased competition for the overall charge as the electrospray droplets form ions. Hence, the steady decrease in the ($B(C_6H_5)_4^-$) intensity and the I^- intensity as I_3^- is formed may be the result of the electrospray ionization process and not an electrochemical phenomena.

The increase in the I_3^- current is rapid from +0.3 V to +0.5 V and slower thereafter. The slower increase beyond +0.5 V is most likely due to increased mass transfer from increasing migration of I^- towards the electrode. Migrational effects are likely due to the low electrolyte concentration and can be substantial. [173]

The decreased concentration of I^- and increased concentration of I_3^- would result in a smaller net mass transfer due to the slower diffusion coefficient of I_3^- [$D(I^-)$, 1.68×10^{-5} cm^2/s; $D(I_3^-)$, 1.55×10^{-5} cm^2/s]. [7]

The steady-state current-voltage curve for I^- at a platinum electrode, which is plotted with the hydrodynamic cyclic voltammogram, is given in Figure 3.6. This data was collected simultaneously with the spectra shown in Figure 3.4. The figure shows that the current rises from baseline to a mass-transfer-controlled limit at $\sim$ 0.9 V. Note also that cell current drops slightly in the mass-transfer-controlled region. The decrease in current occurs at $\sim$ 1.3 V and is accompanied by the increased intensity of tri-iodide as shown in Figures 3.4 and 3.5. The steady-state current-voltage curve is consistent with the hydrodynamic cyclic voltammogram.

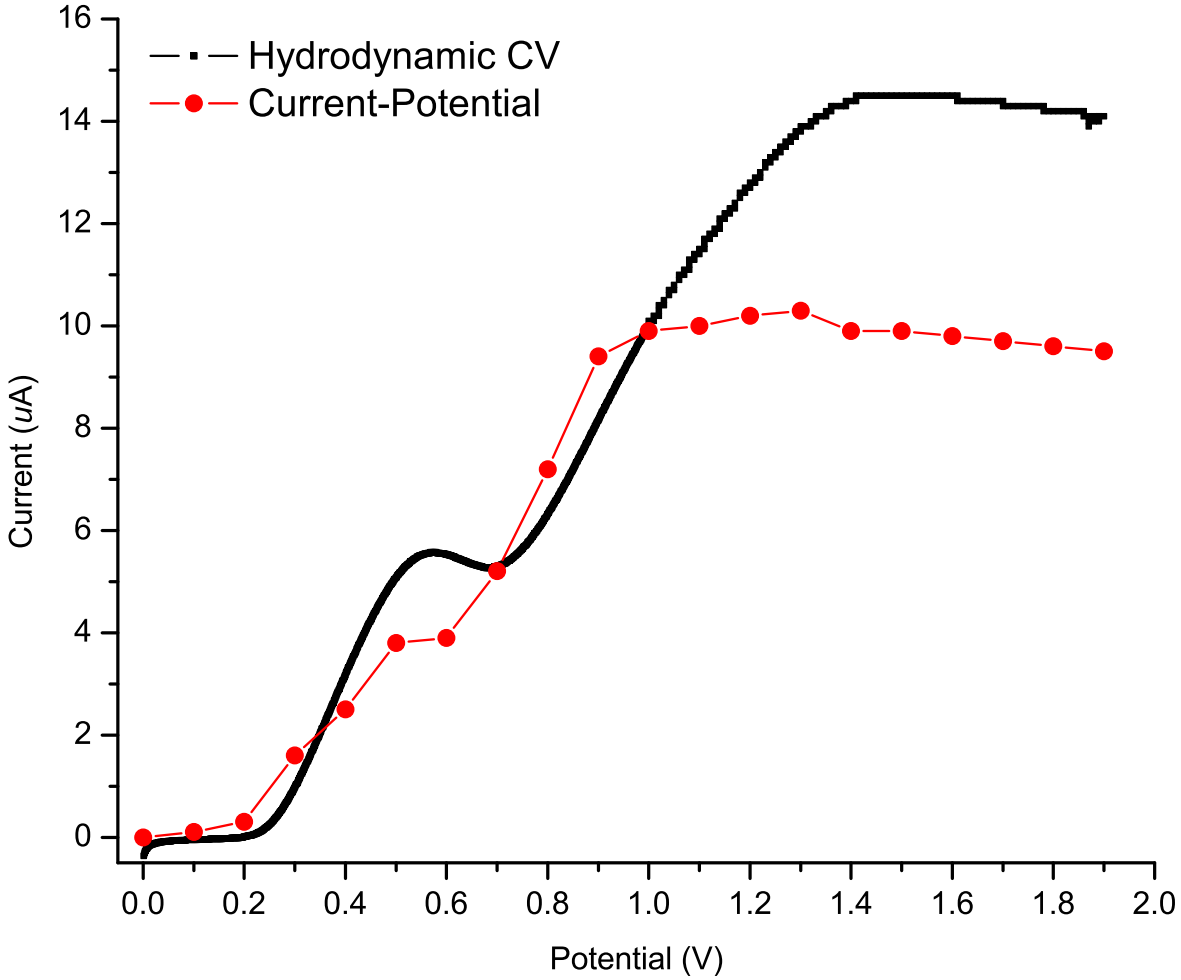

Figure 3.6: Hydrodynamic Cyclic Voltammetry and Current-Potential of I^- at the Platinum Electrode, V *vs.* Ag/AgCl

The concentration changes are confirmed by a color change of the solution around the working electrode due to the characteristic brown color of I_3^-. The current-potential curve in Figure 3.2 shows two waves at $\sim +0.4$ V and $\sim +1.0$ V. These are in agreement with the reported current-potential curve of I^- in acetonitrile solution studied using a rotating-platinum-disk electrode. [7]

Gold Working Electrode. The cyclic voltammogram of KI in acetonitrile at gold electrodes is shown in Figure 3.7. The cyclic voltammogram shows a similarity to the voltammogram at platinum electrodes, two anodic peaks, corresponding to (3.3) and (3.5), and one cathodic peak corresponding to reaction (3.6). However, the EC/ES-MS spectra of KI at gold electrodes in acetonitrile, (shown in Figure 3.8) is quite different.

The difference between Figures 3.4 and Figure 3.8 is clearly evident. As seen in Figure 3.8, the mass peak that changes with potential is AuI_2^- *m/z* 451 at $\sim +0.3$ V. This peak increases with increasing potential and then starts to decrease at $\sim +0.6$ V at which potential *m/z* 381 (I_3^-) begins to increase. The intensity of the peak at *m/z* 381 reaches a maximum at a potential of $\sim +1.7$ V where it starts to gradually decrease. This decrease is also seen in the I^- peak at *m/z* 127. Finally, the peak at *m/z* 451, corresponding to AuI_2^-, starts to increase in intensity at $\sim +1.7$ V. These data indicate that I_3^- accumulates around the gold electrode in the potential range of +0.8 to +1.5 V. At less positive potentials AuI_2^- is formed, and at more positive potentials, AuI_2^- is again formed.

The data from Figure 3.8 are also shown in Figure 3.9 where the absolute intensities of $B(C_6H_5)_4^-$, I^-, I_3^- and AuI_2^- ions are plotted versus the applied electrochemical potential. A slightly decrease of the absolute intensities of $B(C_6H_5)_4^-$ versus applied potential was also recorded in Figure 3.8.

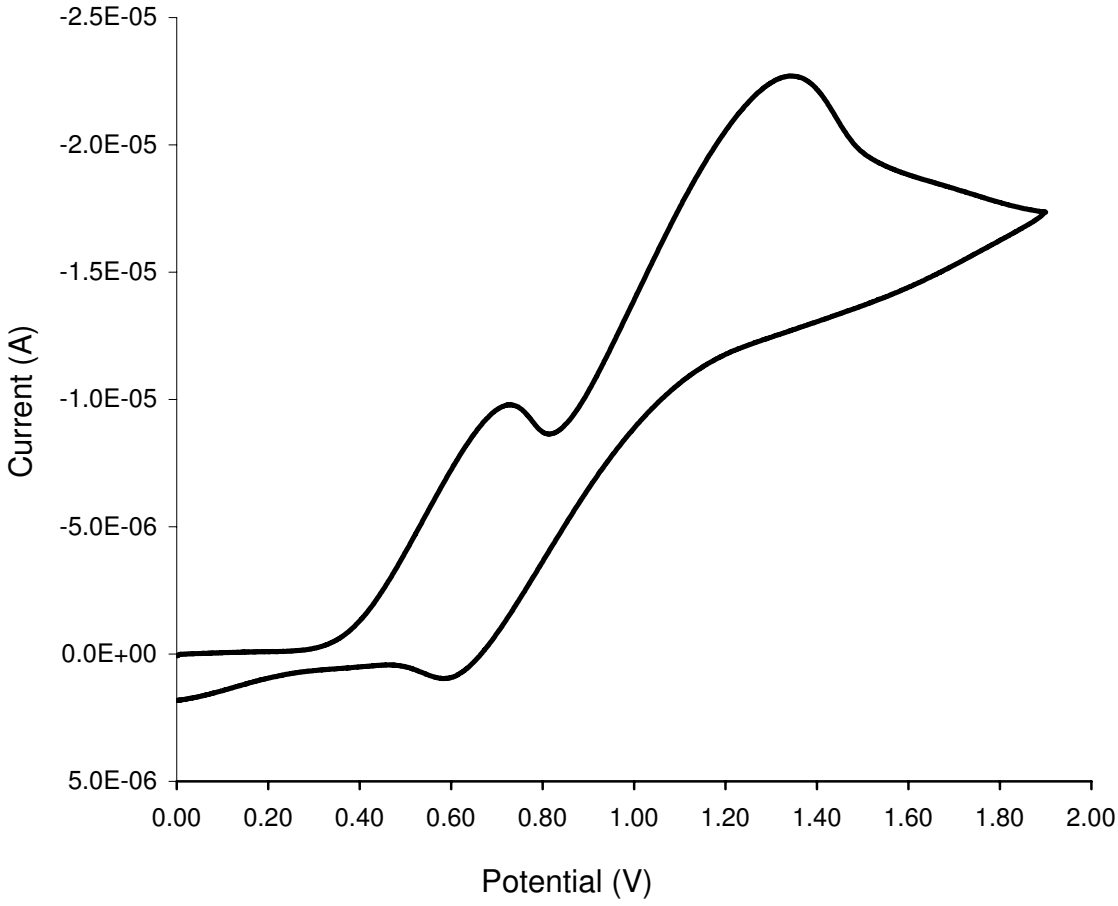

Figure 3.7: Cyclic Voltammetry of I^- at the Gold Electrode, V *vs.* Ag/AgCl

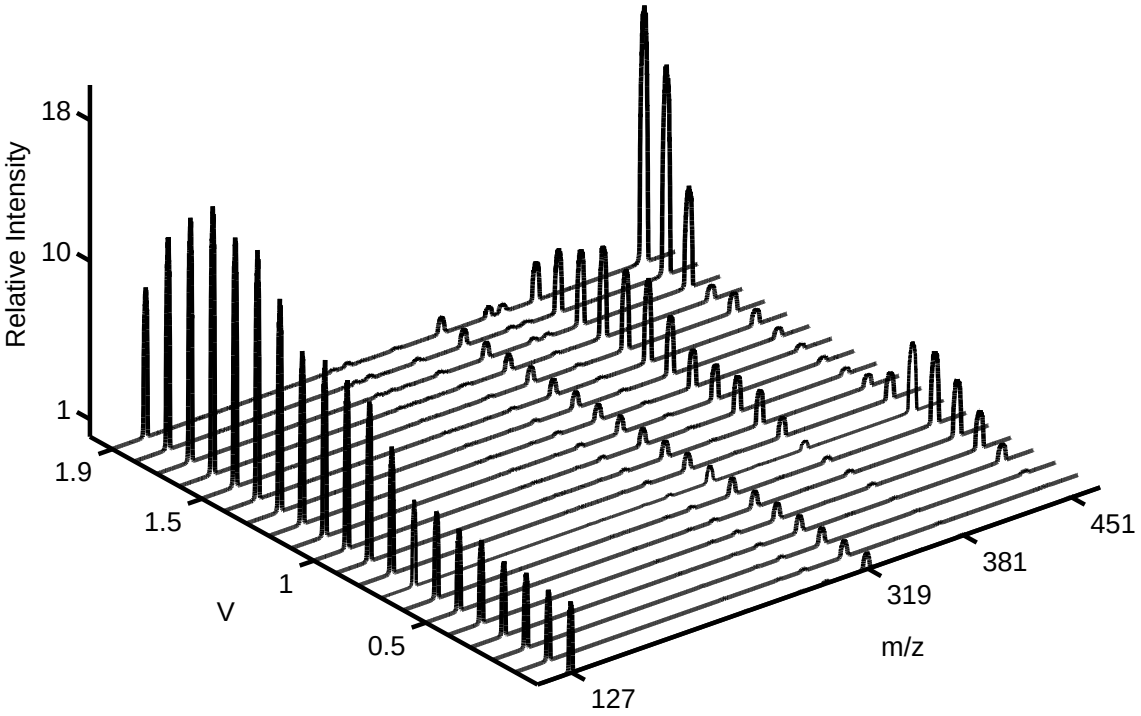

Figure 3.8: Three Dimensional Plot of EC/ES-MS Mass Spectra I^- at the Gold Electrode as a Function of Applied Electrochemical Cell Potential

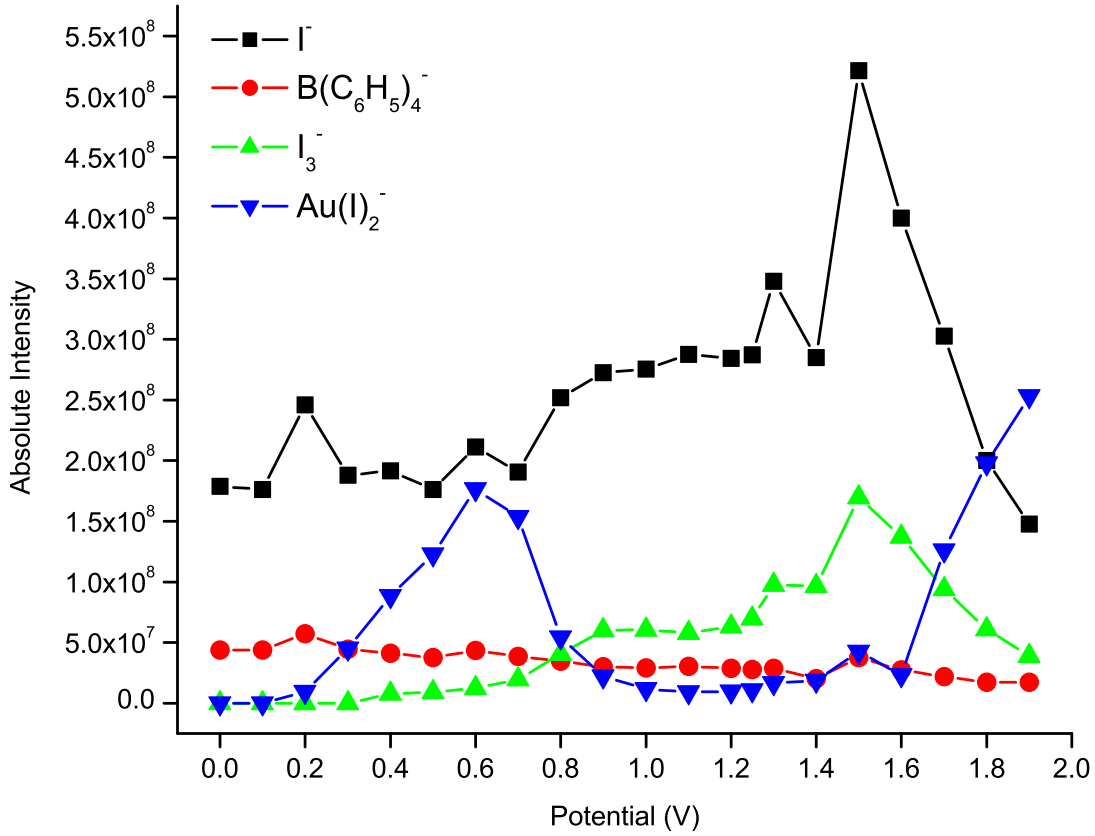

Figure 3.9: Absolute Ion Intensities *vs.* Potential, I^- at the Gold Electrode

The absolute intensities of $B(C_6H_5)_4^-$ decrease as the potential is increased and I_3^- and AuI_2^- are formed. As stated in platinum electrode case, these could be interpreted as increased competition for the overall charge as the electrospray droplets form ions. The observation of the same steady decrease of the $B(C_6H_5)_4^-$ intensity at gold electrode proves that this is the result of the electrospray ionization process and not an electrochemical phenomena.

The current-potential curve of I^- at the gold electrode is also shown in Figure 3.10. Clearly, the current-potential curves at platinum and gold electrodes are very similar from 0 V to about 1.4 V. However, above 1.4 V the current at the gold electrode begins to rise again; this is in the same region where the AuI_2^- reappears, as seen in Figure 3.8.

There are three waves in the current-potential curve at the gold electrode. These correspond to:

$$Au + I^- \rightleftharpoons Au_{(s)} - I^-_{(adsorbed)} \tag{3.7}$$

$$Au_{(s)} - I^-_{(adsorbed)} \rightleftharpoons AuI_{(s)} + e^- \tag{3.8}$$

$$AuI_{(s)} + I^- \rightleftharpoons AuI_2^- \tag{3.9}$$

$$2I^- \rightleftharpoons I_2 + 2e^- \tag{3.10}$$

$$I_2 + I^- \rightleftharpoons I_3^- \tag{3.11}$$

$$Au \rightleftharpoons Au^+ + e^- \tag{3.12}$$

$$Au^+ + 2I^- \rightleftharpoons AuI_2^- \tag{3.13}$$

A plausible interpretation for our observation of AuI_2^- in acetonitrile at *m/z* 451 at low potentials is shown in equations (3.8) and (3.9). Equation (3.8) describes the surface oxidation of the gold iodide adlayer to form AuI on the electrode surface. That reaction is followed by the dissolution of the AuI as AuI_2^- (equation 3.9) driven by the high stability constant of AuI_2^-. A similar mechanism of gold oxidation with I^- in water with (0.1%) acetonitrile was proposed by Kissner. [23]

The standard gold electrode potential (E°_{Au/Au^+}) *vs.* NHE at 20°C in acetonitrile is 1.511 V (1.312 V *vs.* Ag/AgCl), [20] so it is not surprising to see that the AuI_2^- at *m/z* 451 increases at about +1.3 V in Figure 3.8. At high potentials gold atoms are electrochemically oxidized to gold(I), following equations (3.11) and (3.12) above.

As previously stated, the current-potential curves of I^- at platinum and gold are different (shown in Figure 3.10). The gold electrode current does not reach a diffusion-limited region at the most positive potentials. This can be explained by the oxidation of gold to Au^+ that is kinetically limited by the surface area of the electrode and not solution diffusion-limited. A second point is at lower potentials, the current-potential curves do not differ appreciably. Thus, the limiting current due to Au-I(adsorbed) oxidation must be small relative to I^- and I_3^- oxidation.

The other question that we need to address here is the observation of different absolute intensities of I^- between platinum and gold electrodes, shown in Figure 3.4 and 3.8.

The absolute intensity of I^- is relatively constant at all applied potentials at the platinum electrode, shown in Figure 3.4. In the gold electrode case, the absolute intensity of I^- is constant when the surface oxidation of gold electrode is occurring, it increases when the formation of I_3^- (oxidation of I^-) at gold electrode surface begins at

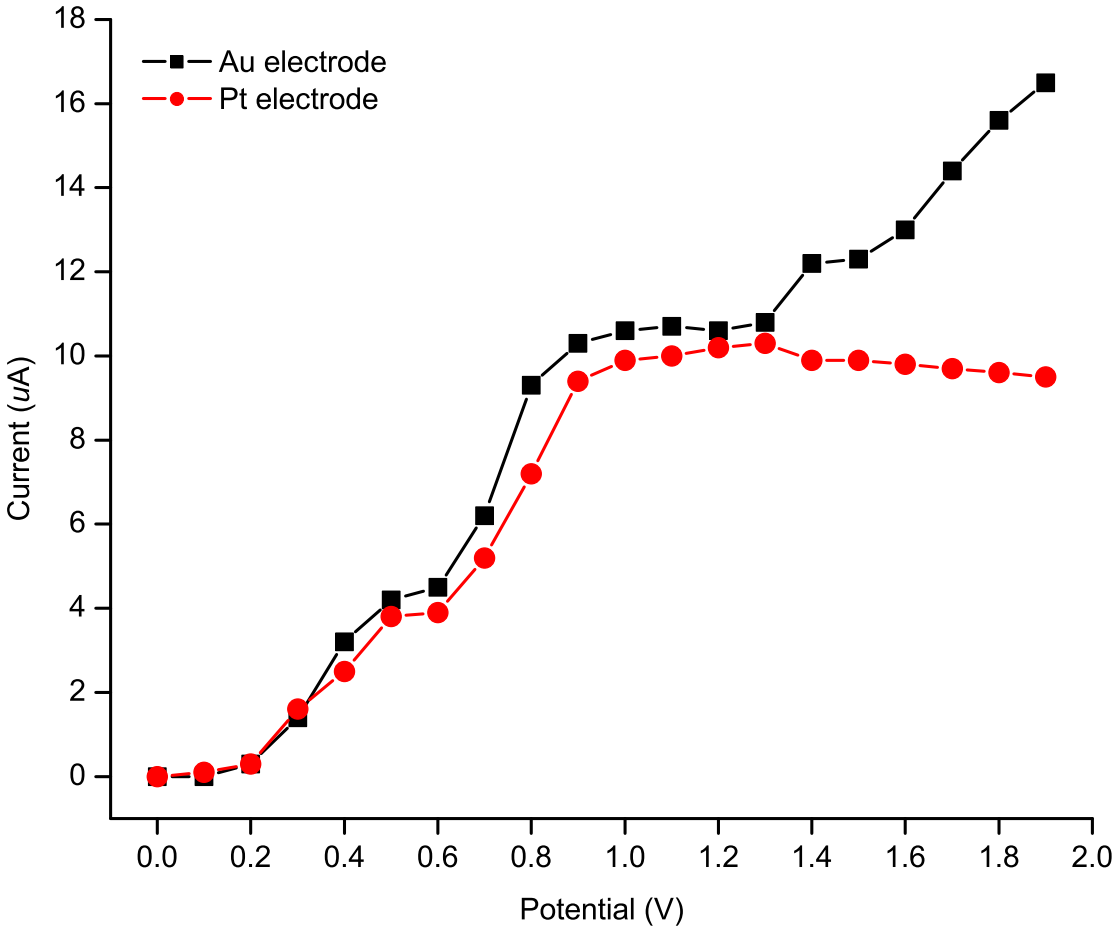

Figure 3.10: Current-Potential of I^- at the Gold and Platinum Electrodes

potentials between 0.9 - 1.4 V. The intensity decreases again when the AuI_2^- dominates the spectra, Figure 3.8.

It is easy to understand that the absolute intensity of the I^- is constant at potentials between 0 and 0.7 V. This is because the surface oxidation of a freshly annealed gold surface has a diffusion-controlled rate determining step. The reaction rate is limited by the rate of AuI_2^- diffusion away the electrode or the I^- diffusing into the electrode double layer, [167] so the absolute intensity of I^- is relatively constant during these processes. [174]

The absolute intensities of I^- begins to differ between platinum and gold electrodes at potentials between 0.9 - 1.4 V. This is not expected under the same experimental conditions, of which only oxidation of I^- at both gold and platinum electrode surface is occurring in this potential range, shown in Figures 3.4 and 3.8. The difference between the trends might indicate a different rate-determining step in the same electrochemical reactions. [175]

Figures 3.5 and 3.9 show that initial absolute intensities of I^- are approximately equal. The later upward trend of absolute intensities of I^- at a gold electrode at potential ranging from 0.9 - 1.4 V could indicate a slow electron-transfer process dominates the heterogenous interface of gold-electrolyte. This causes I^- to accumulate around the working electrode due to the high stability constant of I_3^- in acetonitrile, and the relatively long residue time (18 s) of solution in the "cup" collector at potentials between 0.9 - 1.5 V.

The experiments on iodide at gold and platinum electrodes may be summarized as follows. With gold electrodes, oxidation of gold in the presence of I^- takes place at low potentials as a surface oxidation process. This is followed by oxidation of I^- from solution at higher potentials (this does not involve adsorption). At high potentials

gold atoms are electrochemically oxidized to gold(I), following equations (3.13) and (3.14) above. In contrast, at the platinum electrode, the I^- is adsorbed on the active sites of platinum electrode, [11] but the oxidation of platinum requires much higher potentials so I^- is oxidized to I_3^-.

3.3.2 Cyanide at Platinum and Gold Electrodes

Platinum Working Electrode. Cyanide online oxidation was carried out in acetonitrile solutions at different concentrations of $[Bu_4N]CN$. The concentrations ranged from 0.2 mM to 8 mM. Experimental results show that a 0.5 mM $[Bu_4N]CN$ acetonitrile solution gives the expected oxidation products. Figure 3.11 shows the results of a normalized EC/ES-MS experiment of the oxidation of CN^- from 0.0 V to +2.1 V in 0.1 V increments. All peaks are normalized to cyanide at *m/z* 26.

The peaks at *m/z* 26, 41 and 87 correspond to CN^-, CH_3CN^- and BF_4^-, respectively. A tiny peak at *m/z* 59 can be assigned to $[CH_3CN \cdot H_2O]^-$ possibly arising from the presence of trace amounts H_2O in the acetonitrile. It is not surprising to see these clusters in the spectra since electrospray often results in clustering. It is important to note that these peaks are present over the whole potential range and appear relatively constant. Two voltage dependent peaks are observed, one at *m/z* 130 and the other one at *m/z* 156. The peak at *m/z* 130 first appears at 1.6 V; it increases slowly until 2.1 V, which was the highest potential applied. This peak can be assigned to $C_5N_5^-$. The results shown in Figure 3.11 clearly demonstrate that this peak is potential dependent. The mechanism for the formation of $C_5N_5^-$ in acetonitrile is shown in Figure 3.12. [28]

In the first step, the cyanogen is formed by oxidation of cyanide. [28] The addition of cyanide with the cyanogen gives the unstable tri-cyanide ($C_3N_3^-$) species. $C_3N_3^-$

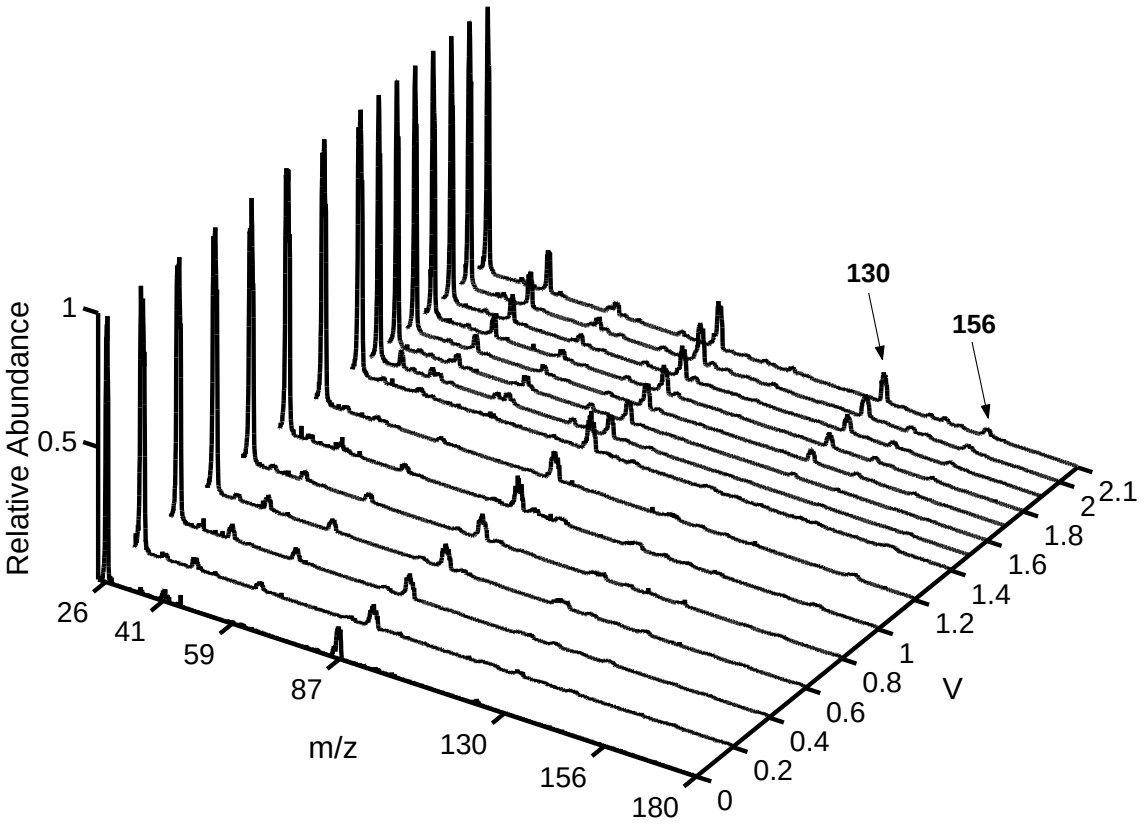

Figure 3.11: Three Dimensional Plot of EC/ES-MS Mass Spectra of CN^- at the Platinum Electrode as a Function of Applied Electrochemical Cell Potentials

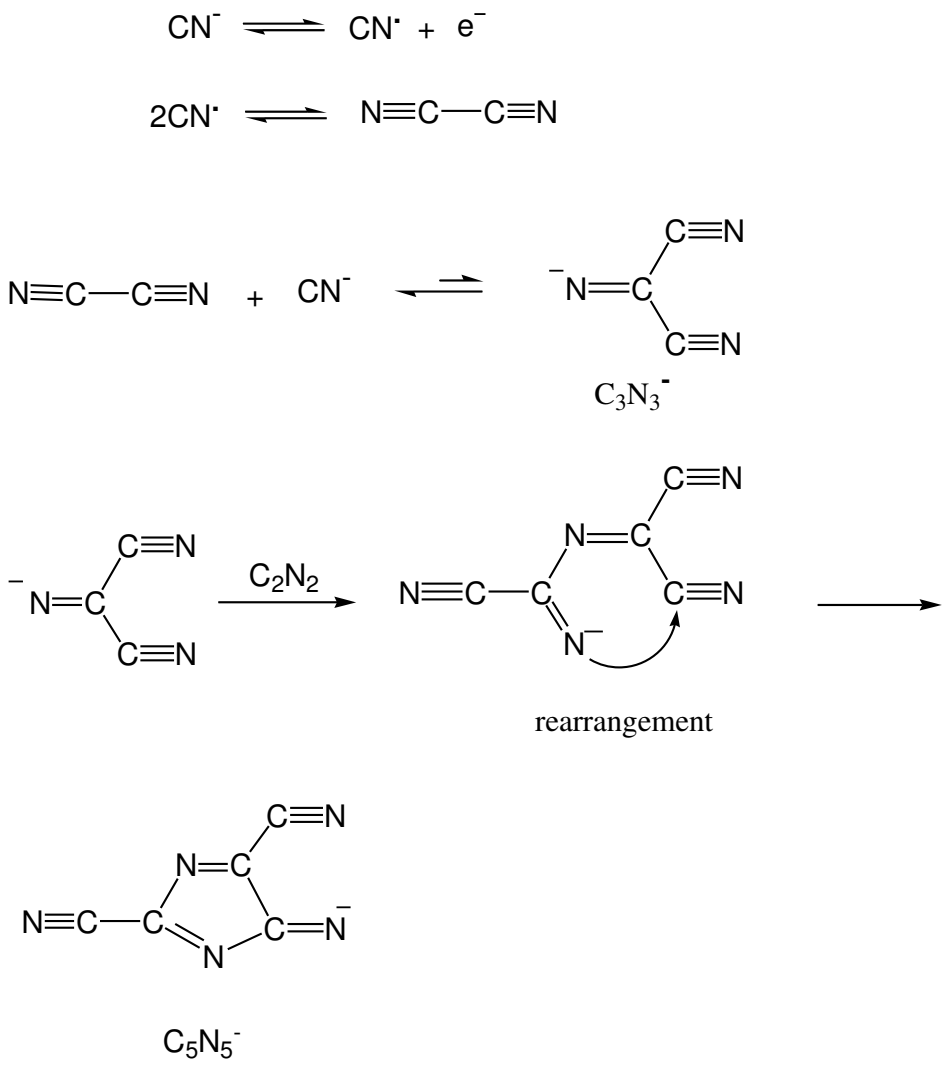

Figure 3.12: Schematic of the Formation of $C_5N_5^-$ by Addition of C_2N_2 to CN^-. [28]

has a stability constant of 0.31 in acetonitrile. [176] A further addition of cyanogen by the tri-cyanide, followed by the rearrangement, shown in Figure 3.12, leads to the formation of $C_5N_5^-$. [28] The observation of $C_5N_5^-$ at high potential could indicate that a relatively high concentration of cyanogen must be present resulting in the formation of $C_5N_5^-$ as showing in Figure 3.12. [28]

The second potential dependent peak at *m/z* 156 seen in Figure 3.11 is not as intense as the peak at *m/z* 130, but it does grow as the potential is increased. We suggest that this small peak may be assigned as $C_6N_6^-$ or $C_{12}N_{12}^{2-}$, [177, 178] which is the trimer of cyanogen. The proposed structure of $C_6N_6^-$, shown in Figure 3.13, has been identified by X-ray in solid state. [177, 178] Observation of negative charged C_6N_6 in our experiment is interesting because C_6N_6 is a neutral species and potentials applied at the platinum electrode are positive. This could indicate that neutral C_6N_6 is formed at the platinum electrode and is reduced to negative $C_6N_6^-$ in the ESI capillary. It has been shown that the $C_6N_6^-$ is an unstable radical and can immediately dimerize at a ring carbon to form $[C_{12}N_{12}]^{2-}$. [178] Unfortunately we were not able to prove this peak by the isotope pattern because of the weak signal and low resolving power of the single quadrupole mass spectrometer.

Comparing these CN^- results with those of iodide at platinum, no peak corresponding to platinum cyanide complexes is observed at any potential studied. Figure 3.14 shows a mass spectrum at 2.0 V and shows the absence of a peak at *m/z* 247. The absence of a complex could be as the result of the low concentration of CN^-. [172] Sawyer, et al. [172] reported that the cyanide oxidation can be inhibited by increasing the concentration of cyanide, this is because the platinum electrode is oxidized rather than cyanide at high potential.

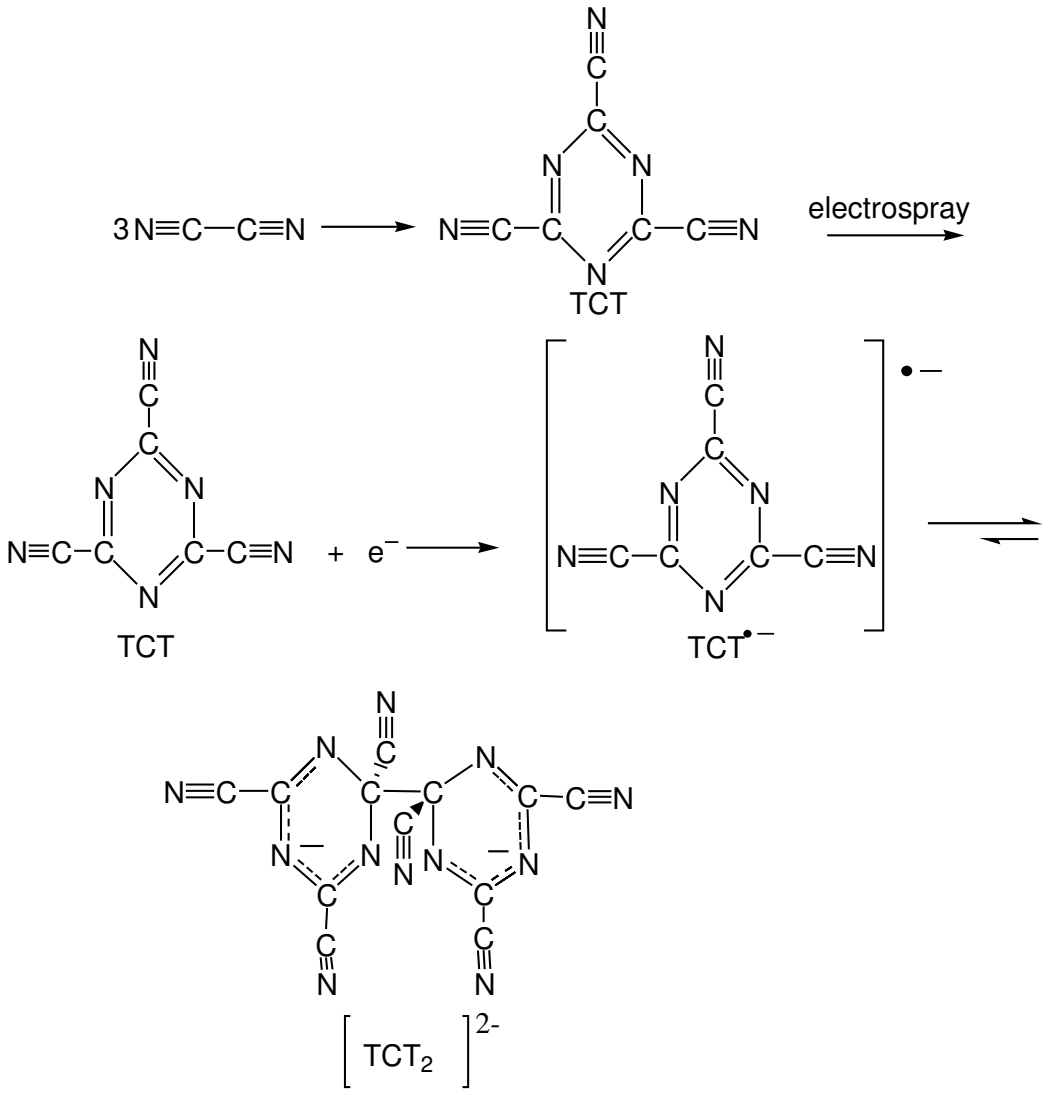

Figure 3.13: Schematic of the Formation of $C_6N_6^-$ and $C_{12}N_{12}^{2-}$ During the Electrospray Process. [177, 178]

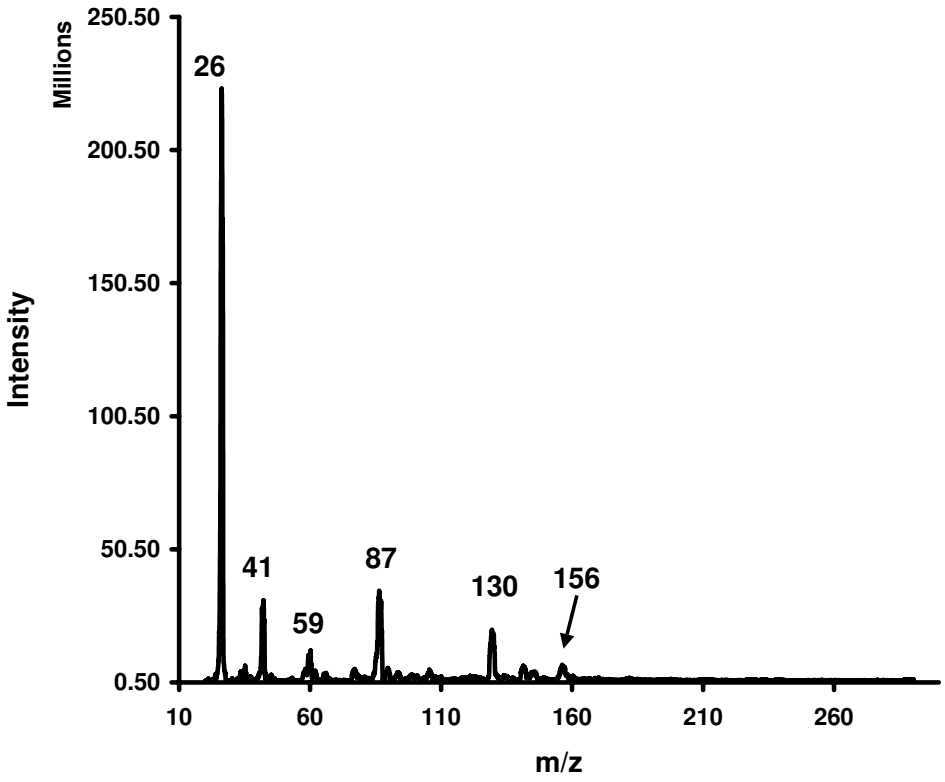

Figure 3.14: Mass Spectrum of the [TBA]CN oxidation at 2.0 V

Gold Working Electrode. The molecular structures are similar for both $Au(CN)_2^-$ and AuI_2^-, consisting of linear two-coordinate complex ions. [179] $Au(CN)_2^-$ is among the most stable two-coordinate complexes of the transition metal ions, with the stability constant 10^{37} M^{-2} in aqueous solution. [180, 181]

The following trend of stability constants of gold(I) complexes in acetonitrile was reported. [24]

$$NCO^- < NCS^- < Cl^- < Br^- < I^- \ll CN^-$$

The above given order ($I^- \ll CN^-$) indicates that $Au(CN)_2^-$ is a very stable complex with a stability constant of 10^{35} M^{-2} in acetonitrile solution. [19]

In this section, we present further results dealing with the surface reaction of a fresh annealed gold electrode in non-aqueous potassium cyanide solution by using EC/ES-MS. Figure 3.15 shows the results of a normalized EC/ES-MS experiment at gold electrodes in the presence of 1 mM potassium cyanide in acetonitrile. The potential ranges from 0.0 V to -1.0 V. The peak at *m/z* 249 corresponds to $Au(CN)_2^-$ and first appears with the strongest peak at 0 V with the potentiostat connected to the cell; it decreases slowly with decreasing potential until ~ -1.0 V. The peak at *m/z* 319 assigned to $B(C_6H_5)_4^-$ appears relatively constant over the entire voltage range. These results clearly demonstrate the formation of $Au(CN)_2^-$ resulting from the surface oxidation of a freshly annealed gold electrode.

A plausible interpretation for our observation of $Au(CN)_2^-$ at 0 V at a gold working electrode is shown in equations (3.17), (3.18) and (3.19). [182] Equation (3.17) describes the surface oxidation of the gold cyanide adlayer to form AuCN on the electrode surface. Reaction (3.17) is followed by the dissolution of the AuCN as $Au(CN)_2^-$ (equation 3.18 and 3.19).

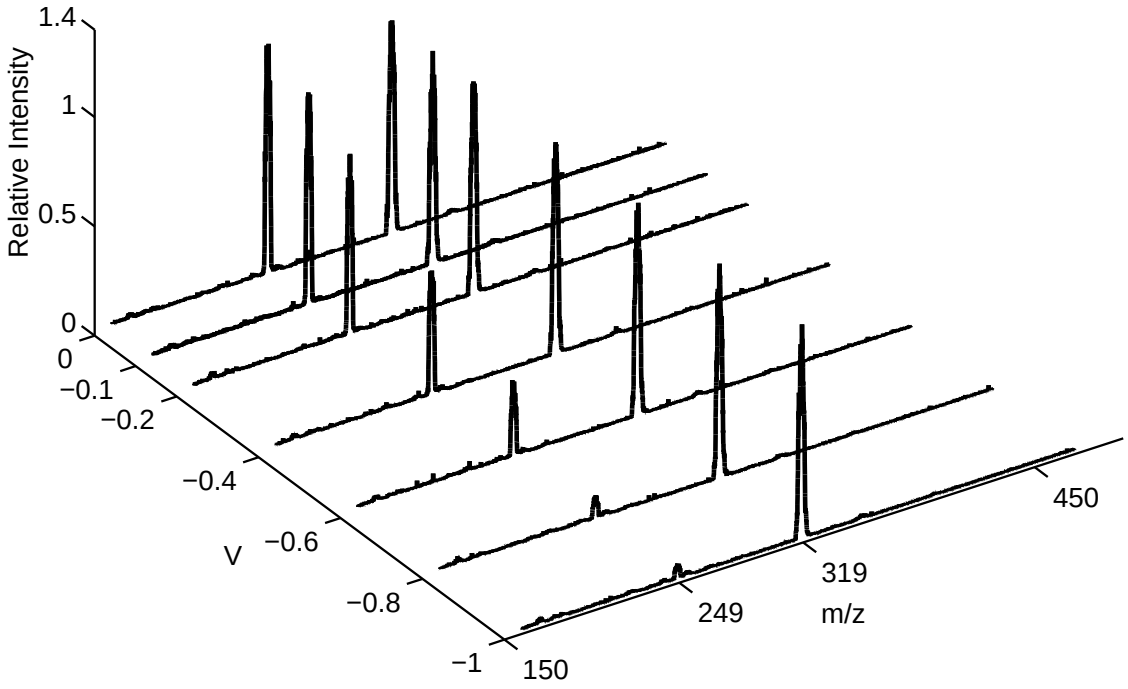

Figure 3.15: Three Dimensional Plot of EC/ES-MS Mass Spectra CN^- at the Gold Electrode as a Function of Applied Electrochemical Cell Potential

$$\mathrm{Au} + \mathrm{CN}^- \rightleftharpoons \mathrm{AuCN}^-_{(\mathrm{ads})} \tag{3.14}$$

$$\mathrm{AuCN}^-_{(\mathrm{ads})} \rightleftharpoons \mathrm{AuCN}_{(\mathrm{ads})} + \mathrm{e}^- \tag{3.15}$$

$$\mathrm{AuCN}_{(\mathrm{ads})} + \mathrm{CN}^- \rightleftharpoons \mathrm{Au(CN)}^-_2 \tag{3.16}$$

The dissolution is driven by the high stability constant of $\mathrm{Au(CN)}^-_2$. Even with potentiostat set at 0 V, a current can flow through the cell. The trace amount of O_2 and water in the acetonitrile could also make the dissolution of the surface gold take place readily. [183] By applying more negative potentials at the working electrode, the surface oxidation step (equation 3.18) slows down, causing the decrease in the intensity of the peak at m/z 249.

3.4 Conclusions

The experimental results presented in this chapter very clearly demonstrate the power of coupling electrochemical experiments to mass spectrometry. These challenging experiments can provide a wealth of detailed information on electrochemical processes. We demonstrated that $\mathrm{B(C_6H_5)}^-_4$ is a suitable internal standard for negative ion in EC/ES-MS studies in acetonitrile. Experiments on I^- at a platinum electrode resulted in well-behaved oxidation to I^-_3. In the CN^- case, the oxidation of CN^- gives cyanogen, addition of two moles of cyanogen to one mole of CN^- leads to the formation $\mathrm{C_5N}^-_5$. The peak at m/z 156 could be assigned to $\mathrm{C_6N}^-_6$ or $\mathrm{C_{12}N}^{2-}_{12}$.

With I^- at gold electrodes we observed AuI^-_2 as well as I^-_3. The AuI^-_2 mass spectrometric ion intensity varies in a non-linear way throughout the applied electrochemical voltage range studied. We suggest that this variation results from the

competition between I^- adsorbed on the gold electrode surface and I^- solution. In the CN^- case, we observed surface oxidation of the gold electrode at 0 V applied at working electrode with a potentiostat connected to the cell. However, as more negative potentials are applied, the AuI_2^- intensity clearly decreases, indicating that the ion is formed at the gold electrode.

Chapter 4

Fullerene

Abstract

Reduction of C_{60} to the 4- state in a mixture of acetonitrile/toluene at 20 °C was studied by using cyclic voltammetry at a scan rate of 100 mV/s. C_{60}^{n-} (n=1,2), generated by using the bulk electrolysis method, was confirmed by ultraviolet spectroscopy. Gas phase observation of C_{60}^{-}, C_{60}^{3-} and C_{60}^{4-} anions generated at platinum electrodes and detected by electrochemistry/electrospray mass spectrometry is reported. The anions were electrochemically generated from solutions of C_{60} dissolved in toluene/acetonitrile. The gas phase observation of C_{60}^{3-} and C_{60}^{4-}, despite the fact that they have negative electron affinities, is a result of a coulombic repulsion barrier to electron loss. These studies, which demonstrate the gas phase kinetic stability of C_{60}^{3-} and C_{60}^{4-}, illustrate the promise of electrochemistry/electrospray mass spectrometry for the study of metastable anions.

4.1 Introduction

One of the most interesting aspects of fullerene chemistry is the ease with which these remarkable molecules accommodate negative charges. It has been said that the electron-accepting ability of C_{60} is its most characteristic chemical property. [146] The fact that C_{60} has three low-lying degenerate unoccupied molecular orbitals allows stepwise electrochemical [29, 41, 121, 123, 184] or alkali metal reduction [185–191] to produce fulleride anions with up to six negative charges. [146,192] Salts of C_{60} with up to three negative charges have been isolated [14, 128, 193] and the ease of generating

C_{60}^{2-} has lead to its use as a reagent in the synthesis of disubstituted fullerenes. [194, 195]

Although it is clear that these multiply charged fullerides exhibit remarkable stability in solution, their observation in the gas phase has been problematic. Thus, while C_{60}^{-} is readily detected in negative ion mass spectrometry [31, 34, 146, 196, 197] and C_{60}^{2-} has been observed by laser desorption mass spectrometry, [151] gas phase detection of fullerides with more than two negative charges has proved elusive. A consideration of the electron affinities (EAs) of C_{60} provides a simple rationale for this fact. Thus, while the first EA is quite positive at 2.66 eV [198] and the second EA has been calculated to be positive, higher EAs are calculated to be negative. [153] The fact that C_{60}^{2-} is only observed under extremely energetic conditions while dianions of higher fullerenes are much more common in negative ion spectrometry has been attributed to more positive EAs for these molecules and the ability of the larger fullerenes to mitigate coulombic repulsion. [41, 152, 156, 199, 200] Dianionic adducts of C_{60} with $F_{47,48}$ and $(CN)_{2,4,6}$ attached are also readily observed.

It is certainly true that negative EAs will render multiply charged fulleride anions metastable and difficult to generate by electron attachment. However, multianions often exhibit a coulombic barrier to electron loss that can temporarily stabilize M^{n-} anions with negative n^{th} EAs. [201–203] Since negatively charged C_{60} anions are readily generated electrochemically, it seemed to us that electrochemistry/electrospray mass spectrometry (EC/ES-MS) [30, 76, 88, 159] would be an ideal technique for the detection of multiply charged C_{60} anions in the gas phase. Although both electrospray mass spectrometry (ES-MS) and EC/ES-MS have been used to study C_{60} anions in the gas phase, neither C_{60}^{3-} nor C_{60}^{4-} has been detected in these studies. We now report EC/ES-MS studies of C_{60} in which these metastable polyanions are observed.

4.2 Experimental Section.

Chemicals. C_{60} was obtained from MER Corporation and used as received. Acetonitrile (MeCN), toluene, and 49% hydrofluoric acid were purchased from Fisher Scientific Co.

Electrochemical grade tetrabutylammonium tetrafluoroborate ($[Bu_4N]BF_4$, 99.5%), tetrabutylammonium perchlorate ($[Bu_4N]ClO_4$, 99.5%), sodium tetraphenylborate ($NaBPh_4$, 99.5%), CaH_2 (99.0%) were obtained from Aldrich Chemical Co. and used as received. Potassium tetraphenylborate ($KBPh_4$) was purchased from Fluka. All solutions were degassed with dried grade 5.0 Ar gas at least 10 mins.

Tetrabutylammonium tetrafluroborate, ($[Bu_4N]BF_4$) and tetrabutylammonium perchlorate were dried at least 72 hours in a vacuum oven at 40 °C prior to use. Acetonitrile was distilled over CaH_2 under N_2 at least 6 hours before use. Toluene was dried over sodium under N_2 at least 10 hours before use.

Cyclic Voltammetry. Cyclic voltammetric measurements were performed with an Epsilon-EC potentiostat (Bioanalytical System Inc. with data system version 1.31.65NT.) in a 5:1 v/v deaerated toluene/acetonitrile mixture. The solvent mixture contained 0.1M $[Bu_4N]BF_4$ as supporting electrolyte. A conventional three-electrode cell with a platinum working electrode and a platinum mesh as the counter electrode was used. All potentials were measured versus a non-aqueous Ag/Ag^+ reference electrode at room temperature, 20 °C. (The values were converted to values vs. SCE by adding 0.29 V. [165])

A non-aqueous reference electrode Ag/Ag^+ was prepared according to a standard procedure. [43] A silver wire, cleaned by sonication in an acetone solution, was immersed in a dried acetonitrile solution containing 0.01 M $AgNO_3$ and the supporting

electrolyte. The concentration of supporting electrolyte usually was the same as the concentration used in the electrolysis solution. The reference electrode solution was contained in a glass tube (ID 5 mm), which was constructed using Pyrex tube with a porous Vycor plug sealed to one end with heat shrink tubing, this tube was then inserted into a 7 mm OD glass salt bridge (E porosity), which was dipped into the C_{60} solution.

All measurements were done twice.

Controlled-Potential Electro-reduction C_{60}. A homemade bulk electrolysis cell, shown in Figure 4.1, was used to perform the experiments of controlled-potential electro-reduction of a C_{60} acetonitrile suspension. The acetonitrile suspension was prepared by adding 0.5 mL saturated C_{60} toluene solution in 7 - 8 mL acetonitrile. The acetonitrile suspension in the working electrode compartment contained 4 mM $[Bu_4N]BF_4$ as supporting electrolyte. In order to minimize the cell resistance, the solution in the counter electrode compartment contained 20 mM $[Bu_4N]BF_4$ as supporting electrolyte. The working electrode compartment has a volume of 8 mL, which is separated from the counter electrode reaction by a fine ceramic frit. The cell body, platinum mesh working electrode and glass salt bridges were dried in a vacuum oven at 80 °C for at least 72 hours prior to use.

The controlled-potential electrolysis was performed in a glove-bag with high purity dried N_2 flowing through it. During the electrolysis, a Teflon-coated stirring bar was used to agitate the solution in the dark. The solution was continuously purged by dried Ar (Grade 5.0) to minimize possible O_2 contamination. The concentration of C_{60} anions in the acetonitrile solution was estimated as 0.23 - 0.26 mM.

The controlled-potentials, corresponding to generation of C_{60}^{n-} (n=1,2,3), were applied at the working electrode sequentially. The calculated elapse time was $\sim$ 50

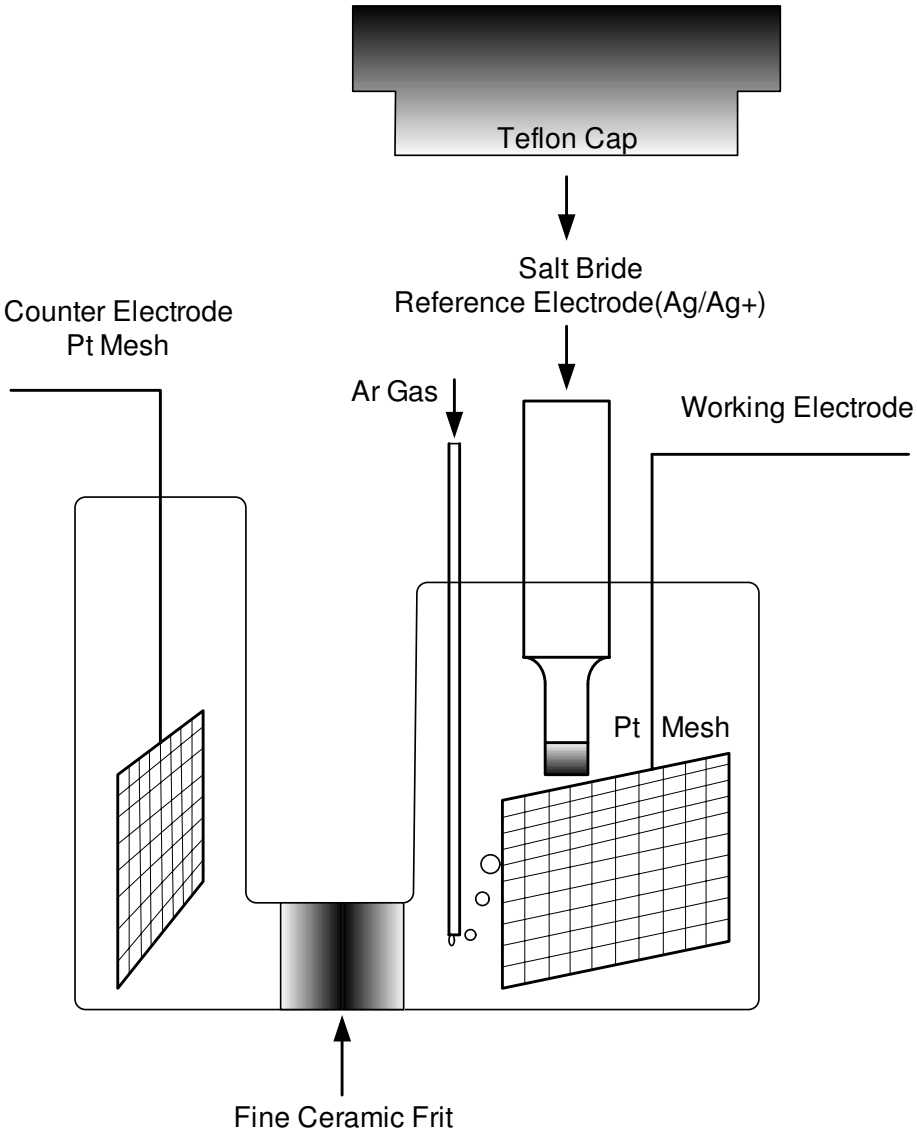

Figure 4.1: Schematic Diagram of the Electrochemical Cell for the Controlled-Potential Electrolysis

mins for each stepwise electrochemical reduction, and the actual experimental elapsed time was 1 hour. The C_{60}^{n-} (n=1,2,3) solution obtained at different potentials was then transferred anaerobically via a 500 μL gas tight syringe to a UV spectrometer and the electrospray mass spectrometer.

Visible Near IR Spectro-electrochemistry. The Vis-NIR spectra were recorded on Hewlett-Packard 5452A and 8453 diode array spectrophotometers which were thermostated at 298 K.

EC/ES-MS Instrumental. Studies of gas phase C_{60}^{n-} polyanions by EC/ES-MS requires finding a suitable solvent medium in which the desired quantity of solid C_{60} can be dissolved. The solvent also needs to support the potential range to be electrochemically studied and needs to to be suitable for electrospray ionization.

In this dissertation, we choose a toluene/acetonitrile solvent mixture and use the "slow" method [212, 215] to prepare the C_{60} solution. It was found that a 5:1 mixture of toluene and acetonitrile with a low concentration $[Bu_4N]BF_4$ as a supporting electrolyte was a satisfactory solvent for the C_{60} EC/ES-MS experiments.

All EC/ES-MS data were collected with a VG-Trios-2000 quadrupole electrospray mass spectrometer. The mass spectra were acquired in negative-ion mode co-adding 50 scans at a scan rate of 0.5 scan/s. The ES tip voltage was $\sim$ 2.89 kV, the source temperature was 60 °C for the toluene/acetonitrile solvent mixture and the cone voltages were typically 20 V. The solutions were pumped with a syringe pump at a flow rate of 5.0 mL/hour.

The electrochemical cell used for EC/ES-MS is shown in Figure 2.1. As described, the cupped collection assembly leads to the mass spectrometer through a fused silica capillary. The working electrode potentials were applied using a Bioanalytical System Inc. CV-27 potentiostat. A platinum-mesh counter electrode and

a Ag/AgCl reference electrode (connected to the cell through a double salt bridge) were used. All potentials are quoted *vs.* aqueous Ag/AgCl. Literature values for C_{60} reduction potentials [192] have been converted to potentials *vs.* Ag/AgCl. Before use, the working electrodes were cleaned by rinsing sequentially with distilled water, 49% hydrofluoric acid, piranha [161] solution, distilled water, HPLC grade methanol and fresh acetonitrile.

4.3 Results and Discussion.

The solubility of C_{60}, up to now, has been determined in up to 150 solvents. [210, 211, 213–217] Table 4.1 lists the solubility of C_{60} in some inexpensive aromatic solvents. Toluene is used in this dissertation, this is because it is a relatively easy to obtain a clean and dry solvent, and is stable over a wide potential range. [42, 43]

Despite the good solubility of C_{60} in toluene, a disadvantage of using pure toluene as solvent is its low dielectric constant, shown in Table 4.1. The low dielectric constant will cause a significant ohmic drop unless high concentrations of supporting electrolytes are added. This problem can be successfully solved by use of a solvent mixture, toluene-acetonitrile.

The properties of solubility, aggregation and electrochemical reduction of C_{60} in the solvent mixtures, toluene-acetonitrile, have been studied extensively. [212, 217–219] Earlier research results [212, 215] show a somewhat unique property of the fullerene's (C_{60}, C_{70}) when dissolved in a toluene-acetonitrile mixtures. As the composition of the solvent mixtures varies, the C_{60} solution undergoes dramatic solvatochromic changes, and the changes are strongly dependent on the C_{60} concentration.

Solvents	Toluene	Dichlorobenzene	Dichloromethane	Benzonitrile	Acetonitrile
Solubility (mg/mL)	3.2[1]/2.8[2]	27[2]	0.26[2]	0.41[2]	0[2]
Dielectric Constant	2.5[3])		8.93[3]	25.2[3]	37.5[3])
Surface Tension mN/m^2	25.97[4]		27.2[4]		19.10[5]

Table 4.1: Solubility of C_{60} in Various Solvents.
(1):reference [214]. (2): reference [213]. (3): reference [209]. (4): reference [207], at 313 K. (5): reference [208]

The solvatochromism is attributed to the formation of C_{60} clusters (dimers and polymers) in the solvent mixtures at a room temperature. The clusters were generated by either "slow" or "fast" addition of acetonitrile to toluene solutions of C_{70} or C_{60}.

Cyclic Voltammetry. Typical cyclic voltammograms of a 0.95 mM C_{60} solution in 5:1 (v/v) toluene-acetonitrile at a platinum electrode (0.10 M $[Bu_4N]BF_4$) is shown in Figure 4.2. The CV was scanned at a rate of 100 mV/s, it proceeds an initial forward scan until the potential is switched at -3.20 V (vs Ag/Ag^+), shown in Figure 4.2. Four clearly well-defined reduction/oxidation peaks are assigned to the generation of 1-, 2-, 3- and 4- anions of C_{60}. Electrochemical reversibility is evident from Figure 4.2.

The four reduction peaks with cathodic peak potentials($E_{(pc)}$) measured relative to Ag/Ag^+ are at -1.02, -1.47, -1.96, -2.50 V. In all cases, the potential separation between any two successive peaks is consistent with the reported value, 450 ± 50 mV. [37, 106, 107]

CV data clearly show that C_{60}^{n-} (n=1,2,3,4) can be generated under the experimental conditions present in this dissertation.

UV-vis-near-IR Spectroscopy. The fullerene anion, C_{60}^-, was prepared by controlled-potential electro-reduction at -1.2 V (vs. Ag/Ag^+) in a C_{60} acetonitrile suspension. The elapsed time for electrolysis was 60 minutes. The reduction of C_{60} to C_{60}^- was confirmed by the conversion of the solution from a brown suspension to a solution with apple-red color. The solution was then anaerobically transferred to an UV cell by a 0.5 mL gas tight syringe. Figure 4.3 curve 1 shows the UV spectrum

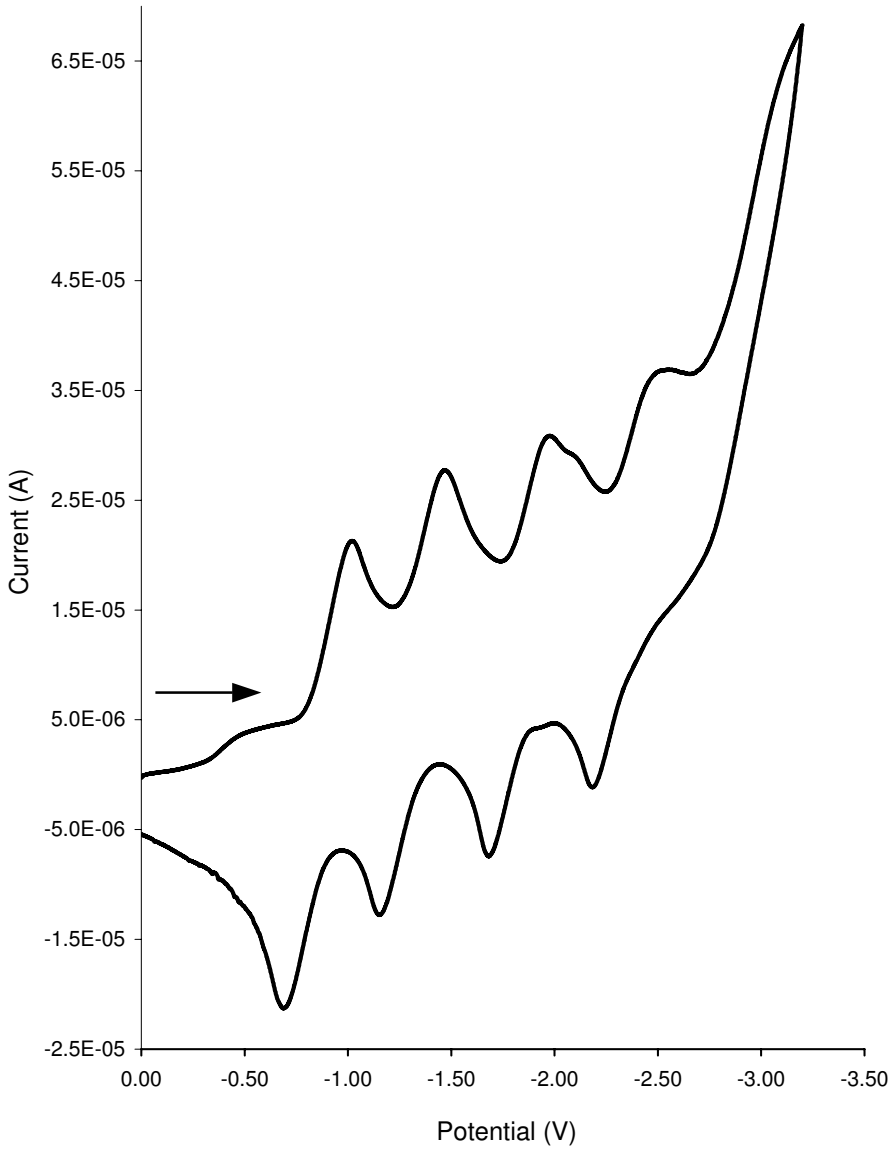

Figure 4.2: Cyclic Voltammogram of C_{60} in Toluene/Acetonitrile at the Scan Rate 100 mV/s, 20°C, V *vs.* Ag/Ag^+

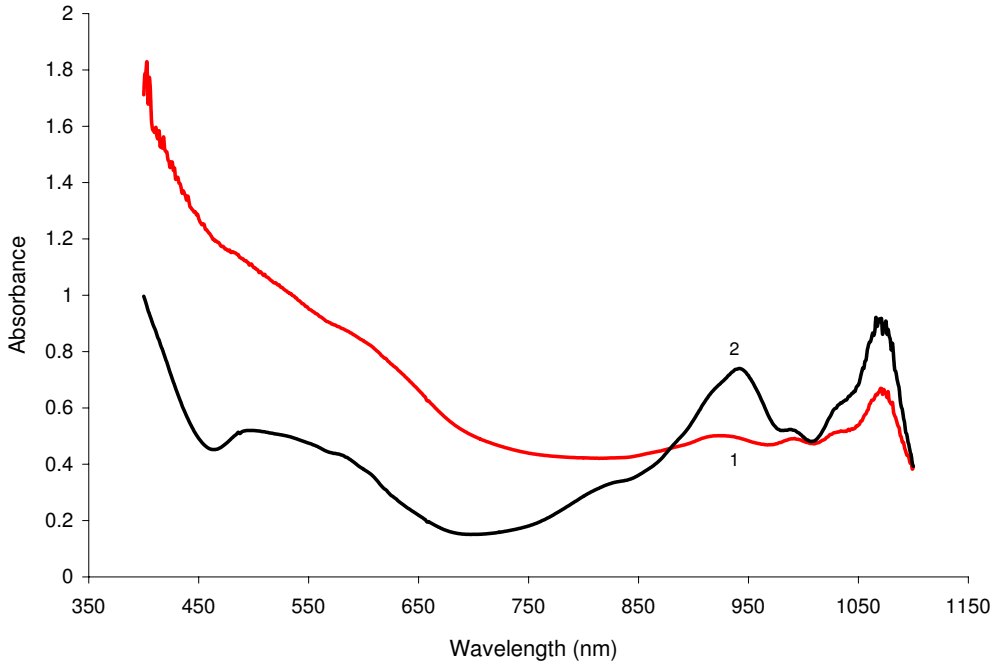

Figure 4.3: Near-IR Spectrum of C_{60}^{n-} (n=1,2) in Toluene/Acetonitrile with $[Bu_4N]BF_4$ at 20°C, Curve (1): IR Absorbance of C_{60}^{-}, Curve (2): the IR Absorbance of C_{60}^{2-}

of the C_{60}^{-} in acetonitrile, it has a strong, characteristic near-IR peak at 1072 nm, (ϵ = 15000 - 20000 $M^{-1} \cdot cm^{-1}$). This peak has been assigned to the allowed t_{1u} to t_{1g} transition, Figure 1.6. [111, 112]

Further electrolysis at -1.8 V led to conversion of C_{60}^{-} to C_{60}^{2-} with a new peak shown in Figure 4.3 curve 2. The absorption peak at 948 nm is in good agreement with the early reports. [31, 206, 220–224] The acetonitrile solution color changed from apple-red to dark-red. The solution was then transferred anaerobically via a 500 μL gas tight syringe to either a UV spectrometer or the electrospray mass spectrometer. Although the C_{60}^{2-} was observed in UV-Vis spectroscopy, we were not able to observe the C_{60}^{2-} by electrospray mass spectrometry.

As the charge on C_{60} increases, the anions become increasingly sensitive to oxygen, water and the solvent purity. Dry-box and vacuum line ($O_2, H_2O <$ 1ppm) techniques are needed for preparation and transportation of the higher charged C_{60} anions solutions. [108, 128, 225–229] Attempts by us to generate C_{60}^{3-} were carried out by further electrolysis at -2.2 V, but we were not able to confirm C_{60}^{3-} by UV-Vis spectroscopy.

EC/ES-MS studies of C_{60}. C_{60} online stepwise electro-reductions were carried out at both platinum and gold electrodes with different supporting electrolytes as well as different concentrations of tetrabutylammonium tetrafluoroborate ($[Bu_4N]BF_4$), tetrabutylammonium perchlorate ($[Bu_4N]ClO_4$) and sodium tetraphenylborate ($NaBPh_4$). The concentration of supporting electrolytes range from 1 mM to 8 mM in a solvent mixture, (5:1 by v/v) toluene-acetonitrile. The toluene solution of C_{60} was prepared first, and then the acetonitrile was slowly added drop by drop using a gas-tight syringe while stirring continuously.

It was found that a 5:1 mixture of toluene and acetonitrile with 4 mM $[Bu_4N]BF_4$ as a supporting electrolyte and 0.05 mM $NaBPh_4$ as an internal standard was a satisfactory solvent for the C_{60} EC/ES-MS experiments. Solutions with this composition were loaded into the electrochemical flow cell, Figure 2.1, and the applied potential was decreased incrementally from 0.0 to -3.4 V. The solution was continuously sprayed into the mass spectrometer. Figure 4.4 shows a three-dimensional plot of the observed mass spectra as a function of the applied potential on the cell. The peaks have all been normalized to the intensity of the internal standard. It can be seen that small amounts of C_{60}^{-}, C_{60}^{3-}, and C_{60}^{4-} are detected at 0.0 V. The intensities of all of these anions increase as the voltage is made more negative, with C_{60}^{4-} showing the most dramatic increase in intensity. In none of these experiments were we able to see evidence of C_{60}^{2-}. In addition, a peak at $m/z = 761$, corresponding to the adduct of C_{60}^{-} and acetonitrile, was observed. Another peak at $m/z = 254$ was observed at potentials between -2.75 and -3.00 V, this peak was assigned as the adduct of C_{60}^{3-} and acetonitrile ($[C_{60} \cdot CH_3CN]^{3-}$).

First, the peaks observed at 0.0 V will be discussed. Since it is known that electrospray sources function as a type of electrochemical cell, [197] it is not surprising that weak -peaks for the fulleride anions are observed when spraying C_{60} solutions from the cell at 0.0 V applied potential. Another probable reason for observation of the fulleride anions at 0 V might be the low dielectric constant of toluene and the surface activity of C_{60}. Early work reported measurements of the surface tension of toluene solutions of C_{60} as a function of temperature and concentration, [207] it was found that C_{60} was surprisingly surface active (Table 4.2); at the largest concentration studied (Table 4.3) C_{60} occupied nearly a monolayer on the surface. In the ion evaporation mode of the electrospray ionization, [2] the mass-analyzed ion intensity

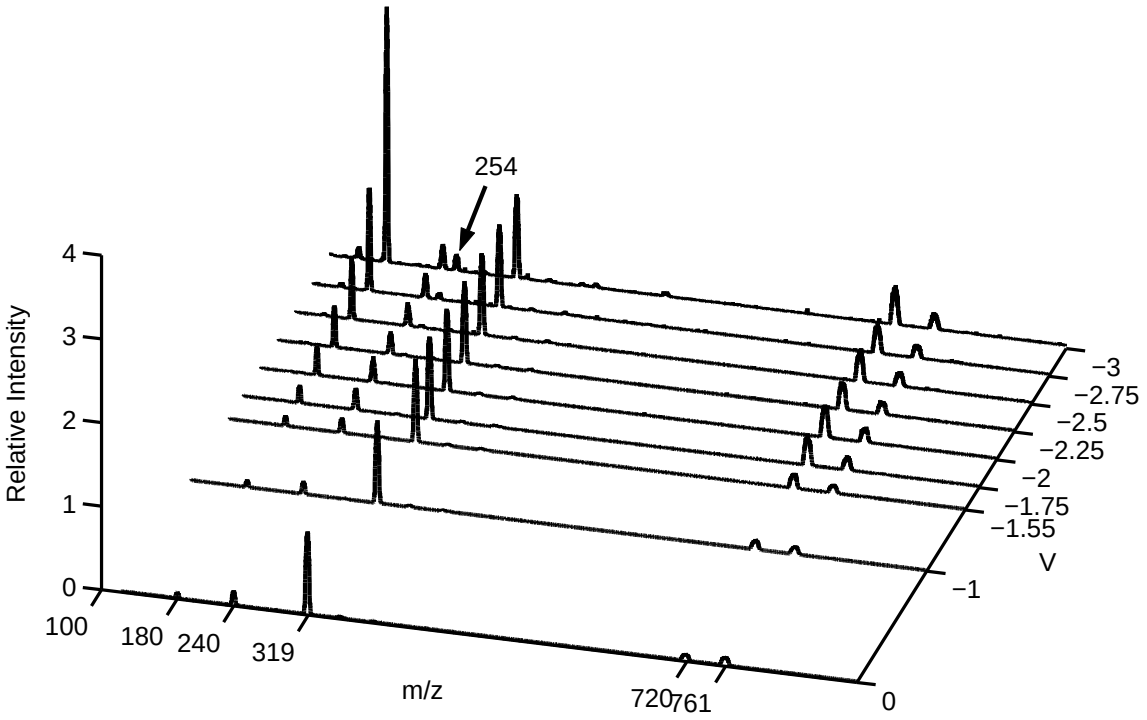

Figure 4.4: Three Dimensional Plot of EC/ES-MS Mass Spectra C_{60} as a Function of Applied Electrochemical Cell Potential

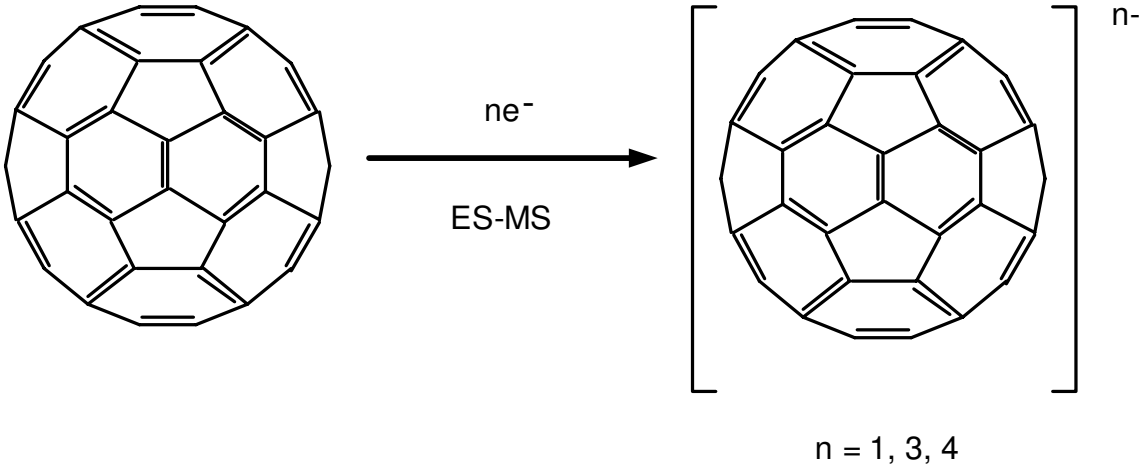

Figure 4.5: C_{60} Reduction

Solution Concentration mM	0	0.208	0.313	0.625	1.250	2.083
			Surface	Tension,	γ (mN/m)	
273 K	30.72	30.18	29.73	29.70	28.99	
303 K	27.35	27.14	27.06	26.78	26.35	25.85
313 K	25.97		25.75	25.64	25.21	25.00

Table 4.2: Surface Tension of C_{60} Solutions in Toluene

- Reference [207]

Solution Concentration mM	0.208	0.313	0.625	1.250	2.083	
		Surface	Excess,	Γ_2^1 (mol/cm)		$d\lambda/dC$
273 K	1.136	1.704	3.406	6.814	11.357	1.238
303 K	0.609	0.913	1.826	3.652	6.085	0.712
313 K	0.406	0.609	1.218	2.436	4.059	0.475

Table 4.3: Surface Excess of C_{60} Solution in Toluene

- Reference [207]

I_A of an analyte ion depends on the surface activity of the analyte ion. [6]

When a charged droplet is formed during the electrospray process, it contains about 10 C_{60} (C_{60} radius: 7Å) units if the radius of the charged-droplet is 10 nm. [2] On the basis of above results, it is clear that most surface sites of a charged droplet will be occupied by solvated C_{60} molecules because of its surface activity in the solvent mixture, toluene/acetonitrile.

On the other hand, by comparing the physical and chemical properties of toluene and acetonitrile, Table 4.1, one can immediately see that approximately same surface tension ($\sim 20\ \mathrm{mN \cdot m^{-2}}$) but remarkably different dielectric constants. The dielectric constants of toluene and acetonitrile are, respectively, 2.4 and 38.8 at 60 °C. A solvent with high dielectric constant usually is capable of holding more charges than a solvent with a low dielectric constant. [230] A solvent with high dielectric constant tends to form solvated ions rather than ion-pairs. [42]

Since C_{60} is an extremely hydrophobic cage-shaped molecule, it is probable that the C_{60} will have non-polar toluene molecules surrounding it rather than an acetonitrile molecule when dissolved in the solvent mixture. Acetonitrile has been proven to be an excellent electrospray solvent for transferring ions from solution phase to gas phase, [5] but a different story might be true for toluene/acetonitrile (5/1 by v/v) mixtures. When a solution of C_{60} passes through the electrospray needle, the presence of high negative electric field at the tip renders the negative charges on the surface of the droplets. [2] Since most available surface sites are occupied by the solvated C_{60}, the negative charge on the surface will be mostly taken by C_{60} molecules because of the electron-accepting ability of C_{60} and the low electric constant of toluene. Furthermore, a charged C_{60} cage allows for the attachment of acetonitrile molecules. This could explain the peak $m/z = 761$ at zero applied potential at the flow cell.

The fact that the peaks in Figure 4.4 increase with increasing applied negative working electrode voltage provides evidence for their electrochemical formation in solution and subsequent transport into the gas phase, Figure 4.5. That we observe no C_{60}^{2-} in these experiments is puzzling since the gas phase dianion has been reported. [151] The reasons that no C_{60}^{2-} was observed are unknown. Given the ease with which this species is generated electrochemically, it must be formed initially in our experiments. It could be possible that C_{60}^{2-} is rapidly removed by the unknown chemical reactions, but it is difficult to imagine a reaction exclusive to C_{60}^{2-} that would not also remove other negatively charged C_{60} species.

As described in Chapter 1, C_{60} has been considered a good candidate for preparation of gas-phase multiply-charged anions, [31,34,146,151,196,197] but, to date, only C_{60}^{2-} and C_{70}^{2-} have been observed by using electrospray and laser desorption methods. [151] In this dissertation, we report for the first time observation of multiply charged C_{60}^{n-} (n=3,4) in the gas phase by using EC/ES-MS. Observation of gas-phase C_{60}^{n-} (n=3,4) by using the EC/ES-MS method is scientifically important for both experimental and theoretical chemistry.

The available techniques for generating, observing and studying long-lived multiply charged anions can be categorized as follows: laser desorption of electrophilic species from a metal surface; [150] electrospray of an aqueous solution containing dianion salts into a vacuum [201,231,232] followed by photodetachment photoelectron spectroscopy; electron capture of neutral clusters of eletrophilic molecules; [233] electron capture by single molecules followed by dimerization to form dianions in the gas phase [234] and formation of multiply charged anions by collision induced dissociation of a high energy monoanion. [235] We demonstrate that the EC/ES-MS method can

be categorized as another experimental method for generating and detecting multiply charged anions in the gas phase by mass spectrometry.

During the past decades, extensive knowledge of physical chemistry has been built on experimental and theoretical studies of single charged anions in the gas phase. [236, 237] But turning to gas-phase multiply charged negative anions (MCAs), both theoretical and experimental information on them are rather insufficient. [236, 237]

MCAs are very common in the condensed phases because they are stabilized by solvation in solution or counter ions in solids, but they are very rare in the gas phase. This is because the difficulty of formation of the multiply-charged anions in the gas phase. A neutral atom or molecule holds its electrons in their orbitals by the electrostatic interaction between the electrons and the positively charged core. Once a neutral molecule binds more than one electron, the dynamic stability (attachment or detachment of electrons) of the gas-phase multiply-charged anions is determined by a coulombic repulsive barrier (CRB) between the anion and the electron. [202] The CRB is formed by the interaction of the long-range Coulomb repulsion among the excess charges and the short-range interaction of electrons in the LUMO. [202] Both the physical and chemical properties of the anions are determined by the CRB. In some cases, the CRB can trap electrons in molecules which have negative EAs. [203, 204] The EA is positive if energy is released during the process of the electron attachment. EA can be high if the incoming electron enters a vacancy of a compact shell and can interact strongly with the nucleus. In most cases, the process of electron attachment on anions is a endothermic, the attaching electron is inevitably repelled by the charge already present in the anion.

Figure 4.6 schematically shows the different EAs and CRB barriers shifting due to the stepwise addition of negative charges to C_{60}. C_{60}^{n-} (n=2,3) have negative EAs.

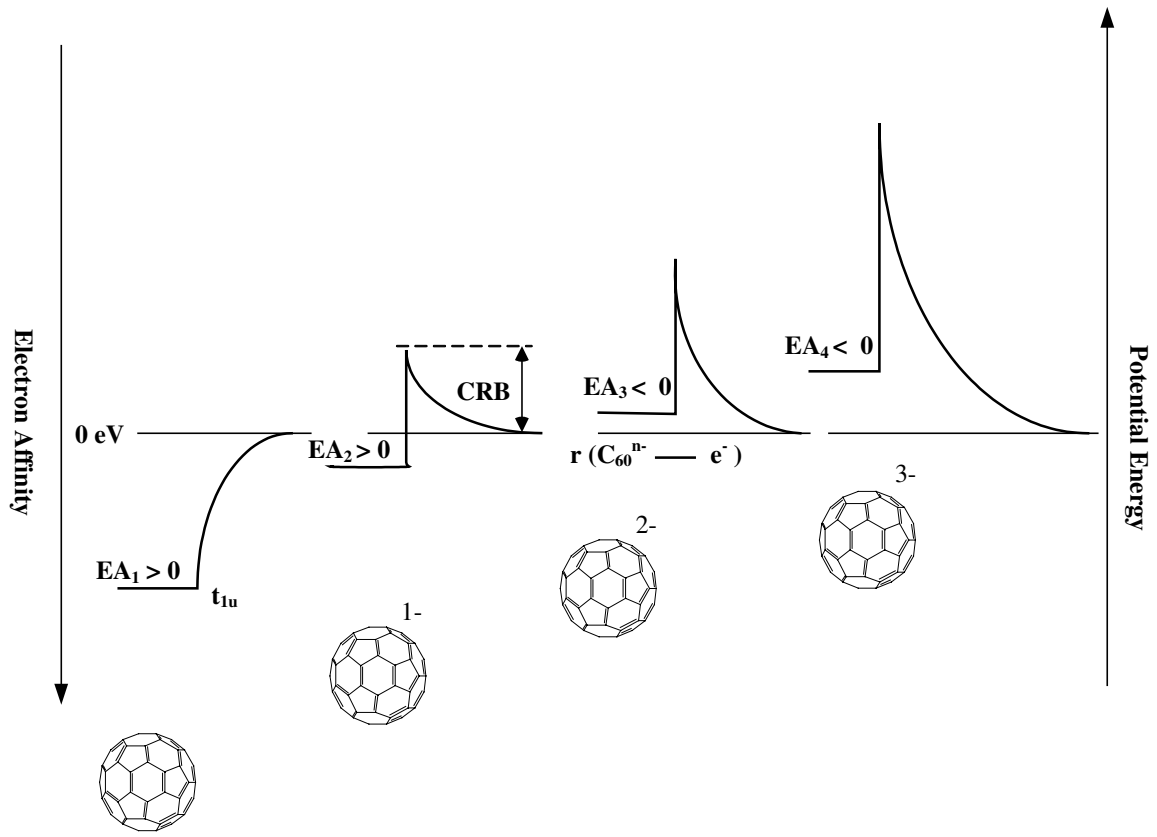

Figure 4.6: Schematic Diagram of the Lowest Unoccupied Molecular Orbitals of C_{60}^{n-} n=0,1,2,3 and the Shifting of the CRB Barrier Heights and the Electron Affinities Due to the Stepwise Addition of Three Negative Charges. The **r** Represents the Electron-Anion Distance

The CRB barrier height increases with the number of the attached negative charges increasing due to the strong mutual Coulomb repulsion of their excess charges.

The negative EAs indicate that C_{60}^{n-} (n=3,4) holds excess electrostatic energy, therefore they are metastable in the gas phase. The common method of generating multiply charged C_{60} anion is to transfer the solid C_{60} into gas phase followed by the stepwise attachment of electrons. Due to the large CRB barriers for C_{60}^{n-} (n=2,3) attachment of electron to the anions forming C_{60}^{n-} (n=3,4) in the gas phase has not been possible.

In the EC/ES-MS method, however, C_{60}^{n-} (n=3,4) is generated in solution where it is stabilized by solvation and then sprayed into the gas phase. Once the C_{60}^{n-} (n=3,4), formed in solution, are transferred into the gas phase, they are immediately trapped inside the CRB barrier, which acts like electrostatic "well". Both the large barrier height and the large molecular size of C_{60} play important roles in the stabilization of C_{60}^{n-} (n=3,4) and in preventing electron detachment. Since electrostatic energy is stored in these multiply charged anions, they can be treated as an electrostatic energy storage medium in gas phase. [203]

This observation of C_{60}^{n-} (n=3,4) with negative binding energy in gas phase greatly enriches the knowledge of the field of gas-phase multiply charged anions in physical chemistry. These results will allow further studies on these and other gas phase multiply charged anions with negative binding energy such as C_{70}.

4.4 Conclusions

The gas phase observation of C_{60}^{-}, C_{60}^{3-} and C_{60}^{4-} in these experiments demonstrate that these metastable polyanions may be observed in the gas phase by first generating them in solution and spraying into the gas phase. The fact that C_{60}^{3-} and C_{60}^{4-} can be

observed despite the fact that they have negative EAs is attributed to a coulombic repulsion barrier to electron loss. As in any EC/ES-MS technique, the method is successful only for those fulleride anions that are soluble. The reason that C_{60}^{2-} was not detected in these experiments is unknown, however we suggest the observation of no C_{60}^{2-} could be due to the unknown chemical reactions. The high concentration of charge in these fulleride polyanions is expected to render them strong nucleophiles and the method promises to become a convenient way of measuring their gas phase reactivities.

Bibliography

[1] Bruckenstein, S.; Gadde, R. R. *J. Am. Chem. Soc.* **1971**, 93, 793-794.

[2] Kebarle, P.; Peschke, M. *Analytica Chimica Acta* **2000**, 406, 11-35.

[3] Wolter, O.; Heitbaum, J. *Ber. Bunsengens. Phys. Chem.* **1984**, 88, 6-10.

[4] Deng, H.; Van Berkel, G. J. *Electroanal.* **1999**, 11, 857-865.

[5] Pramanik, B. N.; Ganguly, A. K.; Gross. M. L. *Applied electrospray mass spectrometry* New York : Marcel Dekker, **2002**.

[6] Tang, L.; Kebarle, P. *Anal. Chem.* **1993**, 65, 3654-3668.

[7] Macagno, V. A.; Giordano, M. C.; Arvía, A. *J. Electrochimica Acta* **1969**, 14, 335-357.

[8] Arvía, A. J.; Giordano, M. C.; Podestá, J. *Electrochimica Acta* **1969**, 14, 389-403.

[9] Swathirajan, S.; Bruckenstein, S. *J. Electroanal. Chem.* **1983**, 143, 167-178.

[10] Iwamoto, R. *Anal. Chem.* **1959**, 31, 955-955.

[11] Bagotsky, V. S.; Vassilyev, Y. B.; Weber, J.; Pirtskhalava, J. N. *J. Electroanal. Chem.* **1970**, 27, 31-46.

[12] Guidelli, R.; Piccardi, G. *Electrochimica Acta* **1967**, 12, 1085-1095.

[13] Popov, A. I.; Geske, D. H. *J. Am. Chem. Soc.* **1958**, 80, 1340-1352.

[14] Bhyrappa, P.; Paul, P.; Stinchcombe, J.; Boyd, P. D. W.; Reed, C. A. *J. Am. Chem. Soc.* **1993**, 115, 11004-11005.

[15] Svensson, P. H.; Rosdahl, J.; Kloo L. *Chem. Eur. J.* **1999**, 5, 305-311.

[16] Lane, R. F.; Hubbard, A. T. *J. Phys. Chem.* **1975**, 79, 808-815.

[17] Sedlmaier, H. D.; Plieth, W. J. *J. Electroanal. Chem.* **1984**, 180, 219-230.

[18] McCarley, R. L.; Bard, A. J. *J. Phys. Chem.* **1991**, 95, 9618-9620.

[19] Goolsby, A. D.; Sawyer, D. T. *Anal. Chem.* **1968**, 40, 1978-1983.

[20] Ahrland, S.; Nilsson, K.; Persson, I.; Yuchi, A.; Penner-Hahn, E. *Inorg. Chem.* **1989**, 28, 1833-1838.

[21] Cahan, B. D.; Villullas, H. M.; Yeager, E. B. *J. Electroanal. Chem.* **1991**, 306, 213-238.

[22] Wagner, D.; Gerischer, H. *J. Electroanal. Chem.* **1989**, 258, 127-137.

[23] Kissner, R. *J. Electroanal. Chem.* **1995**, 385, 71-75.

[24] Roulet, R.; Lan Quang, N.; Mason, W. R.; Fenske, G. P. *Helv. Chim. Acta* **1973**, 56, 2405-2418.

[25] Kunimatsu, K.; Seki, H.; Golden, W. G.; Gordon, J. G.; Philpott, M. R. *Langmuir* **1988**, 4, 337-341.

[26] Abderrahmane Tadjeddine, A.; Le Rille, A. *Electrochimica Acta* **1999**, 45, 601-609.

[27] Brotherton T. K.; Lynn, J. W. *Chem. Rev.* **1959**, 59, 841-883.

[28] Wiley, D. W.; Webster, O. W.; Blanchard, E. P. *J. Org. Chem.* **1976**, 41, 1889-1893.

[29] Kukolich, G. S.; Huffman, D. R. *Chem. Phys. Lett.* **1991**, 182, 263-265.

[30] Schell-Sorokin, A. J.; Mehran, F.; Eaton, G. R.; Eaton, S. S.; Viehbeck, A.; O'Toole, T. R.; Brown, C. A. *Chem. Phys. Lett.* **1992**, 195, 225-232.

[31] Baumgarten, M.; Guegel, A.; Gherghel, L. *Adv. Mater.* **1993**, 5, 458-461.

[32] Baumgarten, M.; Gherghel, L. *Appl. Magn. Reson.* **1996**, 11, 171-182.

[33] Hiraoka, K.; Kudaka, I.; Fujimaki, S.; Shinohara, H. *Rapid Commun. Mass Spectrom.* **1992**, 6, 254-256.

[34] Fullagar, W. K.; Gentle, I. R.; Heath, G. A.; White, J. W. *J. Chem. Soc. Chem. Commun.* **1993**, 6, 525-527.

[35] Disch, R. L.; Schulman, J. M. *Chem. Phys. Lett.* **1986**, 125, 465-466.

[36] Bochvar, D. A.; Galápern, E. G. *Dokl. Akad. Nauk SSSR* **1973**, 209, 610-612.

[37] Xie, Q.; Perez-Cordero, E.; Echegoyen, L. *J. Am. Chem. Soc.* **1992**, 114, 3978-3980.

[38] Smith, P.; Mark, T. D. *Chem. Phys. Lett.* **1993**, 213, 202-206.

[39] Hathiramani, D.; Aichele, K.; Arnold, W.; Huber, K.; Salzborn, E. *Phys. Rev. Lett.* **2000**, 85, 3604-3607.

[40] Robert, J.; Doyle, Jr.; Ross, M. M. *J. Phys. Chem.* **1991**, 95, 4954-4956.

[41] Khairallah, G.; Barrie, P. *Chem. Phys. Lett.* **1997**, 268, 218-222.

[42] Bard, A.; Faulkner, L. R. *Electrochemical Methods: Fundamentals and Applications Application*, **2000,** 2nd ed, New York: John Wiley & Sons, Inc.

[43] Sawyer, D. T.; Sobkowiak, A.; Roberts, J. L. *Electrochemistry For Chemists* 2nd ed, New York: John Wiley & Sons, Inc. **1995**,

[44] Schalley, C. A. *Modern Mass Spectrometry* **2003**, Berlin, New York: Springer, c2003.

[45] Wolter, O.; Heitbaum, J. *Ber. Bunsengens. Phys. Chem.* **1984**, 88, 2-6.

[46] Kotiaho, T.; Lauritsen, F. R.; Choudury, T. K.; Cooks, R. G. *Anal. Chem.* **1991**, 63, 875A-883A.

[47] Hartung, T.; Schmiemann, U.; Kamphausen, I.; Baltruschat, H. *Anal. Chem.* **1991**, 63, 44-48.

[48] Dülberg, A. *In Institut Für Physikalische Chemie,* Universität Witten-Herdecke: Witten-Herdecke, 199, page 164

[49] Tegtmeyer, D.; Heindrichs, A.; Heitbaum, J. *Ber. Bunsenges. Phys. Chem.* **1989**, 93, 201-206.

[50] Arpino, P. *Mass Spectr. Rev.* **1990**, 9, 631.

[51] Hambitzer, G.; Heitbaum, J. *Anal. Chem.* **1986**, 58, 1067-1070.

[52] Hambitzer, G.; Heitbaum, J.; Stassen, I. *J. Electroanal. Chem.* **1998**, 447, 117-124.

[53] Stassen, I.; Hambitzer, G. *J. Electroanal. Chem.* **1997**, 440, 219-228.

[54] Volk, J. K.; Lee, M. S.; Yost, R. A.; Brajter-Toth, A. *Anal. Chem.* **1988**, 60, 720-722.

[55] Volk, J. K.; Yost, R. A.; Brajter-Toth, A. *Anal. Chem.* **1992**, 64, 21A-26A,30A-33A.

[56] Volk, J. K.; Yost, R. A.; Brajter-Toth, A. *Anal. Chem.* **1989**, 61, 1709-1717.

[57] Yamashita, M.; Fenn, J. B. *J. Phys. Chem.* **1984**, 88, 4451-4459.

[58] Yamashita, M.; Fenn, J. B. *J. Phys. Chem.* **1984**, 88, 4671-4675.

[59] Iribarne, J. V.; Thomson, B. A. *J. Chem. Phys.* **1976**, 64, 2287-2290

[60] Thomson, B. A.; Iribarne, J. V. *J. Chem. Phys.* **1979**, 71, 4451-4459

[61] Bartmess, J. E.; Philips, L. R. *Anal. Chem.* **1987**, 59, 2012-2014.

[62] Huang, E. C.; Wachs, T.; Conboy, J. J.; Henion, J. D. *Anal. Chem.* **1990**, 62, 713A-725A.

[63] Volk, K. J.; Yost, R. A.; Brajter-Toth, A. *J. Electrochem. Soc.* **1990**, 137, 1764-1771.

[64] Volk, K. J.; Yost, R. A.; Brajter-Toth, A. *Anal. Chem.* **1989**, 474, 231-243.

[65] Dole, M.; Mack, L. L.; Hines, R. L.; Mobley, R. C.; Ferguson, L. D.; Alice, M. B. *J. Chem. Phys.* **1968**, 49, 2240-2249.

[66] Aleksandrov, M. L.; Gall, L. N.; Krasnov, V. N.; Nikolaev, V. I.; Pavlenko, V. A.; Shkurov, V. A. *Dokl. Akad. Nauk SSSR,* **1984**, 277, 379.

[67] Reyleigh, L. *Philas. Mag.* **1882** 14, 184.

[68] Reid, R. C.; Prausnitz, J. M.; Sherwood, T. K. *The properties of Gases and Liquids*. 3rd ed., **1977**. New York: McGraw-Hill. The surface tension of a luiquid is defined as the force per unit length exerted in the plane of the liquid's surface. Te unit if surface tenion is dyn$(cm)^{-1}$.

[69] Röllgen, F. W.; Bramer-Wegne, E.; Buttering, L. *J. Phys. Colloq.* **1984**, 45, supplement 12, C9-297.

[70] Schmelzeisn-Redeker, G.; Buttering, L.; Röllgen, F. W. *Int. J. Mass Spectrom. Ion Processes* **1989**, 90, 139.

[71] Loscertales, I. G.; Fernández De La Mora, J. *J. Chem. Phys.* **1995**, 103, 5041-5080.

[72] Pretty, J. R.; Duckworth, D. C.; Van Berkel, G. J. *Anal. Chem.* **1997**, 69, 3544-3551.

[73] Pretty, J. R.; Deng, H.; Goeringer, D. E.; Van Berkel, G. J. *Anal. Chem.* **2000**, 72, 2066-2074.

[74] Deng, H.; Van Berkel, G. J. *Anal. Chem.* **1999**, 71, 4284-4293.

[75] Van Berkel, G. J.; Asano, K. G.; Kertesz, V. *Anal. Chem.* **2002**, 74, 5047-5056.

[76] Zhou, F.; Van Berkel, G. J. *Anal. Chem.* **1995**, 67, 3643-3649.

[77] Zhang, T.; Palii, S. P.; Eyler, J. R.; Brajter, A. *Anal. Chem.* **2002**, 74, 1097-1097.

[78] Zhang, T.; Brajter-Toth, A. *Anal. Chem.* **2000**, 72, 2533-2540.

[79] Regino, M. C. S.; Weston, C.; Brajter-Toth, A. *Anal. Chim. Act.* **1998**, 369, 253-262.

[80] Regino, M. C. S.; Brajter-Toth, A. *Anal. Chem.* **1997**, 69, 5067-5072.

[81] Hambitzer, G.; Heitbaum, J. *Anal. Chem.* **1998**, 70, 838-842.

[82] Gun, J.; Modestov, A.; Lev, O.; Poli, R. *Eur. J. Inorg. Chem.* **2003**, 12, 2264-2272.

[83] Diehl, G.; Karst, U. *Anal. and Bioanalytical Chem.* **2002**, 373, 390-398.

[84] Kertesz, V.; Dun, N. M.; Van Berkel, G. J. *Electrochimica Acta* **2002**, 47, 1035-1042.

[85] Permentier, H. P.; Bruins, A. P. *J. Am. Soc. Mass Spec.* **2004**, 15, 1707-1716.

[86] Bond, A. M.; Colton, R.; D'Agostino, A.; Downnard, A. C.; Traeger, J. C. *Anal. Chem.* **1995**, 67, 1691-1695.

[87] Xu, X.; Lu, W.; Cole, R. B. *Anal. Chem.* **1996**, 68, 4244-4253.

[88] Lu, W.; Xu, X.; Cole, R. B. *Anal. Chem.* **1997**, 69, 2478-2484.

[89] Zhang, T.; Palii, S. P.; Eyler, J. R.; Brajter-Toth, A. *Anal. Chem.* **2002**, 74, 1097-1103.

[90] Pretty, J. R.; Van Berkel, G. J. *Rapid Comm. Mass. Spectrom.* **1998**, 12, 1644-1648.

[91] Kertesz, V.; Van Berkel, G. J. *Electroanal.* **2001**, 13, 1425-1430.

[92] Hambitzer, G.; Heitbaum, J.; Stassen, I. *Anal. Chem.* **1998**, 70, 838-842.

[93] Modestov, A. D.; Gun, J.; Mudrov, A.; Lev, O. *Electroanal.* **2004**, 367-378.

[94] Austad, T.; Esperas, S. *Acta. Chem. Stand.* A28, **1974**, 892-896.

[95] Sharpe, A. G. *Inorganic chemistry* New York : Wiley, c1992. 3rd ed.

[96] DeKOCK, R. L.; Caswell, D. S. *Inorganica Chimica Acta* 37, **1979**, L469-L470.

[97] Kroto, H. W.; Heath, J. P.; O'Brien, S. C.; Curl, R. F.; Smalley, R. E. *Nature* **1985**, 318, 162.

[98] Dresselhaus, M. S.; Dresselhaus, G.; Eklund, D. C. *Sciences of Fullerernes and Carbon Nanotubes*, **2000** A John Wiley Sons, Inc. 1st ed.

[99] Kadish, K. M.; Ruoff, R. S. *Fullerenes Chemistry, Physics, and Technology*, **2000**, A John Wiley Sons, Inc. 1st ed.

[100] Haddon, R. C.; Brus, L. E.; Raghavachari, K. *Chem. Phys. Lett.* **1986**, 125, 459-464.

[101] Haymet, A. D. J. *Chem. Phys. Lett.* **1985**, 122, 421-424.

[102] Krätschmer, W.; Lamb, L. D.; Fostiropoulus, K.; Huffman, D. R. *Nature* **1990**, 347, 354-358.

[103] Johnson, R. D.; Meijer, G.; Bethune, D. S. *J. Am. Chem. Soc.* **1990**, 112, 8983-8984.

[104] Taylor, R.; Hare, J. P.; Abdul-Sada, A. K.; Kroto, H. W. *J. Chem. Soc. Chem. Commun.* **1990**, 115, 1423-1425.

[105] Niyazimbetov, M. E.; Evans, D. H.; Lerke, S. A.; Cahill, P. A.; Henderson, C. C. *J. Phys. Chem.* **1994**, 98, 13093-13098.

[106] Ohsawa, Y.; Saji, T. *J. Am. Chem. Soc.* **1992**, 114, 3978-3980.

[107] Zhou, F.; Jeboulet, C.; Bard, A. *J. Am. Chem. Soc.* **1992**, 781-782.

[108] Khaled M. M.; Carlin, R. T.; Trulove, P. C.; Eaton, G. R.; Eaton, S. S. *J. Am. Chem. Soc.* **1994**, 116, 3465-3474.

[109] Olsen, S.; Bond, A. M.; Compton, R. G.; Lazarev, G.; Mahon, P. J.; Marken, F.; Raston, C. L.; Tedesco, V.; Webster, R. D. *J. Phys. Chem. A* **1998**, 102, 2641-2649.

[110] Koh, W.; Dubois D.; Kutner W.; Thomas Jones, M.; Kadish, K. M. *J. Phys. Chem.* **1993**, 97, 6871-6879.

[111] Lawson, D. R.; Feldheim, D. L.; Foss, C. A.; Dorhout, P. K.; Elliott, C. M.; Martin, C. R.; Parkinson, B. *J. Electrochem. Soc.* **1992**, 139, L68-L71.

[112] Fullagar, W. K.; Gentle, I. R.; Heath, G. A.; White, J. W. *J. Chem. Soc., Chem. Commun.* **1993**, 525-527.

[113] Heath, G. A.; McGrady, J. E.; Martin, R. L. *J. Chem. Soc., Chem. Commun.* **1992**, 1272-1274.

[114] Bruno, C.; Doubitski, I.; Marcaccio, M.; Paolucci, F.; Paolucci, D.; Zaopo, A. *J. Am. Chem. Soc.* **2003**, 125, 15738-15739.

[115] Garcia, E.; Kwak, J.; Bard, A. J. *Inorg. Chem.* **1988**, 27, 4377-4382.

[116] Ceroni, P.; Paolucci, F.; Paradisi, C.; Juris, A.; Roffia, S.; Serroni, S.; Campagna, S.; Bard, A. J. *J. Am. Chem. Soc.* **1998**, 120, 5480-5487.

[117] Bard, A. J.; Garcia, E.; Kucharenko, S.; Stretlets, V. V. *Inorg. Chem.* **1993**, 32, 3528-3531.

[118] Ruoff, R. S.; Tse, D. S.; Malhotra, R.; Lorents, D. C. *J. Phys. Chem.* **1993**, 97, 3379-3383.

[119] Sivaraman, N.; Dhamodaran, R.; Kaliappan, I.; Srinivasan, T. G.; Rao, P. R. V.; Mathews, C. K. *J. Org. Chem.* **1992**, 57, 6077-6079.

[120] Haddon, R. C.; Hebard, A. F.; Rosseinsky, M. J.; Murphy, D. W.; Duclos, S. J.; Lyons, K. B.; Miller, B.; Rosamilia, J. M.; Fleming, R. M.; Kortan, A. R.; Glarum, S. H.; Makhija, A. V.; Muller, A. J.; Eick, R. H.; Zahurak, S. M.; Tycko, R.; Dabbagh, G.; Thiel, F. A. *Nature* **1991**, 350, 320-322.

[121] Bausch, J. W.; Prakash, G. K. S.; Olah, G. A. *J. Am. Chem. Soc.* **1991**, 113, 3205-3206.

[122] Ederlé, Y.; Mathis, C. *Macromolecules* **1997**, 30, 4262-4267.

[123] Chi, Y.; Bhonsle, J. B.; Canteenwala, T.; Huang, J.-P.; Shiea, J.; Chen, B.-J.; Chiang, L. Y. *Chem. Lett.* **1998**, 465-466.

[124] Janiak, C.; Mühle, S.; Hemling, H.; Köhler, K. *Polyhedron* **1996**, 15, 1559-1563.

[125] Chen, J.; Huang, Z. E.; Cai, F. F.; Shao, Q. F.; Chen, S.-M.; Ye, H.-J. *J. Chem. Soc. Chem. Commun.* **1994**, 2177-2178.

[126] Stinchcombe, J.; Peónicaud, A.; Bhyrappa, P.; Boyd, P. D. W.; Reed, C. A. *J. Am. Chem. Soc.* **1993**, 115, 5212-5217.

[127] Stinchcombe, J.; Peónicaud, A.; Bhyrappa, P.; Boyd, P. D. W.; Reed, C. A. *J. Am. Chem. Soc.* **1994**, 116, 6484-6484.

[128] Boyd, P. D. W.; Bhyrappa, P.; Paul, P.; Stinchcombe, J.; Bolskar, R. D.; Sun, Y.; Reed, C. A. *J. Am. Chem. Soc.* **1995**, 117, 2907-2914.

[129] Sun, Y.; Reed, C. A. *J. Chem. Soc. Chem. Commun.* **1997**, 747- 748.

[130] Connelly, N. G.; Geiger, W. E. *Chem. Rev.* **1996**, 96, 877-910.

[131] Chen, J.; Huang, Z. E.; Cai, R. F.; Shao, Q. F.; Ye, H. J. *Solid State Commun.* **1995**, 95, 233-237.

[132] Chen, J.; Cai, R. F.; Huang, Z. E.; Shao, Q. F.; Chen, S. M. *Solid State Commun.* **1995**, 95, 239-243.

[133] Chen, J.; Cai, F. F.; Shao, Q. F.; Huang, Z. E.; Chen, S. M. *J. Chem. Soc. Chem. Commun.* **1996**, 1111-1112.

[134] Shabtai, E.; Weitz, A.; Haddon, R. C.; Hoffman, R. E.; Rabinovitz, M.; Khong, A.; Cross, R. J.; Saunders, M.; Cheng, P.-C.; Scott, L. T. *J. Am. Chem. Soc.* **1998**, 120, 6389-6393.

[135] Peónicaud, A.; Hsu, J.; Reed, C. A.; Koch, A.; Khemani, K. C.; Allemand, P.-M.; Wudl, F. *J. Am. Chem. Soc.* **1991**, 113, 6699-6700.

[136] Walch, B.; Cocke, C. L.; Vöpel, R.; Salzborn, E. *Phys. Rev. Lett.* **1994**, 72, 1439-1479.

[137] Christian, J. F.; Wan, Z.; Anderson, S. L. *J. Chem. Phys.* **1993**, 99, 3468-3479.

[138] Takayama, M. *Int. J. Mass Spectrom. Ion Process.* **1991**, 121, R19-R25.

[139] Farizon, B.; Farizon, M.; Gaillard, M. J.; Gobet, F.; Carré M.; Buchet, J. P.; Scheier, P.; Märk, T. D. *Phys. Rev. Lett.* **1998**, 81, 4108-4111.

[140] Yeretzian, C.; Hansen, K.; Beck, R. D.; Whetten, R. L. *J. Chem. Phys.* **1993**, 98, 7480-7484.

[141] Dünser, B.; Lezius, M.; Scheier, P.; Deutsh, H.; Märk, T. D. *Phys. Rev. Lett.* **1995**, 74, 3364-3367.

[142] Andersen, J. U.; Brink, C.; Hvelplund, P.; Larsson, M. O.; Bech Nielsen, R. B.; Shen, H. *Phys. Rev. Lett.* **1996**, 77, 3991-3994.

[143] Scheier, P.; Düser, B.; Märk, T. D. *Phys. Rev. Lett.* **1995**, 74, 3368-3371.

[144] O'Brien, S. C.; Heath, J. R.; Curl, R. F.; Smalley, R. E. *J. Chem. Phys.* **1988**, 88, 220-230.

[145] Campbell, E. E. B.; Ulmer, G.; Hertel, I. V. *Phys. Rev. Lett.* **1991**, 67, 1986-1988.

[146] Reed, C. A.; Bolskar, R. D. *Chem. Rev.* **2000**, 100, 1075-1120.

[147] Fullagar, W. K.; Gentle, I. R.; Heath, G. A.; White, J. W. *J. Chem. Soc. Chem. Commun.* **1993**, 6, 525-527.

[148] Hampe, O.; Neumaier, M.; Blom, M. N.; Kappes, M. N. *Chem. Phys. Lett.* **2002**, 354, 303-309.

[149] Kozlovski, V.; Brusov, V.; Sulimenkov, I.; Pikhtelev, A. *Rapid Commun. Mass. Spectrom.* **2004**, 18, 780-786.

[150] Hettich, R. L.; Compton, R. N.; Ritchie, R. H. *Phys. Rev. Lett.* **1991**, 67, 1242-1245.

[151] Limbach, P. A.; Schweikhard, L.; Cowen, K. A.; McDermott, M. T.; Marshall, A. G.; Coe, J. V. *J. Am. Chem. Soc.* **1991**, 113, 6795-6798.

[152] Zhou, F.; Van Berkel, G.; Donovan, B. T. *J. Am. Chem. Soc.* **1994**, 116, 5485-5486.

[153] Luo, J.; Peng, L. M.; Xue, Z. Q.; Wu, J. L. *J. Chem. Phys.* **2004**, 120, 7998-8001.

[154] Yang, S. H.; Pettiette, C. L.; Conceicao, J.; Cheshnovsky, O.; Smalley, R. E. *Chem. Phys. Lett.* **1987**, 139, 233-238.

[155] Ehrler, O. T.; Weber, J. M.; Furche, F.; Kappes, M. M. P. *Phys. Rev. Lett.* **2003**, 91, 113006/1-113006/4.

[156] Khairallah, G.; Peel, J. B. *Chem. Phys. Lett.* **1998**, 296, 545-548.

[157] Balades, A. T.; Ikonomou, M. G.; Kebarle, P. *Anal. Chem.* **1991**, 63, 2109-2114.

[158] Van Berkel, G. J.; McLuckey, S. A.; Glish, G. L. *Anal. Chem.* **1992**, 64, 1586-1593.

[159] Van Berkel, G. J.; Zhou, F. *Anal. Chem.* **1995**, 67, 2916-2923.

[160] Van Berkel, G. J.; Asano, K. G.; Granger, M. C. *Anal. Chem.* **2004**, 76, 1493-1499.

[161] Licht, S.; Cammarata, V.; Wrighton, M. S. *J. Phys. Chem.* **1990**, 94, 6133-6140.

[162] Bard, A.; Faulkner, L. R. *Electrochemical Methods: Fundamentals and Applications*, New York: Wiley, c2001, 2nd ed, page 333.

[163] Schlichting, H. *Boundary-Layer Theroy,* **1999**, John Wiley & Sons, Inc. 9th ed.

[164] Coetzee J. F.; Cunningham G. P.; McGuire D. K.; Padmanabhan G. R. *Anal. Chem.* **1962**,34, 1139-1143.

[165] Mann, C. K.; Banes, K. K. *Electrochemical Reactions in Nonaqueous Systems*, **1970** John Wiley & Sons, Inc. 2nd ed.

[166] Sawyer, D. T.; Sobkowiak, A.; Roberts, J. L. *Electrochemistry For Chemists*, 2nd ed. **1995**, John Wiley & Sons, Inc. p.318.

[167] Bard, A.; Faulkner, L. R. *Electrochemical Methods: Fundamentals and Applications*, New York: Wiley, c2001, 2nd ed. p231.

[168] Von Stackelberg, M.; Pilgram, M.; Toome V. Z. *Elektrochem.* **1953**, 57, 342-350.

[169] Bard, A.; Faulkner, L. R. *Electrochemical Methods: Fundamentals and Applications*, New York: Wiley, c2001, 2nd ed. p.147

[170] Bard, A.; Faulkner, L. R. *Electrochemical Methods: Fundamentals and Applications Application*, New York: Wiley, c2001, 2nd ed. p.31

[171] Bard, A.; Faulkner, L. R. *Electrochemical Methods: Fundamentals and Applications*, New York: Wiley, c2001, 2nd ed. p.165

[172] Sawyer, D. T.; Day, R. J. *J. Electroanal. Chem.* **1963**, 5, 195-207.

[173] Ciszkowska, M.; Osteryoung, J. G. *Anal. Chem.* **1995**, 67, 1125-1130.

[174] The surface oxidation rate could be determined by the I^- diffusion becasue of the observation of the constant absolute intensity of I^-.

[175] The available surface area of Au electrode could limit the Au oxidation rate, but this can not explain that the approximately equal absolutely intensity of I^- observed with both Au and Pt electrode at 0 V in Figure 3.2 and 3.7.

[176] Beck, M. T.; Gáspár V.; Goel, D. P. *Inorganica Chimica Acta* **1979**, 33, L147-L148.

[177] Del Sesto, R. E.; Arif, A. M.; Miller, J. S. *Chem. Commum.* **2001**, 2730-2731.

[178] Rico, E.; Del Sesto, R. E.; Arif, A. M.; Novoa, J. J.; Iwona Anusiewicz, I.; Skurski, P.; Simons, J.; Dunn, B. C.; Edward, M.; Eyring, E. M.; Joel, S.; Miller, J. S. *J. Org. Chem.* **2003**, 68, 3367-3379.

[179] Holleman, A. F.; Wiberg, E. *Inorganic Chemistry* Academic Press, **1995**, 3ed.

[180] Puddephatt, R. J. *The Chemistry Of Gold* **1978**, Elsevier Scientific Publishing Company, London, st ed.

[181] Sharpe, A. G. *The Chemistry of Cyano Complexes of the Transition Metals* **1976**. Academic Press: London

[182] Kirk, D. W.; Foulkes, F. R. *J. Electrochem. Soc.* **1980**, 127, 1993-1998.

[183] McCarley, R. L.; Bard, A. J. *J. Phys. Chem.* **1992**, 96, 7410-7416.

[184] Buffinger, D. R.; Ziebarth, R. P.; Stenger, V. A.; Recchia, C.; Pennington, C. H. *J. Am. Chem. Soc.* **1993**, 115, 9267-9270.

[185] Haufler, R. E.; Conceicao, J.; Chibante, L. P. F.; Chai, Y.; Byrne, N. E.; Flanagan, S.; Haley, M. M.; O'Brien, S. C.; Pan, C.; Xiao, Z.; Billups, W. E.; Ciufolini, M. A.; Hauge, R. H.; Margrave, J. L.; Wilson, L. J.; Curl, R. F.; Smalley, R. E. *J. Phys. Chem.* **1990,** 94, 8634-8636.

[186] Loy, D. A.; Assink, R. A. *J. Am. Chem. Soc.* **1992**, 114, 3977-3978.

[187] Ohsawa, Y.; Saji, T. *J. Chem. Soc. Chem. Commun.* **1992**, 10, 781-782.

[188] Allemand, P. M.; Koch, A.; Wudl, F.; Rubin, Y.; Diederich, F.; Alvarez, M. M.; Anz, S. J.; Whetten, R. L. *J. Am. Chem. Soc.* **1991,** 113, 1050-1051.

[189] Cox, D. M.; Behal, S.; Disko, M.; Gorun, S. M.; Greaney, M.; Hsu, C. S.; Kollin, E. B.; Millar, J.; Robbins, J.; Robbins, W.; Sherwood, R. D.; Tindall, P. *J. Am. Chem. Soc.* **1991,** 113, 2940-2944.

[190] Dubois, D.; Kadish, K. M.; Flanagan, S.; Haufler, R. E.; Chibante, L. P. F.; Wilson, L. J. *J. Am. Chem. Soc.* **1991,** 113, 4364-4366.

[191] Dubois, D.; Kadish, K. M.; Flanagan, S.; Wilson, L. J. *J. Am. Chem. Soc.* **1991**, 113, 7773-7774.

[192] Echegoyen, L.; Echegoyen, L. E. *Accts. Chem. Res.* **1998**, 31, 593-601.

[193] Paul, P.; Xie, Z.; Bau, R.; Boyd, P. D. W.; Reed, C. A. *J. Am. Chem. Soc.* **1994**, 116, 4145-4146.

[194] Allard, E.; Riviere, L.; Delaunay, J.; Dubois, D.; Cousseau, J. *Tetrahedron Lett.* **1999**, 40, 7223-7226.

[195] Allard, E.; Delaunay, J.; Cheng, F.; Cousseau, J.; Orduna, J. *J. Org. Lett.* **2001**, 3, 3503-3506.

[196] Hampe, O.; Neumaier, M.; Blom, M. N.; Kappes, M. N. *Chem. Phys. Lett.* **2002**, 354, 303-309.

[197] Kozlovski, V.; Brusov, V.; Sulimenkov, I.; Pikhtelev, A.; Dodonov B. *Rapid Commun. Mass. Spectrom.* **2004**, 18, 780-786.

[198] Wang, X.-B.; Ding, C.-F.; Wang, L.-S. *J. Chem. Phys.* **1999**, 110, 8217-8220.

[199] Ehrler, O. T.; Weber, J. M.; Furche, F.; Kappes, M. M. *Phys. Rev. Lett.* **2003**, 91, 113006/1-113006/4.

[200] Jin, C.; Hettich, R. L.; Compton, R. N.; Tuinman, A.; Kovacs-Derechskei, A.; Marynick, D. S.; Dunlap, B. I. *Phys. Rev. Lett.* **1994**, 73, 2821-2824.

[201] Wang, L.-S.; Wang, X.-B. *J. Phys. Chem.* A **2000**, 104, 1978-1990.

[202] Sheller, M. K.; Compton, R. N.; Cederbaum, L. S. *Science* **1995**, 270, 1160-1166.

[203] Wang, X.-B.; Wang, L.-S. *Nature* **1999**, 400, 245-248.

[204] Electron Affinity: EA is the energy that released when a electron attaches to a gas phase atom, molecule or ion. Usually an EA is positive if energy is released during the process of the electron attachment. Electron affinity can be great if the coming electron enters vacancy in a compact shell and can interact strongly with the nucleus. In most cases, the process of electron attachment on anions is a endothermic, the coming electron is inevitably repelled by the charge already present in the compact shell.

[205] Koh, W.; Dubois, D.; Kutner, W.; Jones, M. T.; Kadish, K. M. *J. Phys. Chem.* **1992**, 96, 4163-4165.

[206] Mehran, F.; Schell-Sorokin, A. J.; Brown, C. A. *Phys. Rev.* B **1992**, 46, 8579-8581.

[207] Xu, Q.; Liu, H.; Frisch, H. L.; William E.; Broderick, W. E. *J. Chem. Phys.* **1993**, 98, 9648-9650.

[208] Weast R. C.; Astle, M. J. *CRC Handbook of Physics and Chemistry* **1982** 63rd Ed, CRC Press, Boca Raton, Florida.

[209] Sawyer, D. T.; Sobkowiak, A.; Roberts, J. L. *Electrochemistry For Chemists*, 2nd ed, **1995**, John Willy & Sons, Inc. p.332

[210] Sun, Y.; Bunker, C. *Nature* **1993**, 365, 398.

[211] Sun, Y.; Ma, B.; Bunker, C.; Liu, B. *J. Am. Chem. Soc.* **1995**, 117, 12705 -12711.

[212] Bezmelnistin, V. N.; Eletskii, A. V.; Stepanov, E. V. *J. Phys. Chem.* **1994**, 98, 6665-6667.

[213] Ruoff, R. S.; Tse, D. S.; Malhotra, R.; Donald, C.; Lorents, D. C. *J. Phys. Chem.* **1993**, 97, 3379-3383.

[214] Kazuhiro, K.; Hirose, T.; Moriuchi, K.; Ken, H.; Araki, T.; Tanaka, N. *Anal. Chem.* **1995**, 67, 2556-2561.

[215] Ghosh, H. N.; Sapre, A. V.; Mittal, J. P. *J. Phys. Chem.* **1996**, 10, 9439-9443.

[216] Ying, Q.; Maracek, J.; Chu, B. *Chem. Phys. Lett.* **1994**, 219, 214-218.

[217] Ajie, H.; Alvarez, M. M.; Anz, S. J.; Beck, R. D.; Diederich, F.; Fostirooulos, K.; Huffman D. R.; KrÄtschmer, W.; Rubin, Y.; Schriver, K. E.; Sensharma, K.; Whetten, R. L. *J. Phys. Chem.* **1990**, 40, 8630-8633.

[218] Jehoulet, C.; Bard, A. J. *J. Am. Chem. Soc.* **1991**, 113, 5456-5457.

[219] Olsen, S. A.; Bond, A. M.; Compton, R G.; Lazarev. G.; Mahon P. J.; Marken, F.; Rason, C. L.; Tedesco, V.; Webster, D. *J. Phys. Chem. A* **1998**, 102, 2641-2649.

[220] Kato, T.; Kodama, T.; Shida, T.; Nakagawa, T.; Matsui, Y.; Suzuki, S.; Shiromaru, H.; Yamauchi, K.; Achiba, Y. *Chem. Phys. Lett.* **1991**, 180, 446-450.

[221] Greaney, M. A.; Gorun, S. M. *J. Phys. Chem.* **1991**, 95, 7142- 7144.

[222] Kato, T.; Kodama, T.; Oyama, M.; Okazaki, S.; Shida, T.; Nakagawa, T.; Matsui, Y.; Suzuki, S.; Shiromaru, H.; Yamauchi, K.; Achiba, Y. *Chem. Phys. Lett.* **1991**, 186, 35-39.

[223] Thomas, R. N. *Anal. Chim. Acta* **1994**, 289, 57-67.

[224] Catalan, J.; Saiz, J. L.; Laynez, J. L.; Jagerovic, N.; Elguero, J. *Angew. Chem. Int. Ed. Engl.* **1995**, 34, 105-107.

[225] Fukuzumi, S.; Suenobu, T.; Hirasaka, T.; Arakawa, R.; Kadish, K. M. *J. Am. Chem. Soc.* **1998**, 120, 9220-9227.

[226] Fukuzumi, S.; Nakanishi, I.; Maruta, J.; Yorisue, T.; Suenobu, T.; Itoh, S.; Arakawa, R.; Kadish, K. M. *J. Am. Chem. Soc.* **1998**, 120, 6673-6680.

[227] Tanaka, T.; Kitagawa, T.; Komatsu, K.; Takeuchi, K. *J. Am. Chem. Soc.* **1997**, 119, 9313-9314.

[228] D'Souza, F.; Choi, J. P.; Kutner, W. *J. Phys. Chem. B* **1998**, 102, 4247-4252.

[229] Cliffel, D. E.; Bard, A. J. *J. Phys. Chem.* **1994**, 98, 8140-8143.

[230] Dielectric Constant

[231] Yang, X.; Wang, X-B.; Niu, S.; Pickett, C. J.; Ichye, T.; Wang, L-S. *Phys. Rev. Lett.* **2002**, 89, 163401-1(4).

[232] Yang, X.; Wang, X-B.; Wang, L-S. *J. Phys. Chem.* **2002**, 106, 7607-7616.

[233] Leiter, K.; Ritter, W.; Stamatovic, A.; Märk, T. D. *Int. J. Mass Spectrom. Ion Processes* **1986**, 68, 341-346.

[234] Dougherty, R. C. *J. Chem. Phys.* **1969**, 50, 1896-1897.

[235] Maas, W. P. H.; Nibbering, N. M. M. *Int. J. Mass Spectrom. Ion Proc.* **1989**, 88, 257-266.

[236] Kalchei, J.; Sax, A. F. *Chem. Rev.* **1994**, 94, 2291-2318.

[237] Hotop, H.; Lineberger, C. *J. Phys. Chem.* Ref. Data (a) **1975**, 4, 539, (b) **1985**, 14, 731